The Design, Synthesis and Characterisation of Subtype Selective Dipeptide-linked Fluorescent Ligands for Human β_1 and β_2–Adrenoceptors

Lea Tita Santu, MChem.

Thesis submitted to the University of Nottingham for the degree of Doctor of Philosophy

September 2016

ABSTRACT

Beta-adrenoceptors belong to the superfamily of G-protein coupled receptors (GPCR) and remain an important target for drug discovery. The complexity of GPCR pharmacology in terms of its signaling profile has led to a desire to further the study of receptor-ligand interaction and obtain more detailed information regarding ligand affinity and efficacy. Development of selective fluorescent ligands targeted at human β_1 and β_2–adrenoceptors may facilitate drug discovery programs in terms of understanding receptor pharmacology and receptor localisation in both recombinant and primary cells from healthy and diseased tissue. Fluorescent ligands are usually designed and synthesized by tethering the ligand to a fluorophore *via* a linker to form a conjugate. This thesis reports the synthesis of a series of novel dipeptide-linked congeners which, when coupled to commercially available fluorophore active esters (BODIPY-X-630/650 or BODIPY–FL), afford a series of seventeen red- and green-emitting dipeptide-linked fluorescent ligands for human β_1 and β_2–adrenoceptors.

Pharmacological characterization of the dipeptide-linked fluorescent ligands was achieved using the NanoBRET assay, a novel proximity-based assay. The most promising synthesised compounds propranolol-Gly-Ala FL and propranolol-Gly-Ser-FL (both nanomolar range K_D), showed a respective 87-fold and 26-fold selectivity for the β_2–adrenoceptor versus the β_1–adrenoceptor [pK_D = 8.59 ± 0.11 and 7.74±0.03 (β_2); 6.65±0.09 and 6.32±0.20 (β_1)]. Additionally, these compounds were used in a NanoBRET displacement binding experiment as tracer ligands, with known unlabelled compounds (such as CGP20712a, cimaterol, propranolol (hydrochloride) and ICI 118551) and newly-synthesised acetylated ligands at the Nluc β_2 AR in order to determine their K_D in this system. The displacement binding data agreed with literature values obtained by whole-cell binding assay in both CHO-K1 and Nluc HEK cells. Furthermore,

[^{3}H]-CGP 12177 whole-cell binding experiments were conducted in Nluc HEK 293 and CHO-K1 β_1 and β_2-AR and the results show good correlation with the NanoBRET saturation data and data obtained from another assay, the CRE-SPAP reporter gene assay. In cells expressing β_2-AR, confocal microscopy studies revealed specific membrane labelling with selected ligands which was inhibited by propranolol and ICI 118551.

These novel ligands have potential as tools for exploring the pharmacology of β–adrenoceptors in native systems where more than one receptor subtype is present in terms of imaging and in providing a replacement for radioligands in binding studies.

ACKNOWLEDGMENTS

I would like to express my sincere gratitude to the University of Nottingham, School of Pharmacy for offering a place, for nurturing my scientific passion and contributing to my personal development.

Special thanks both my supervisors Profs. Barrie Kellam and Stephen Hill for their guidance, sound advice and moral support. I grateful for Dr. Christophe Fromont and Dr Leigh Stoddart for technical guidance and support in the laboratory.

I am grateful for the support from the ICS team, to Marleen and Rick for tissue culture training; to Tim Self and Sjima for confocal imaging training and to Mark Soave for being a good friend and a good lab partner, a happy SPAPer. Additionally, I am thankful to Jackie Glenn, Sarah Cully and Amanda Wheal for proofreading my work.

I would like to thank my family "Les Santus" for their tremendous support. And to my husband Sedu, you are the real star; your invaluable support has taken me this far. I thank you all for being my cheerleaders; my heart beats for all you.

ABBREBIATIONS

Ala	alanine
AR	adenosine receptors
β-Ala	beta-alanine
Boc	*tert*-butylcarbonyl
Brine	saturated NaCl
BODIPY®	boron-dipyrromethene
Boc	*tert*-Butyloxycarbonyl
BRET	bioluminescence resonance energy transfer
B_{max}	receptor maximum occupency
$CHCl_3$	chloroform
Calcd.	calculated
cAMP	cyclic adenosine monophosphate
Cbz	carboxybenzyl group
COPD	chronic obstructive pulmonary disease
CRE	cAMP response element
d	doublet

dd	doublet of doublet
DCM	dichloromethane
DIPEA	diisopropylamine
DMAP	4-dimethylaminopyridine
DMEM\F12	Dulbecco's Modified Eagle Medium
DMF	*N*,*N* – Dimethylformamide
DMSO	dimethyl sulphoxide
EDTA	2,2',2",2"'-(Ethane-1,2-diyldinitrilo)tetraacetic acid
Et_2O	diethyl ether
EtOAc	ethyl acetate
Fmoc	fluorenylmethyloxycarbonyl
FRET	fluorescent resonance energy transfer
FCS	Fluorescence Correlation Spectroscopy
FACS	Fluorescence activated cell sorting
FCC	flash column chromatography
G-protein	guanine nucleotide binding protein
GPCR	g-protein coupled receptor

GDP	guanine diphosphate
GTP	guanine triphosphate
Gln	glutamine
Gly	glycine
HBTU	N,N,N′,N′-Tetramethyl-O-(1H-benzotriazol-1-yl)uronium hexafluorophosphate
HBSS	Herpes Balanced Salt Solution
HCl	hydrochloric acid
HEK	human embryonic kidney
H_2O	deionised water
HFIP	hexafluoro-2-propanol
IR	infrared spectroscopy
K_D	Dissociation constant
LC-MS	liquid chromatography tandem with mass spectroscopy
LCM	Laser Scanning Confocal Microscopy
m	multiplet
meas.	measured
MeCN	acetonitrile

MeOH	methanol
$MgSO_4$	anhydrous magnesium sulphate
Mp	melting point
NaH	sodium hydride
NaOH	sodium hydroxide
NanoBRET	BRET system that uses the luciferase, Nanoluc
Nluc	Nanoluc
Na_2SO_4	anhydrous sodium sulphate
NH_4Cl	saturated ammonium chloride solution
NH_3	ammonium solution
NMR	nuclear magnetic resonance spectroscopy
PBS	Phosphate Buffered Saline
PEG	polyethylene glycol
Pd	palladium
Phe	phenylalanine
PKA	Protein kinase A
Ppm	part per million

PET	petroleum ether (40-60%)
t	triplet
theo.	theoritical
Tyr	tyrosine
s	singlet
SAR	structure activity relationship
SPAP	secreted placental alkaline phosphatase
Ser	serine

All amino acids are referred to by standard IUPAC nomenclature, using three letter codes.

CONTENTS

1 INTRODUCTION

Guanine nucleotide binding Protein Coupled Receptors (GPCRs) represent one of the main families of cell-surface receptors which allow a cell to sense and respond to external stimuli[1-6]. Approximately one third of clinically prescribed drugs target members of this receptor family and they remain one of the main targets for drug design[7].

According to Navigant Consulting, "GPCRs are among the most heavily investigated drug targets in the pharmaceutical industry"[8]. This is because GPCRs are widely spread across all key body organs, and their proven involvement in pathologies *e.g.* central nervous system disorders, cardiovascular disease and cancer[2]. GPCRs therefore remain an attractive and relevant drug target for current and future drug discovery programmes across both large and small pharmaceutical industries[9].

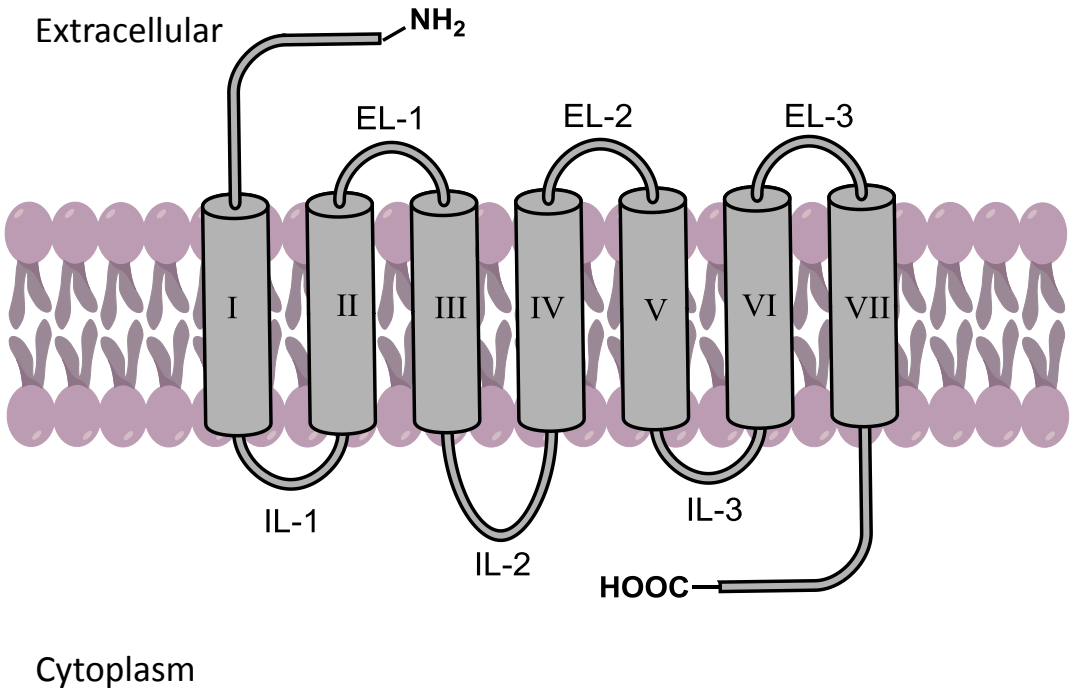

Figure 1-1| General schematic for GPCR. The seven transmembrane spanning alpha-helices (grey) are numbered by roman numerals and pass through the phospholipid membrane (pantone) seven times. The receptor poses structural characteristics that include three intracellular loops (IL-1, IL-2, IL-3) and three extracellular loops (EL-1, EL-2, EL-3).

A GPCR molecular structure consists of a single polypeptide chain which can vary between 311 to 1490 amino acids residues[10]. GPCRs consist of seven transmembrane (TM) spanning α-helices, defined by their primary sequences in which seven regions are embedded into the phospholipid cell membrane with extracellular *N*-terminus and intracellular *C*-terminus domains of varying length (Figure 1-1). The intracellular (IL) and extracellular loops (EL) link together the seven hydrophobic TM spanning α-helical regions. The extracellular loops often possess cysteine residues that form disulphide cross-links stabilising the overall receptor structure[11]. The receptor evokes a cellular response primarily *via* activation

of a heterotrimeric guanosine triphosphate-binding protein[8]. *In vitro* studies have demonstrated that the 7TM receptor can also signal *via* G protein–independent mechanisms[12]; in rat hippocampus cells, for example, mGluR1's synaptic activation by mossy fibre stimulation evokes an excitatory postsynaptic response which is independent of G-protein function[13].

GPCRs can be classified into three major classes, which share the seven transmembrane α-helices but differ in the length of the *N*-terminus and location of the antagonist binding domain (as seen in Figure 1-2)[14]. Alternatively, the five main GPCR families (Glutamate, Rhodopsin, Adhesion, Frizzled/Taste2, and Secretin) can be grouped based on their homology sequences and their functional similarity forming the GRAFS classification system[15]. These are as follows: Class A (rhodopsin-like), Class B (secretin receptor family), Class C (metabotropic glutamate receptor family), Class D (the fungal mating pheromone receptors), Class E (cAMP receptor) and Class F (frizzled/smoothened)[15].

Class A, (rhodopsin-like family) is the largest group comprising mainly monoamine and neuropeptide receptors that have a short *N*-terminal region[16-18].

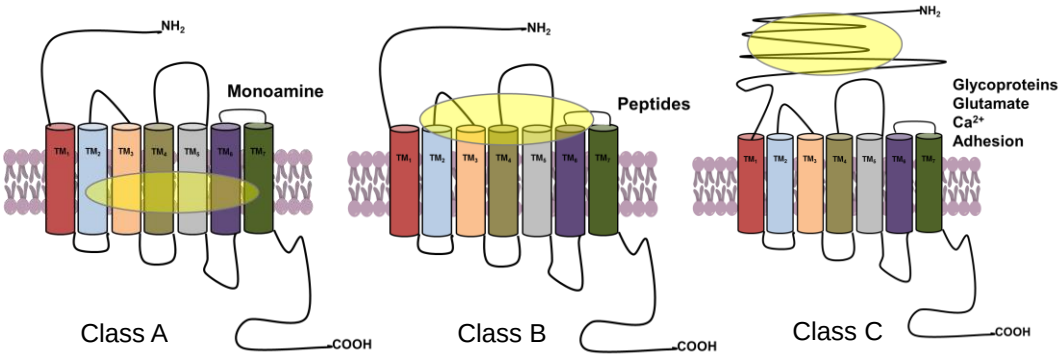

Figure 1-2| Schematic based on Kobilka's illustration of the agonist binding site location and the secondary structure for GPCR major classes[19]. Class A binding site is embedded in the transmembrane, Class B agonist binding site is located between the transmembrane protein and the *N*-terminus extracellular domain whereas Class C agonist binding site is located within the *N*-terminus extracellular domain.

Class B, the secretin (glucagon) receptor family, responds to peptide hormones and are primarily G_s-coupled[20]. Their structural features consist of an intermediate *N*-terminal region that also incorporates the ligand-binding domain[16-18].

Class C is the smallest class, and includes the metabotropic glutamate receptor/ calcium sensor family that responds to divalent cations and amino acids. They are the largest in size as their *N*-terminal region comprises of 950-1200 amino acid residues including the ligand-binding domain[16-18]. Class C GPCRs have a unique characteristic; they only exist as homodimers (mGlu and CaS receptors) or heterodimers (GABAB receptor and T1Rs)[21, 22].

Class D (fungal mating pheromone receptors) and E (cyclic AMP receptors) are not found in vertebrates[23].

Class F consists of 10 Frizzled (FZD) and Smoothened (SMO) proteins. The FZDs are activated by secreted cysteine-rich lipoglycoproteins termed Wnt. They are

involved in cell proliferation and polarity during metazoan development[24]. The SMO proteins are indirectly activated by the Hedgehog signalling proteins acting on the transmembrane protein Patched (PTCH) and are involved in embryogenesis and carcinogenesis[25].

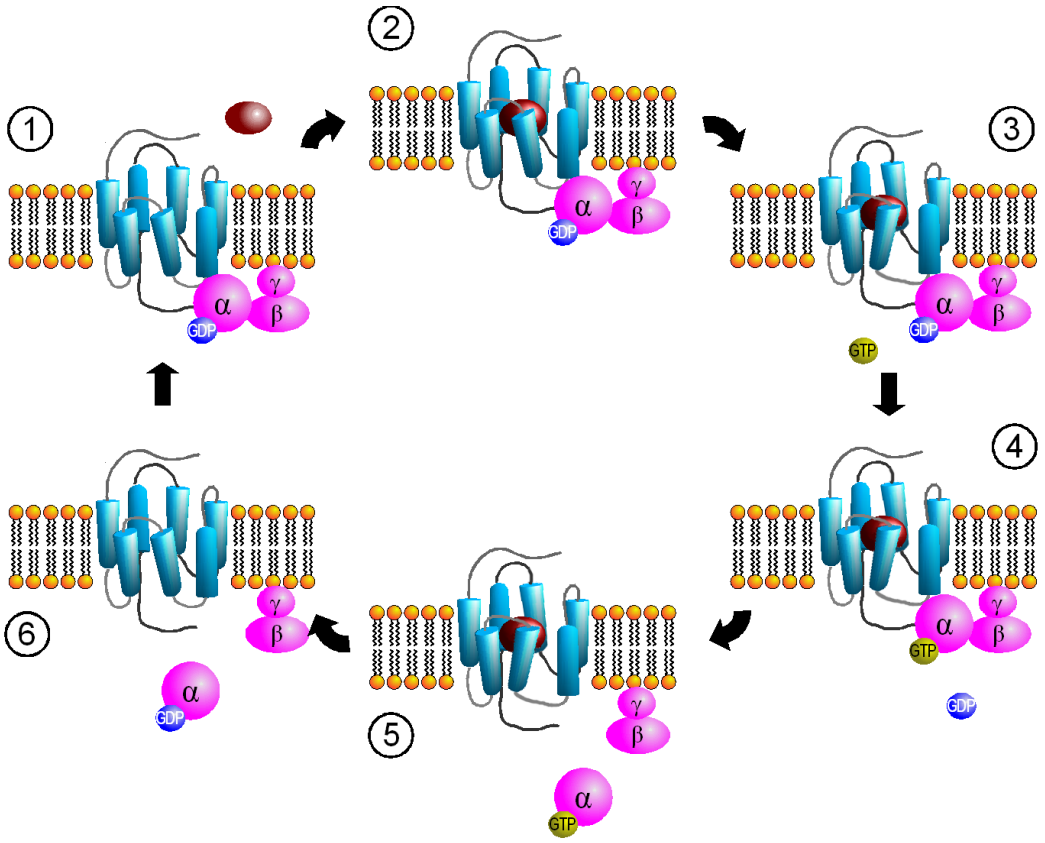

1. The GPCR in its inactive form is bound to the heterotrimeric G-protein. The G-protein α-subunit in this inactive complex is bound to guanine diphosphate (GDP).

2 - 3. The agonist binds to the receptor, which then undergoes a conformational change.

4. The activated receptor induces the replacement of GDP for guanine triphosphate (GTP) on the G-protein α-subunit.

5. GTP binding induces the G-protein α-subunit to dissociate from the βγ subunit

6. The G-protein α-subunit possesses intrinsic GTPase activity leading to the formation of GDP from GTP. The GDP-bound α-subunit can then re-associate with βγ subunit and return the GPCR to the inactive state.

Figure 1-3| Illustration of the G-protein activation cycle by G-protein-coupled receptors[10, 26]. **Source**: Hamm, Biol. Chem. 1998, 273, 669-672.

Binding of an agonist to the receptor leads to activation and dissociation of the G-protein, consequently activating a cascade of intracellular signals. After activation, the receptor engages a heterotrimeric G protein and catalyses release of GDP from the G protein α-subunit (Gα) as illustrated in Figure 1-3. Intracellular GTP then binds the nucleotide-free G protein, allowing it to regulate downstream effectors (adenylyl cyclase, phospholipase C, ion channels) which in turn elicit cellular responses[7]. In some cases, GPCRs are constitutively active in the absence of the agonist; it was first demonstrated in recombinant cell lines and in transgenic animal tissues due to mutation or overexpression of the receptor[27].

1.1 G-proteins

G-proteins are proteins with a specific ability to bind the nucleotides guanosine diphosphate (GDP) and guanosine triphosphate (GTP)[28]. There are two general classes of GTP-binding protein, the heterotrimeric and monomeric G-proteins. Heterotrimeric G-proteins are associated with GPCRs and are composed of three distinct subunits (α, β, and γ). In humans, there are 21 α, 6 β, and 12 γ subunits, allowing several trimeric G-protein permutations[29]. Regardless of the specific composition of the heterotrimeric G-protein, the α subunit binds to the guanine nucleotide, either GTP or GDP[30]. Agonist binding to the GPCR induces a conformational change that causes the exchange of GDP with GTP by the G-protein. GPCR activation leads to a structural and a biochemical cascade event that effects a target protein (illustrated in Figure 1-4)[31].

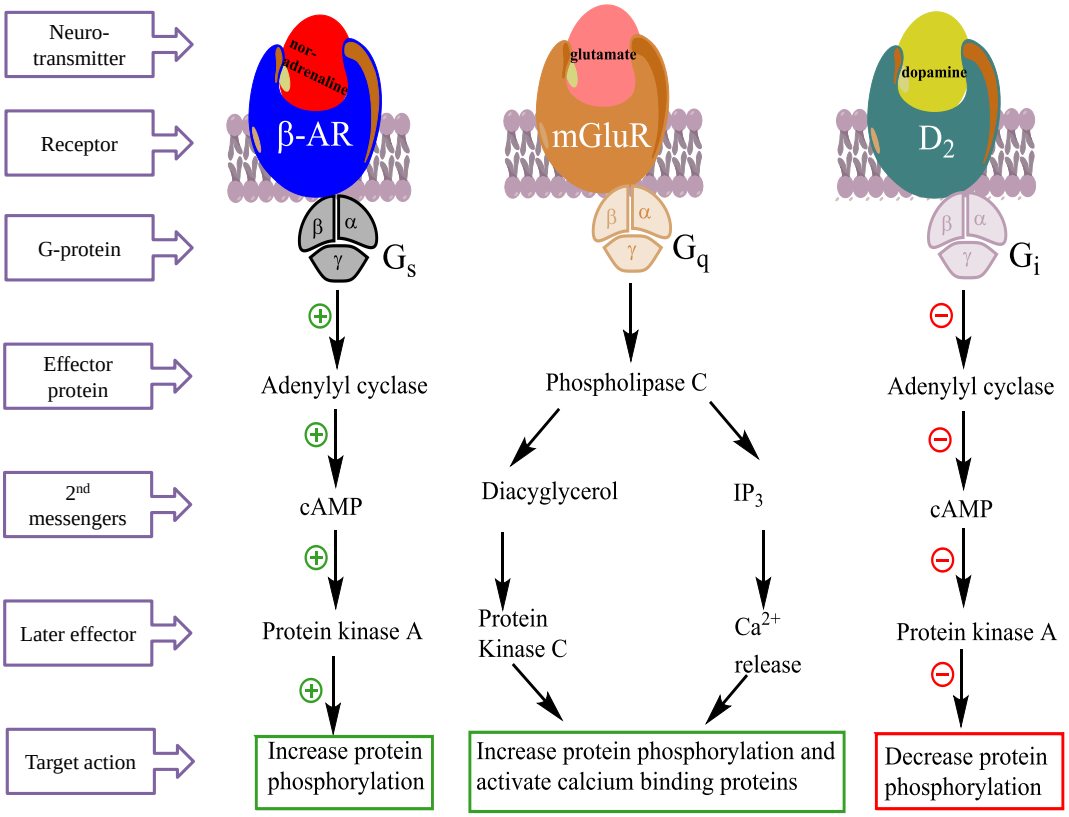

Figure 1-4 | Effector pathways associated with G-protein-coupled receptors and examples of three different types of heterotrimeric G-protein (G_s, G_q and G_i) illustrated from Neuroscience 5th edition, figure 7.6 [32]. The binding of a neurotransmitter to a receptor leads to activation of a G-protein and subsequent recruitment of second messenger pathways.

The monomeric G-proteins (small G-proteins or small GTPase) also relay signals from activated cell surface receptors to intracellular targets such as the cytoskeleton and the vesicle trafficking apparatus of the cell[33]. This family of proteins is homologous to the Ras GTPases and are also called the Ras superfamily of GTPases. Ras is a molecule that helps regulate cell differentiation and proliferation by relaying signals from receptor kinases to the nucleus. There are a large number of small G-proteins that have been identified and can be classified into five different subfamilies with different functions. For example, some are involved in vesicle

trafficking in the presynaptic terminal or elsewhere in the neuron, while others play a central role in protein and RNA trafficking into and out of the nucleus[34].

1.2 Studying GPCRs as A Drug Target

1.2.1 X-Ray Crystallography

Current insight into GPCR function and structure is primarily based on high-resolution X-ray crystal structures of the inactive and active state of the rhodopsin family[19, 35]. Indeed, X-ray crystallography is an important and powerful tool in drug discovery[36]. The detailed analysis of crystal structures of protein-ligand complexes allows the study of the specific interactions of a particular drug with its protein target at the atomic level. It is used for drug design and improvement[37]. The use of receptor chimeras and mutations produced by judicious amino acid deletions/replacements has greatly aided exploration of the functional domains of the human β-adrenoceptor[11, 38]. This work led to an important finding, which was that the location of the ligand-binding site was contained in the transmembrane-spanning regions[39].

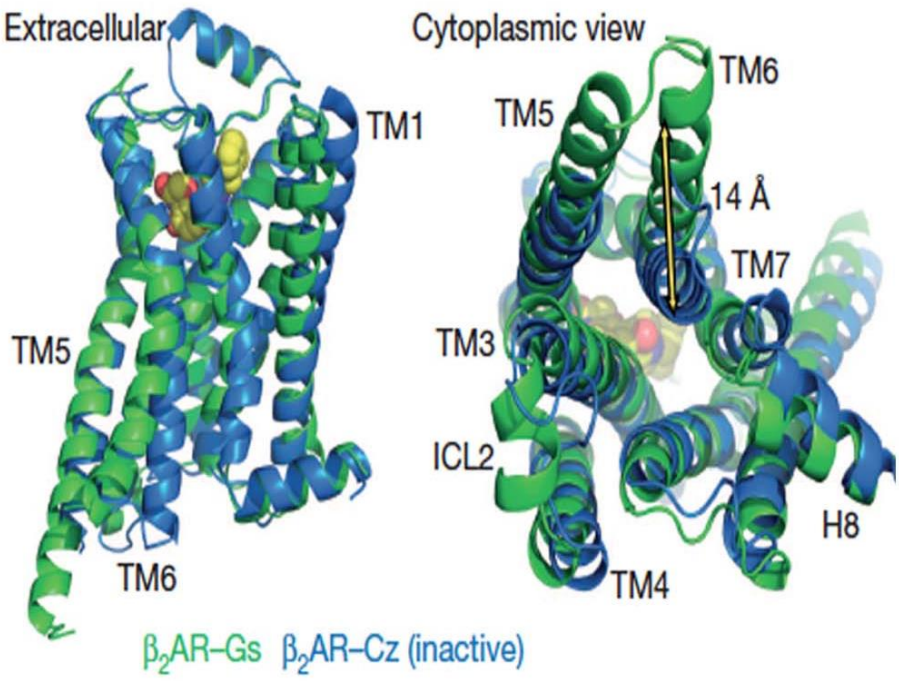

Figure 1-5| The illustration of active and inactive β_2AR crystal structures. The agonist was superimposed onto the structure of the human β_2 receptor which was crystallized in a lipid environment when bound to the inverse agonist carazolol (PDB: 2RH1). Side and cytoplasmic views of the β_2AR–Gs structure (green) compared to the inactive carazolol-bound β_2AR structure (blue). Important structural changes are observed in the intracellular domains of TM5 and TM6, where TM5 is stretched by two helical turns whereas TM6 is moved outward by 14Å as measured at the α-carbons of Glu 268 (yellow arrow) in the two structures[35]. **Source**: Rasmussen *et al*. Nature. 2007 Nov 15;450 (7168):383-7.

Palczewski *et al*. successfully solved the first high resolution mammalian GPCR crystal structure of bovine rhodopsin[40-42]. The introduction of high resolution crystal structure have provided further insight on ligand binding and GPCR confirmation changes that occurs during receptor activation[43]. Seven years later, Rasmussen *et al*. reported the crystallization of the human β_2- AR (illustrated in Figure 1-5)[44]. The high resolution β_2–AR crystal structure has confirmed the presence of essential binding site amino acid residues such as Asp[113], Ser[203] and [207], Asn[293] and [312] which

were elucidated *via* mutagenesis techniques[45]. The analysis of regions outside the native ligand binding pocket had allowed the identification of non-conserved residues; aiding with the design of sub-type selective ligands. GPCRs such as the k-opioids[46], dopamine, D_3[47, 48], muscarinic, M_2[49], histamine H_1[50] and many others [25, 51, 52] were determined as a result of prior knowledge of previously solved crystal structures. The reasons for GPCR crystallography success can be attributed to several innovative protein engineering techniques and crystallography methods such as engineering disulphide bridges or thermostabilization of GPCRs by systematic scanning mutagenesis[40]. Crude X-ray data are interpreted as a set of atomic coordinates, which are then fitted into a protein backbone. If resolution permits, a sequence is added and hence a model can be built. The preliminary model undergoes a series of computational refinement that can proof the model. Crystal structures are used as the basis for computational techniques such as molecular modelling[53].

1.2.2 Molecular Modelling

Molecular modelling is an assortment of techniques, often computational-based, that enables derivation, representation and manipulation of molecular structures and reactions in space[54]. Computational modelling methods are now used as standard tools by organic chemists for rationalising and predicting the structure and reactivity of organic, bio-organic and organometallic molecules[55].

In order to study GPCR as a drug target, scientists have taken different approaches in their quest for answers for drug design and discovery programs[56]. Some research groups have used homology models based on the rhodopsin crystal structure for

structure-activity studies of GPCR ligands; others focus on the site-directed mutagenesis approach (neoceptors are either modelled or re-engineering of known GPCRs biding sites)[57] based on the rhodopsin homology model[58, 59]. The homology modelling approach focuses on studying ligand properties and their effect on receptor structure and various applications detailed by Vyas and colleagues[60]. The neoceptor approach is used to tease out certain amino acid function in the binding site that are important for binding of both agonists and antagonists[61]. Structure-based drug design methods include virtual screening and *de novo* drug design techniques; these serve as an efficient tool when used alongside the high throughput screening (HTS) approach.

Detailed crystal structure and computational methods have enabled thorough investigation of the atomic and molecular interactions between the ligand and target receptor, aiding in the identification and optimization of new drugs. The use of molecular modelling in the study of GPCR as a drug target has proven to be quicker and more cost effective than HTS in cases where a lead molecule is discovered[62].

1.2.3 GPCR Pharmacology

Small molecule, peptide and protein ligands can induce a broad range of signalling responses at a GPCR as illustrated in Figure 1-6. An agonist can be classified as either full, partial or inverse. Full agonists bind and active the receptor by inducing the maximal G-protein signalling response, while partial agonists bind and activate the receptor by inducing submaximal signalling relative to the full agonist. An inverse agonist binds to the agonist binding site but produces negative efficacy,

which is characterised by a decrease in basal levels of signalling. An agonist is defined as a ligand that binds to a receptor and produces a response. Conversely, the ability of a ligand to bind to a receptor without inducing a response is antagonism only if it binds to the same site as the agonist[63]. Some ligands can act as agonists of one signalling pathway while acting as inverse agonists of an alternative pathway (biased agonists)[64, 65].

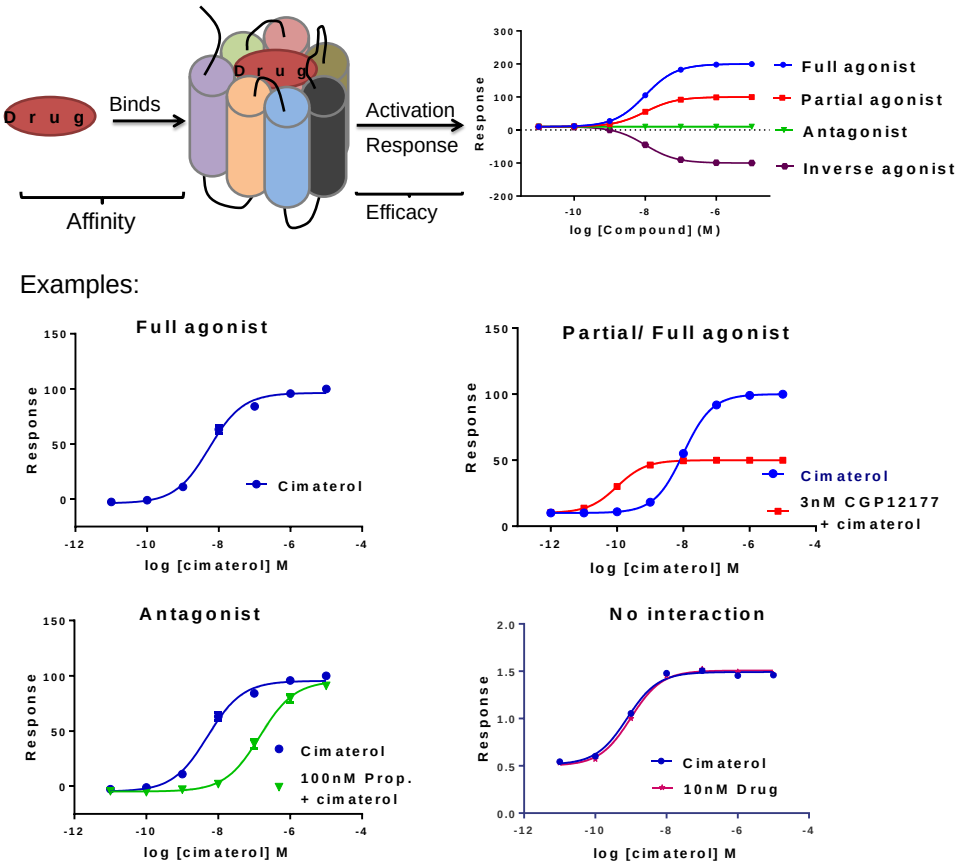

Figure 1-6| Schematic and experimental examples of ligand action on receptors: Affinity and Efficacy. The top panel illustrates the action of a drug on the receptor, which induces a response. The fact that a drug binds is a measure of affinity while efficacy is the ability of a drug to activate the receptor and induce a response that may vary from full agonism to partial agonism[66]. The bottom panel shows experimental examples of affinity and efficacy. Cimaterol is a classic example of a β_2-AR agonist whereas CGP12177 shows a partial agonist profile in the presence of cimaterol[67, 68]. For an antagonist profile, propranolol was used[69-71] and an unnamed drug showed no interaction with the receptor.

Ligands interact with their target at equilibrium in a reversible manner that involves various interactions such as electrostatic, hydrogen bonding and Van der Waals forces depending on both the target and the ligands involved. These binding interactions influence the overall ligand properties of affinity and, in the case of agonists, efficacy[66]. Affinity is the measure of how tightly a drug binds to a receptor. Mathematically, affinity is defined as $1/K_D$. The equilibrium dissociation constant (K_D) value represents the concentration of ligand required to occupy 50% of the available receptors.

Efficacy is the ability of a drug to bind and activate the receptor and induce a physiological response[72]. Efficacy is a concept and numerical term introduced by Stephenson to express the degree to which different agonists are able to activate receptors[73]. The scale of ligand efficacy ranges from 1 (full agonist) to -1 (full inverse agonist) and neutral antagonists are defined very precisely as possessing zero efficacy[65].

In order to study GPCR pharmacology, a wide range of assays has been developed. The assays discussed below are not exhaustive as there are numerous types of assays used in GPCR screening technology that includes calcium[74] and cAMP assays[75] and GTPγS binding assays[76]. Comprehensive reviews by Zhang and Thomsen *et al.* provides a detailed account of the GPCR screening tool box[74, 77].

1.2.3.1 Radioligand binding assay

A radioligand binding assay is used to characterize the interaction between a receptor and its ligands. This includes kinetics profile and the determination of receptor density in tissue or cells. There are three types of radioligand binding assay:

saturation, competition and kinetics assays. The saturation assay determines the maximal receptor occupancy of the ligand (B_{max}) and affinity, K_D. Competition binding assays are used to determine the IC_{50} of an unlabeled ligands by displacement of the radioligands. The IC_{50} is an empirical value, dependent upon the concentration and affinity of the radioligand used, therefore the Cheng Prusoff correction is used to derive K_i (concentration of competitor required to bind 50% receptor sites). Kinetic studies determine the direct measurement of association (K_{on}) and dissociation rates (K_{off}) of a radioactive and unlabeled ligands in equilibrium. Important drawbacks of this technique includes cost, and health and safety issues associated with disposal of waste materials. Additionally, some of the radioisotopes have short half-lives. These factors have driven the development of sensitive and robust non-radioactive alternatives[78].

1.2.3.2 Reporter gene assay

A reporter gene is a DNA sequence whose product is synthesized in response to activation of the signalling cascade under investigation. The DNA sequence has three integral parts, a promoter (which controls transcription), a reporter gene and a transcription stop signal. GPCR activation alters gene transcription *via* responsive elements for second messengers including the cAMP response element (CRE) located in the upstream region of a promoter, which in turn regulates the expression of selected reporter proteins[77].

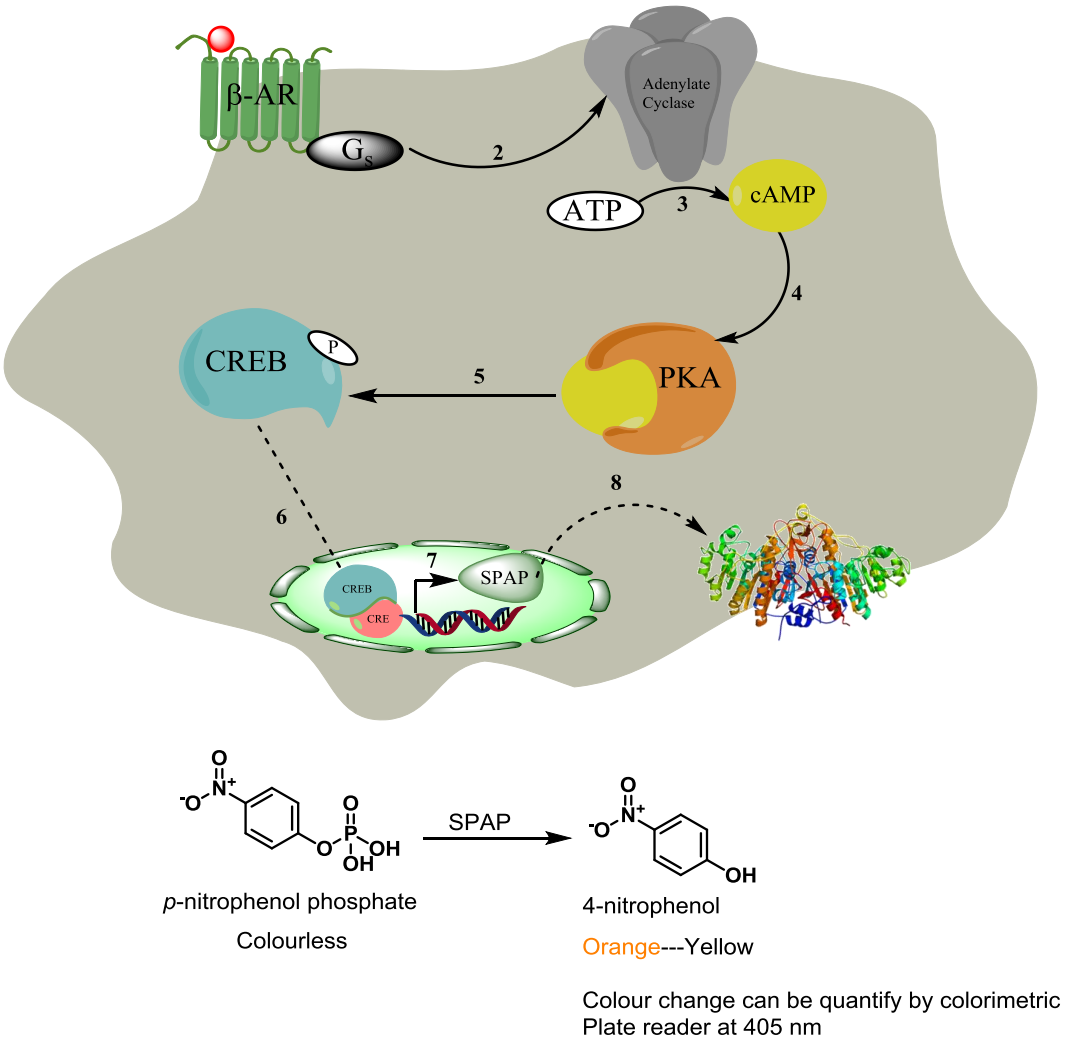

Figure 1-7| Secreted Placental Alkaline Phosphatase (SPAP) assay mechanism of action. (1) Agonist activates the β-AR-Gs complex, which stimulates adenylate cyclase (2) leading to the production of cAMP from ATP (3). cAMP then binds to protein kinase A (PKA) (4) which leads to the phosphorylation of cAMP response element binding protein (CREB) (5). The newly phosphorylated CREB binds to cAMP response element (CRE) (6) leading to the translation of secreted placental alkaline phosphatase (SPAP) (7), which is then secreted outside the cell (8). A colorimetric test is used to measure the level of SPAP produced. It relies on the colour change that arises when *p*-nitrophenol phosphate (PNPP) is dephosphorylated by the SPAP protein leading to the production of 4-nitrophenol, which is quantify by the colorimetric plate reader at 405nm[79].

The assay is used to accurately determine the affinity of antagonist and the efficacy and relative potencies of agonists at the GPCR. A reporter gene assay allows the

study of live cells by providing a cheap and safe alternative to radioligand binding assay. Despite the benefits, the assay requires long incubation periods which can lead to receptor desensitization. Another limitation involves significant signal amplification between ligand binding and subsequent transcription that causes false positives[80]. A false positive refers to a test result that indicates the presence of an entity when it actually not present. For example, in luciferase reporter-gene assays, it was reported that analogues of *N*-pyridin-2-ylbenzamide were competitive inhibitors of luciferase activity rather receptor antagonists. Luciferase activity is recorded as luminescent readout at 562 nm. The reported compounds quench the luciferase signal with an absorption peak around 550 nm, which leads to a false positive readouts.[81]

1.3 Adrenoceptors and The Sympathetic Nervous System

The sympathetic nervous system is a component of the peripheral nervous system, which controls smooth and cardiac muscles, organs and the adrenal medulla[82]. The fight or flight response is a classic example of a sympathetic nervous system-controlled response[18]. The hormones adrenaline and noradrenaline released from the adrenal medulla act on both central and peripheral adrenoceptors resulting in a range of physiological effects[69].

Adrenoceptors belong to the GPCR family. There are two sub-families of adrenoceptors; α and β as classified by their pharmacology. Within the alpha adrenoceptors (αAR), there are two main subtypes (α_1 and α_2) and each of these is

divided into three further subtypes[83, 84]. In general, activation of α_1-AR leads to vasoconstriction, salivary secretion, relaxation of gastrointestinal smooth muscle and hepatic glycogenolysis[85]. Activation of α_2-AR results in the inhibition of neurotransmitter release (including noradrenaline **(1)** and acetylcholine release from autonomic nerves), platelet aggregation, smooth muscle vasoconstriction and inhibition of insulin release[84].

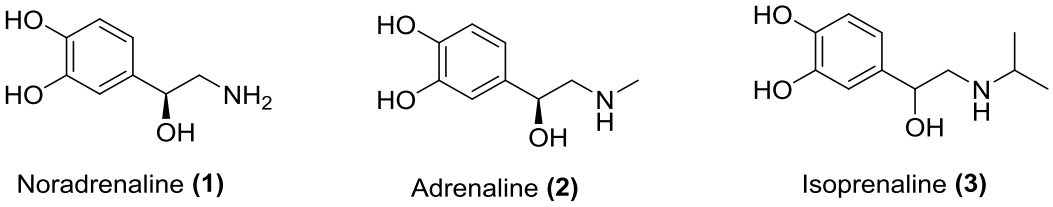

Figure 1-8| Endogenous catecholamine: noradrenaline (1) and adrenaline (2) and the synthetic non-selective β-adrenoceptor selective agonist isoprenaline (3).

The focus of this project is the beta-adrenoceptors; therefore the remainder of the introduction will be devoted to this receptor.

1.3.1 Beta-adrenoceptors

β-adrenoceptors belong to the super family of G-protein coupled receptors and remain an important drug discovery target for the treatment of cardiovascular diseases. The existence of three distinct human genes, which encode for β-adrenoceptor subtypes, β_1, β_2 and β_3 have been proven by molecular biology techniques [3]. Both α and β- adrenoceptors are expressed in smooth muscle cells, nerve terminals and endothelial cells[86].

β_1 adrenoceptors (β_1AR) are mainly found in the heart where they regulate the positive ionotropic and chronotropic effects of catecholamines (Figure 1-8), The β_2 adrenoceptor (β_2AR) is expressed in vascular smooth muscle, lymphocytes, endothelial cells, pulmonary and cardiac myocyte tissue[86], and performs a pivotal role in smooth muscle relaxation in humans[87].

The β_3 adrenoceptor (β_3AR) is predominantly expressed in adipose tissue and is involved in thermogenesis in brown adipose tissue[5] and in mediating lipolysis in white adipose tissue[88]. Stimulation of β_3AR is responsible for a variety of pharmacological effects such as enhancement of energy expenditure[89], increase in fat oxidation and improvement of glucose absorption in the gut of rodent models of obesity and diabetes[90].

β-Adrenoceptors are broadly distributed in various tissues of the body hence their involvement in many pathologies[91].

1.3.2 Therapeutic Indications for β_1 and β_2-adrenoceptors

For decades, β-blockers have been widely used in hypertension treatments and more recently, investigated potentially as effective agents in cancer therapy through blockade of adrenoceptors in tumour tissues[92]. β_2-agonists are bronchodilators that have been used for the management of asthma and chronic obstructive pulmonary disease (COPD)[93]. The availability of crystal structure analyses of membranes has revolutionised drug discovery programs[37, 64]. It allows deep understanding on the active topology of the receptor and the nature of ligand-receptor interactions[94].

Figure 1-9 sections B and D show amino acid residues within both β_1 and β_2 adrenoceptor binding sites that are involved in making important interactions with ligands. The following interactions were observed in β_2 AR: Ser^{207} was found to H-bond to the phenolic hydroxyl, while Ser^{204} and Ser^{203} were found to interact with the primary benzylic hydroxyl. A potential H-bonding interaction was identified between Asn^{293} and the asymmetric benzylic hydroxyl, while Asp^{113} and the amine were in proximity, allowing for a strong charge interaction. The middle ether oxygen in the chain was observed to be positioned within H-bonding range of Asn^{318} (TM7) while the benzylic ether oxygen was ideally situated to form H-bonds to both Ser^{120} (TM3) and Asn^{322} (TM7)[95].

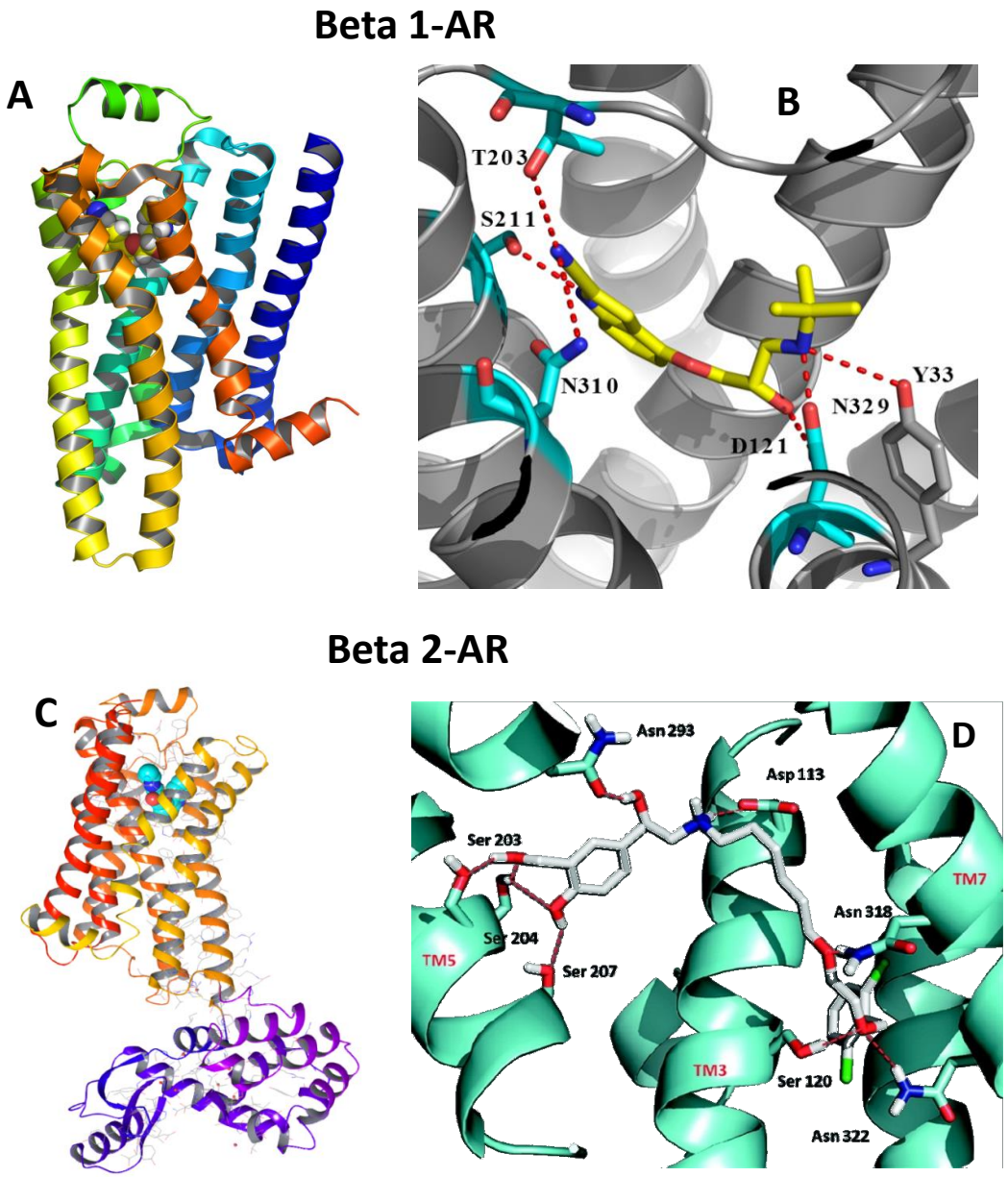

Figure 1-9| (A)[45] & (C)[95] The structures of ligand bound β_1 & β_2 ARs respectively (B) Ligand binding pocket of the mutated turkey β_1-AR co-crystalysed with cyanopindolol (yellow) by polar interactions (aquamarine) or non-polar interactions (grey)[45] (D) Agonist interaction with amino acid residues at the human β_2 AR binding pocket[95]. The agonist was superimposed onto the structure of the human β_2 receptor which was crystallized in a lipid environment when bound to the inverse agonist carazolol. **Source**: Warne *et al*. Nature 429, 241–244 and Procopiou *et al*. *J. Med. Chem.* 2010, 53, 4522-4530 (PDB: 4BVN and 2RH1).

A. β-blockers

The Nobel Prize winner Sir James Black pioneered the development of the first β-blockers, which to-date remain one of the most successfully prescribed drug classes[96]. The clinical application of β-blockers has significantly surpassed the boundaries of their original conception; which was to treat coronary heart diseases such as cardiac arrhythmias and angina[97]. Now they are routinely used in the treatment of anxiety[98], migraine[99], glaucoma[100] and cardiac failure[101]. In angina, the coronary arteries are partially congested by atherosclerosis, leading to reduction in blood flow to cardiac muscle. During periods of physical activity or stress there is an increase in the force of contraction and heart rate, and in the normal heart the coronary artery blood flow is increased as necessary[102]. However, in the case of angina, insufficient blood flow leads to myocardial ischaemia (lack of oxygen supply) resulting to overwhelming chest pain, which is a characteristic of angina pectoris[103].

Recent research has speculated that these drugs may also be of use in diseases such as cancer[104], osteoporosis[105] and malaria[106]. Beta-blockers act at both β_1 and β_2-adrenoceptor to varying degrees. This explains the observation that β_2-adrenoceptors inhibition can cause bronchoconstriction (bronchospasm) even when selective β_1-adrenoceptor blockers are used; therefore asthmatic and patients with COPD have to be cautious while on β-blockers. The therapy can also cause impotence and cold extremities[106, 107]. The exact mechanism of action of the β-blockers in hypertension is somewhat uncertain; the drug might decrease cardiac output *via* inhibition of β_1-adrenoceptors, or might inhibit the action of β-

adrenoceptors on renal juxtaglomerular cells[108]. For coronary heart diseases such as angina, beta-blockers reduce cardiac output and rate, which in turn improves coronary blood flow and chest pain[109].

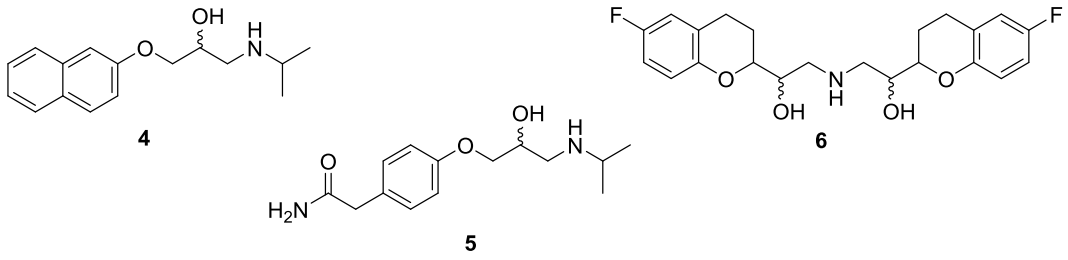

Figure 1-10| The three generations of beta blockers: (4) Propranolol, (5) Atenolol and (6) Nebivolol.

Sir James Black developed Propranolol (**4**), a first generation, non-selective beta-blocker while working for Imperial Chemical Industries. This drug has revolutionized medical practice worldwide and remains in clinical use today for the treatment of arrhythmias, anxiety, ischaemic heart disease (IHD), essential tremor, hypertension, thyrotoxicosis, migraine and portal hypertension[96, 110].

Atenolol (**5**) is a second-generation beta-blocker that is used to treat migraine, hypertension, IHD and arrhythmias. It is a β_1AR antagonist, which is selective (-6.66±0.05 and -5.99±0.14) but non-specific. Atenolol lacks intrinsic sympathomimetic activity with a superior efficacy on cardiac than vascular or bronchial adrenoreceptors, leading to decrease in blood pressure primarily by reducing heart rate and cardiac contractility. This implies that it might act to some extent on β_2-adrenoceptors[111], indeed numerous reports have shown that atenolol

therapy leads to non-specific expiratory reductions and airway resistance increases in COPD patients[112].

Nebivolol (**6**) is a third-generation selective beta-blocker that is clinically used for the treatment of hypertension and heart failure[113]. Nebivolol is a cardioselective beta-blocker that has been reported to be potent and well tolerated in patients with hypertension. Clinical data suggests a mortality rate reduction in patients with heart failure[114].

B. β_2-adrenoceptors agonists

β_2-adrenoceptors are mainly located in bronchial and vascular smooth muscles, which makes them an excellent target in the treatment of pulmonary disorders such as COPD or asthma. Asthma is due to inflammation of the bronchi. It causes narrowing of the bronchi, which leads to mucus production[82]. The condition is manageable but incurable therefore inhalers and other forms of medications are used to relieve and prevent symptoms[115]. Inhaled β_2-agonists have been an essential part of asthma management for decades and work by interacting with β_2-adrenoceptors on bronchial at the epithelial cells to induce bronchodilatation through muscle relaxation. Currently, there are three types of inhaled β_2AR agonist which are clinically available: short and ultra- long acting[116].

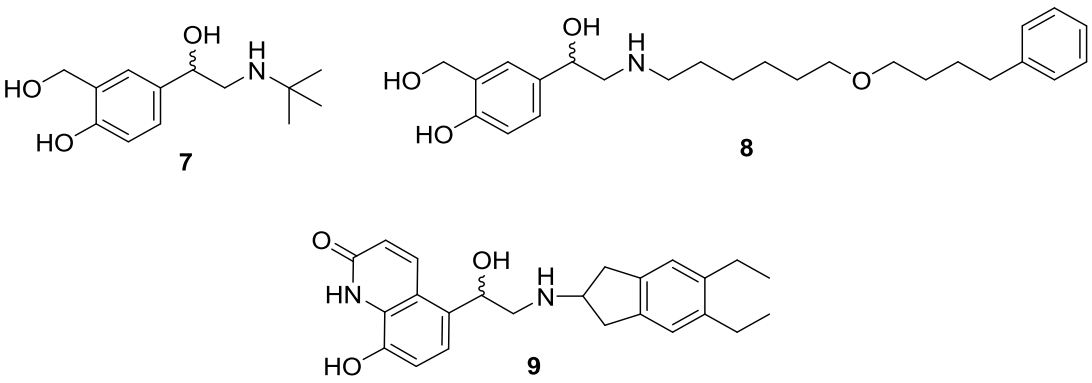

Figure 1-11| The three generations of beta agonists: (**7**) Salbutamol (**8**) Salmeterol and (**9**) Indacaterol.

Short-acting β_2-adrenoceptor agonists (SABAs) are the first generation β_2AR agonist, which have been accessible for about 40 years, and have a fast response and duration of action of about 4 h. They are primarily used effectively and safely in COPD and asthmatic for relief of bronchoconstriction symptoms.

The introduction of the second generation β_2AR agonists, the long-acting β_2-adrenoceptor agonists (LABAs) such as salmeterol were designed specifically for consistent use, as their therapeutic window varies within 16h. In essence, they control symptoms as they are used for preventing future symptoms and attacks from physical activity. Ultra-long acting specific agonists (uLABAs) are the third generation of β_2-AR agonist[117]. They are fast-acting and very efficacious with full agonism on-set action with 24h bronchodilation duration[118].

Current assay technologies are falling short in GPCR drug discovery because GPCRs are studied in transfected or mutated cells, where they are in a modified environment[2, 119]. Development of novel approaches, which offers the screening of

both fragment-like and drug molecules at GPCRs in a whole cell assays would be an important step to the drug discovery process[6].

1.4 The Use of Fluorescent Ligands in GPCR Screening

In their native environment, GPCRs are highly organized in membrane domains with signalling proteins involved in complex signal trafficking between intracellular membrane compartments[120]. This complexity of GPCR pharmacology has led to a desire to further the study of receptor-ligand interaction and details of ligand affinity and efficacy[121].

Increasing knowledge on GPCR pharmacology such as receptor trafficking, oligomerization[122, 123] and biased signaling[124] implies that there is a need to further characterize GPCRs. Non-fluorescent assays previously discussed show limitations. They cannot probe GPCRs at single cell and single molecule, enabling receptor localisation, visualisation and quantification. These limitations can be resolved with the utilisation of fluorescent techniques[125].

1.4.1 Fluorescence

Fluorescence is a cyclic three stage process which consists of: (1) fluorophore excitation due to light energy absorption, (2) a transient excited lifetime with minimal energy loss and (3) the fluorophore returns to its ground state, causing light emission (

Figure **1-12**).

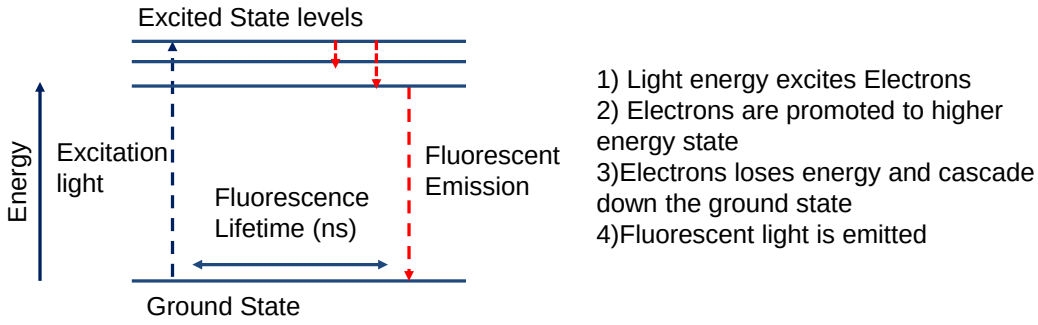

Figure 1-12| The fluorescence principal as shown by the Jablonski energy diagram[126].

The emitted light energy has a longer wavelength compared to the absorbed light energy, due to the energy lost throughout the transient excited lifetime. Therefore emitted and absorbed light are detectable as different areas or colors on the visible spectrum. The fluorophore can undergo photobleaching, which occurs throughout the excited lifetime stage, due to structural degradation of the fluorophore. High-intensity light energy can lead to structural change of the fluorophore and it therefore loses its ability to fluoresce[126].

Fluorescence-based techniques have been around for decades however their use was limited to histological stains[127]. Attempts have been made to couple fluorophores to drugs in the hope of identifying their binding sites. The experimental aim was to synthesise a high affinity fluorescent probe that will remain bound to the target receptor after the washing step. Early examples of fluorescent ligands include histamine, neurotensin and various opioids, as well as ligands for nicotinic receptors and α and β-adrenoceptors[128]. Because of the hydrophobic nature of the fluorophores

utilized in the synthesis of the fluorescent probes above, background fluorescence was interfering with microscopic studies. To overcome this limitation, previously synthesised fluorescent probes photophysical properties required improvement[129].

Fluorescent ligands are efficient biological tracers used for the detection of target location and activation, and to trace biological processes *in vivo*[130]. They offer the possibility of analysis of GPCR pharmacology at the level of the single molecule and single cell[131]. For example, the use of fluorescent ligands to monitor the kinetics of ligand binding to GPCRs at real time in live cells without the washing step (separation of bound and unbound ligands) is a key advantage that radioligands cannot offer[132]. Additionally, fluorescence correlation spectroscopy (FCS) studies with fluorescent probes for adenosine receptor has enabled insights into GPCR membrane organization[133]. Receptor location can be revealed by the fluorescent ligands bound to them, reversible ligands can provide pharmacological details such as binding affinity and their molecular interaction[134].

1.4.2 Fluorescent Techniques: Advantages and Disadvantages

Fluorescent techniques provide a broader spectrum of additional details in pharmacological investigations, such as receptor localisation, which was not available with traditional techniques such as radioligand binding assays. It is ideal for the characterisation and quantification of particular ligand-receptor interactions in single living cells and at the single molecule level[2, 119]. Also fluorescent ligands offer benefits compared to radioligands in competitive binding assays, eliminating the health and safety issues and disposal cost associated with radioactivity[74]. The

use of fluorescent techniques presents many advantages over the radioligand assay such as:

- Increased sensitivity and safety[135]
- No disposal costs required compared to the radioligand which requires scintillation disposal costs[136]
- Greater spatial resolution compared to autoradiography[136, 137]
- Experiments can be performed in a live assay with small tissue samples or single cells (miniaturization)[125, 133]
- Results can be obtained immediately[137, 138]
- Fluorophores can be tailored to experimental requirements; eg. for imaging studies, receptor co-localisation is enabled by the utulisation of covalently bonded cells with a fluorescent protein such as SNAP-tag[139]
- Provides visual confirmation for receptor localization and binding[140]
- Stable signal from the fluorophore[128]

The fluorescence technique has opened up a range of possibilities for pharmacologists, but there are disadvantages associated with the technique:

- The fluorophore, which is usually a large molecule, increase the overall molecular size of the ligand, hence altering the chemical properties which, in turn can alter the potency and affinity of the compound of interest
- Tissue auto-fluorescence and bleaching can increase background fluorescence
- Sensitive detectors are required for low fluorescent ligand concentrations [141]

1.4.3 Existing Fluorescent-based Assays

Perkin Elmer and Molecular Probes have pioneered fluorescent techniques. Originally, chelating lanthanides were used that had intense and long lasting emission, allowing the quantification of fluorescence intensity to be recorded after excitation[142]. There are a wide range of fluorescence techniques that have been used for the study of GPCRs. The current toolbox utilizes fluorescent techniques, which includes fluorescent activated cell sorting (FACS)[143, 144], fluorescent correlation spectroscopy (FCS)[145-147], fluorescent resonance energy transfer (FRET)[125] and total internal reflection fluorescence microscopy (TIRFM)[148]. Several comprehensive reviews have been published by Stoddart *et al*.[125, 137], Zhang *et al.* [77] and many others have highlighted the advantages and disadvantages of fluorescent-based assay[132, 136]. This report would focus on the techniques relevant to this project.

1.4.3.1 Bioluminescence Resonance Energy Transfer (BRET)

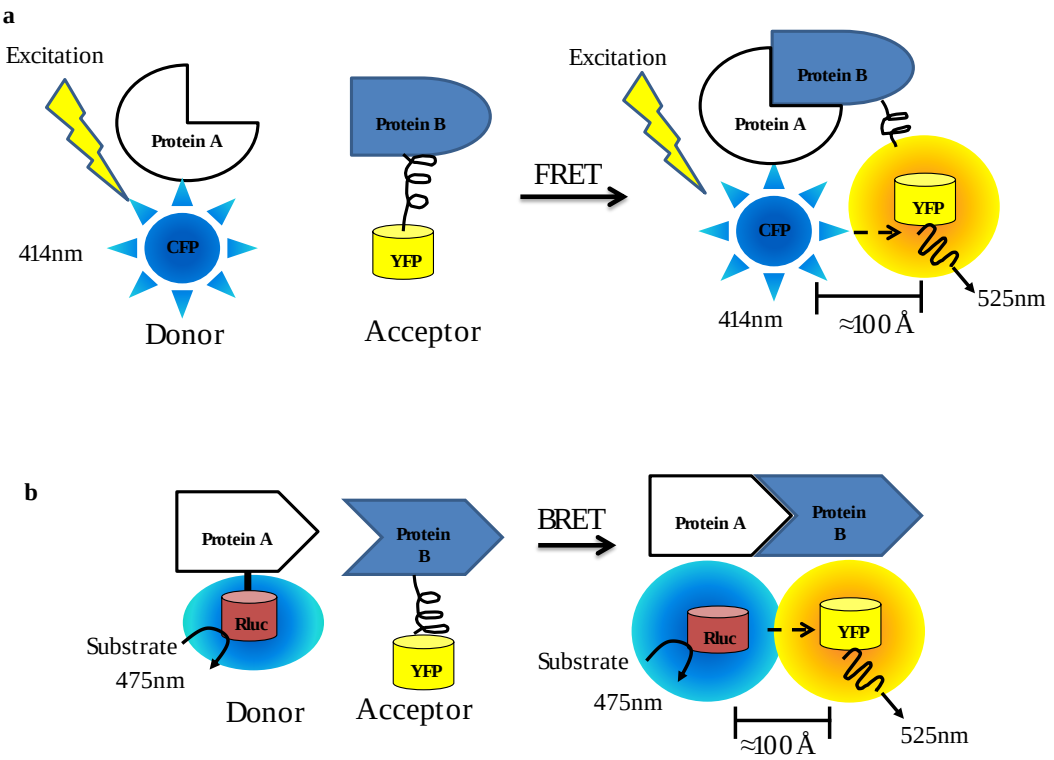

Figure 1-13| Schematic representation of resonance energy transfer between donor and acceptor in either FRET or BRET. a) The top panel illustrates the FRET assay where cyan fluorescent protein (CFP) is the donor and yellow fluorescent protein (YFP) is the acceptor. Upon donor excitation with an external energy source (given the proteins are in close proximity), energy is transfer occurs. b) The bottom panel illustrates the BRET assay where Renilla luciferase enzyme (Rluc) is the donor and the YFP is the acceptor. Addition of Rluc substrate produces bioluminescent light that excites the YFP. Given that both receptors are in close proximity, BRET occurs[125].

BRET quantifies the binding interaction between a fluorescent ligand (as an acceptor) and the receptor of interest, which itself is fused to a bioluminescent donor. On binding of the fluorophore to the receptor, the bioluminescent donor; (usually a luciferase) excites the fluorophore by resonance non-radioactive energy transfer through dipole-dipole coupling. Bioluminescence technology provides a reproducible, sensitive, reliable and easy to use tool for the study of protein-protein

interaction or ligand-receptor interaction[149]. Recently, Hall *et al.* have engineered a small luciferase, NanoLuc (Nluc), which has allowed further study of GPCR by providing high sensitivity and adaptability to existing BRET methodologies[150]. NanoLuc is a 19.1 kDa, ATP-independent luciferase that utilizes a novel coelenterazine analogue (furimazine) to produce high intensity, glow-type luminescence as illustrated in Figure 1-13. The bioluminescent protein displays excellent physiochemical properties; it is stable under a range of pH, temperature and urea fluctuations[151]. Stoddart *et al.* used the NanoBRET™ approach to investigate ligand-protein interaction in live cells. The development of the NanoBRET™ assay has enabled the interrogation of GPCR in recombinant cells in real time using various receptors and fluorophore types[71].

1.4.3.2 Laser Scanning Confocal Microscopy (LSM)

Confocal microscopy represents an important tool for the characterization of fluorescent ligands. One of the pre-requisites of a good fluorescent probe is selective binding to the receptor of choice (with minimum cytosolic uptake), which can be displaced by an unlabeled ligand[135]. It allows the study of the cellular and tissue localization of the receptor with high resolution. Confocal systems enable study of cell function and structure using live-cell imaging in cell cultures and organisms such as bacteria at speeds and durations not previously possible[152]. There are examples of live cell imaging in our laboratory, where a range of GPCRs have been characterised. LSM allows the presentation of cellular images in 3D without

compromising the cells by fixing them. It provides a platform for receptor visualization and quantification at the single cell level[153].

1.4.4 Current Fluorescent Ligands

Fluorescent ligands are an exciting alternative to radioligands. They represent a powerful and diverse toolbox for the study of GPCRs since their varied applications can interrogate the receptor in live single cells in their native environment, providing valuable information regarding receptor-ligand pharmacology. Several comprehensive reviews by Lochner[154], Vernall[155] and Sridharan[136] *et al*. reviewed fluorescent ligands currently used for the study of GPCR class A receptor have been published; they cover fluorescent probes design and applications in both live and recombinants cells. In this section a review of current, small molecule-based fluorescent conjugates that have been designed for the study of GPCR class A receptor, with a focus on the adenosine receptor and adrenoceptor is discussed.

Adenosine receptors are by far the receptors with the most fluorescent ligands, synthesised predominantly for A_1 and A_3-ARs.

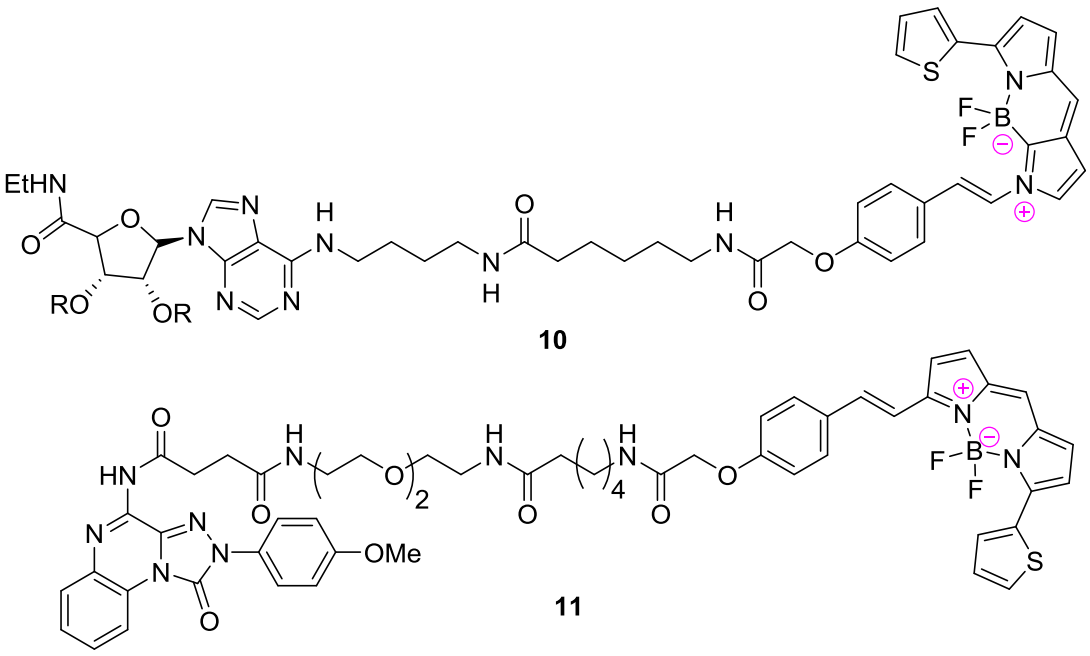

Figure 1-14| Structure of fluorescent labelled adenosine AR ligands[156, 157].

The reported probes are either agonists or antagonists which benefit from a range of ligands and fluorophores. Currently A_1 and A_3-ARs fluorescent ligands are confidently used as a suitable alternative for whole cell binding assay for screening purposes. Briddon *et al.* have described the used of A_1-AR antagonist fluorescent probe (**13**) in imaging and FCS studies[156]. Membrane localisation was enabled *via* laser scanning confocal microscopy while FCS was used to quantify ligand−receptor interactions in microdomains of single living cells [157]. Baker *et al.* have investigated the influence of fluorophore and linker composition on the pharmacology of fluorescent adenosine A_1 receptor ligands. NECA (**18**) derivatives were synthesised and characterised *via* confocal microscopy, radioligand and reporter gene assay. The investigation have shown that the linker length can affect the fluorescent probe binding affinity and the ligand efficacy[131]. Compound **10**, which was linked with a

short aliphatic linker (C3) displayed the highest affinity at A_1-AR compared to its parent ligand NECA[131].

Within the same group, Vernall *et al.* were able to synthesize a highly potent and selective fluorescent antagonist of the human A_3-AR based on the quinoxan-1-one scaffold. The lead probe (**11**) showed enhanced affinity while maintaining excellent selectivity toward A_3-AR compared to the endogenous ligand. Given its affinity and selectivity profile, the quinoxan-1-one based compound was used as a tool for live cell assays and imaging studies[119]. Further work in the same group by Vernall and colleagues on peptide-modified fluorescent adenosine receptor (AR) ligands have shown that the peptide linker contributed in enhancing the ligand binding affinity compared to the parent ligand (xanthine amine congener) illustrated in Figure 1-15. Compound **14** showed clear improvement on the membrane binding, which was displaced by unlabeled ligands as demonstrated with a laser scanning microscopy technique[158].

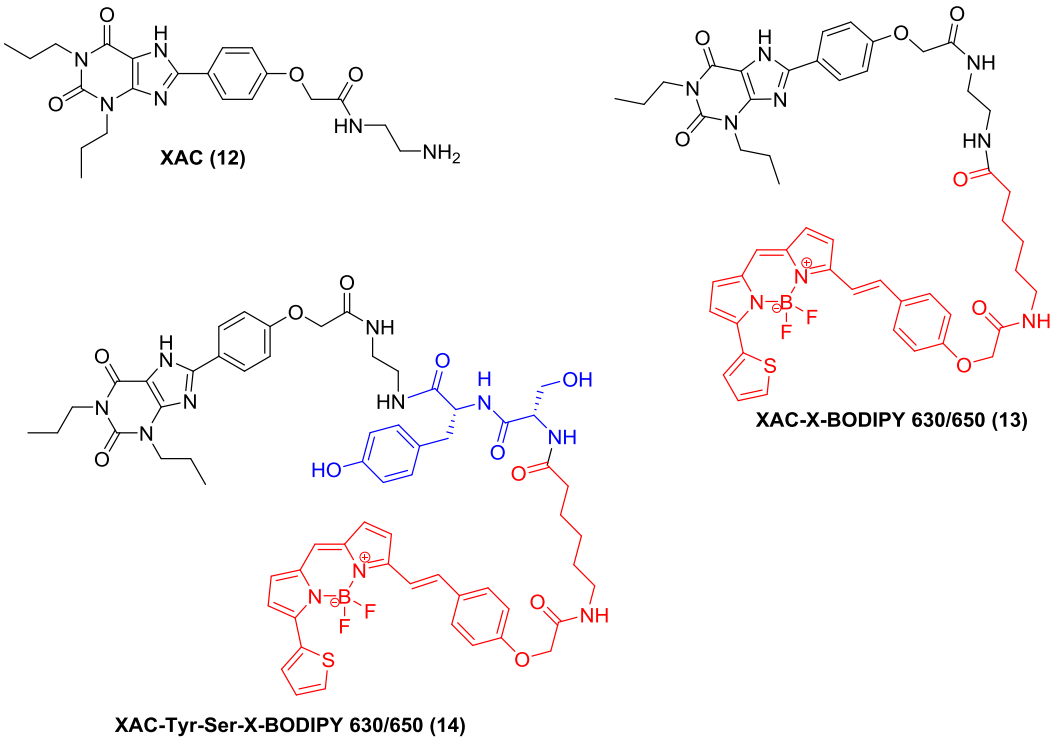

	hA_1 pK_i	hA_2 pK_i	A_3/A_1
XAC	7.30	7.80	3.1
XAC-X-BY630/650	8.03	7.51	0.3
XAC-Tyr-Ser-X-BY630/650	7.62	9.12	31.6

Figure 1-15| Binding affinity of XAC-derived compounds at human A_1AR and A_3AR[158].

The adrenoceptor receptor benefits from a range of commercially available fluorescent probes especially developed for the study of this receptor. Their pharmacological profile range from agonists to antagonists. These agonist or antagonist fluorescent ligands have been synthesised with different linker and fluorophore make up, which makes them diverse as a tool for adrenoceptor pharmacology studies.

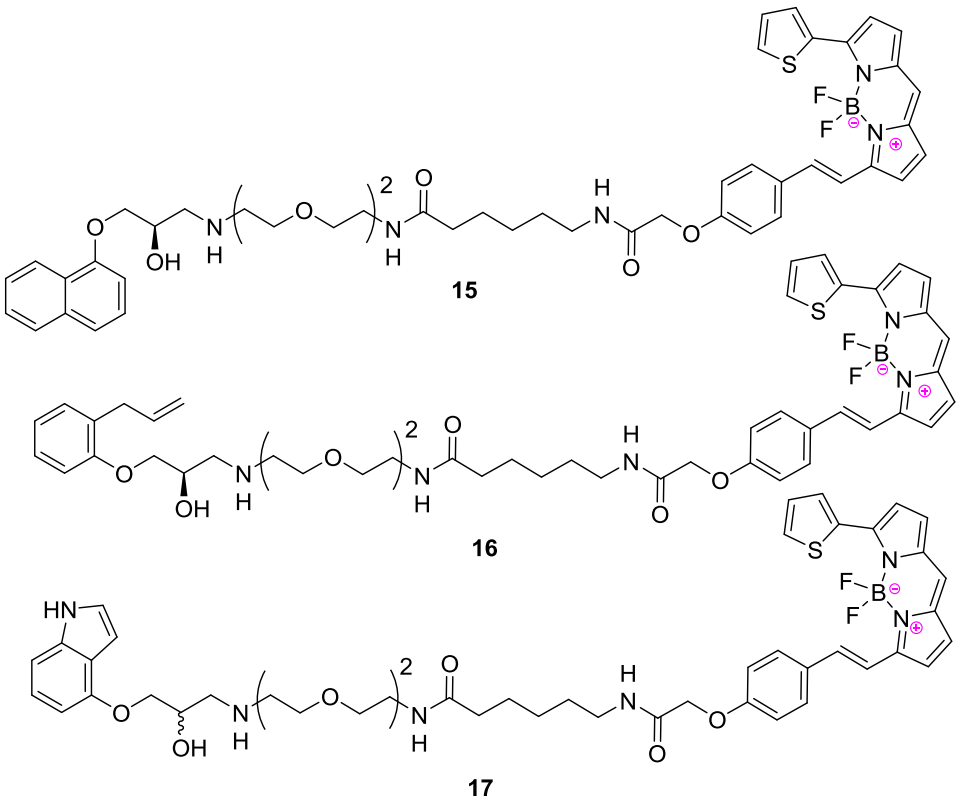

Figure 1-16 | Structure of fluorescent labelled β_2-AR ligands[2].

A series of red-shifted fluorescent β-adrenoceptor ligands were synthesised based on β-blockers propranolol (**4**), alprenolol and pindolol. Eight propranolol derivatives with various linker lengths from C2 to polyethylene glycol (PEG) both racemic and enantiomerically pure (S) were synthesised and characterised at the β_1, β_2 and β_3-ARs[2]. This study confirmed the hypothesis supported by Daly[134, 159], Jacobson[153] and many others[128, 160] that states that minor changes in the linker chemistry can affect the overall pharmacology of the final conjugate[159]. Additionally, these results supported the effect of linker size on probe pharmacology as seen in adenosine ligands by Middleton[157].

The best in this series in terms of affinity at both β_1 and β_3-ARs was a red emitting compound **15**, which displayed a antagonist profile, as does its parent compound, propranolol [β_1-AR (Log K_D = -8.22) and β_2-AR (Log K_D = -9.21)]. It was 28-fold more potent at the β_2-AR (Log K_D = -9.22) compared to β_1-AR (Log K_D = -7.76) with affinity for the β_2-AR that mirror propranolol affinity. It was further used for confocal imaging in CHO cells stably expressing the human β_2-AR. Compound **15** showed specific membrane binding at 3 nM, which was displaceable by unlabelled β_2- selective antagonist ICI 118551. This compound is still used as a reference for various assays in our laboratories.

Alprenolol-based fluorescent ligand had modest affinity for the β-AR compared to propranolol-based ligands. There were four synthesised ligands with different linker composition (C2 and PEG-8: S enantiomer and racemate). The C2-linked compounds data displayed non-selectivity for either β_1- or β_2-AR with 10-fold less affinity when compared to alprenolol [β_1-AR (Log K_D = -7.95) and β_2-AR (Log K_D = -9.30)]. PEG-8-linked compound **16** within the alprenolol-based probes was comparable to the parent ligand, alprenolol. In contrast, pindolol-based ligand (**17**) was 10-fold less potent at the β-AR compared to its parent molecule pindolol [β_1-AR (Log K_d = -8.58) and β_2-AR (Log K_d = -9.27)]. Pindolol-based ligands were the least potent in the series of fluorescent probes and therefore was not characterised further with microscopic studies.

1.5 Fluorescent Ligand Design

A fluorescent ligand consists of three distinct parts: the ligand, the fluorophore and the linker region, which connects both previous components. In order to develop successful fluorescent probes; the ligand, fluorophore and linker have to be carefully considered and tailored to meet the project objectives, which is to investigate GPCRs pharmacology in recombinant cells and later on in their native environment. Fluorescent ligands must have certain key characteristics in order to be suitable for live cell screening[2, 106, 161]

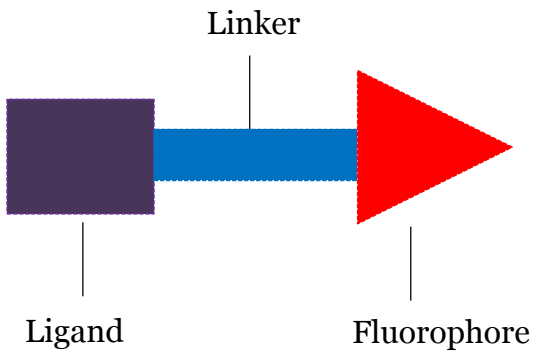

Scheme 1-1| Fluorescent ligand components.

Designing GPCR fluorescent ligands requires careful consideration of key factors such as photophysical, pharmacological, and physicochemical properties. These include selectivity and structure activity relationship (SAR) studies between the ligand and the target receptor, the length and chemical composition of the linker between the pharmacophore and fluorophore; the chemical composition and photo-physical properties of the pharmacophore and fluorophore[121, 139, 157].

It is critical to carefully choose a ligand, which is ideally endorsed by SAR studies that suggest the optimal position for the linker/fluorophore combination. The molecular weight of commercial fluorophores varies within a range of 400-1,000 Da, therefore they can considerably increase the final size of the molecular probe, which in turn may alter the pharmacological properties of the final conjugate. It is also important to choose the linkage point carefully with respect to efficacy and binding affinity[160].

The choice of the fluorophore is primarily determined by its photo-physical properties such as fluorescence lifetime, quantum yield, and excitation and emission spectrum for the assay of choice. The optical set up and the light sources have an influence on the optimal excitation-emission combination. For live cell assays, the choice of excitation wavelength is crucial as photo-bleaching might occur when imaging[162]. The fluorophore can also be quenched in an aqueous environment, can be beneficial in discriminating between membrane bound from free ligands, which will affect the results. It is also important to consider the physiochemical properties of a fluorophore with the linker. Hydrophobic fluorophores may increase non-specific binding or increase partitioning into the cell membrane and the amount of visible intracellular ligand.

The choice of the linker, in terms of its chemical structure and length, is worth considering. For example in the A_1AR, the linker length was shown to affect the binding affinity and the ligand efficacy[130, 131, 157].

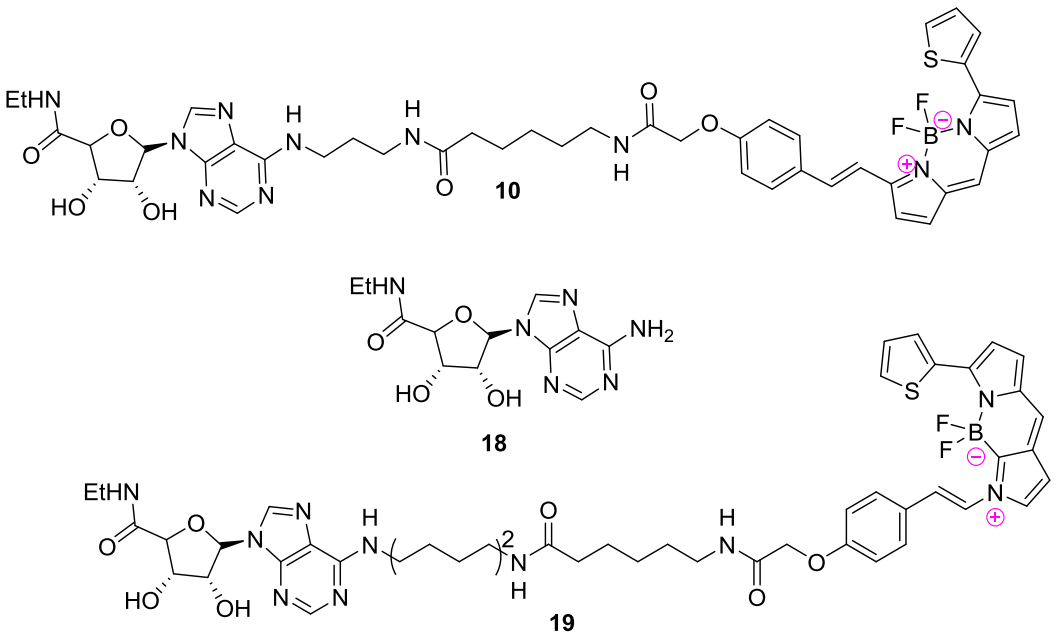

Compounds	Linker size	LogK$_D$
10	3	8.21±0.11
18	-	7.43±0.04
19	8	7.32±0.09

Figure 1-17| Fluorescent agonists **10** and **19** with the parent molecule 5'-(N-ethylcarboxamindo)-adenosine **18** (NECA) acting at the human A_1AR[131, 157].

Figure 1-16 illustrates the effect of fluorophore and linker length on the efficacy and potency of A_1AR fluorescent ligand[157]. Potency and efficacy are enhanced with shorter linker length. The potency varies with the fluorophore and the receptor of choice, allowing the chemical property of the linker to balance that of the fluorophore.

The β-adrenoceptor fluorescent ligands previously reported by Baker *et al*. were explored using living cell assays in order to study the spatial and temporal aspect of

ligand-protein interaction at β-adrenoceptor. However, the fluorescent ligand synthesised did not ideally meet the required characteristics such as the photochemical properties, hence their imaging properties required improvement (as illustrated in the aims and objectives section), therefore a redesign program was necessary in order to successfully achieve the objective of studying the selectivity of β-adrenoceptor subtypes[2].

Fluorescent ligands are usually designed and synthesized by tethering the ligand to a fluorophore *via* a linker to form a conjugate[6]. As such, it is desirable to develop methods that favor affinity and selectivity for the target especially if they have subtypes[131]. Jacobson and colleagues investigated whether minor chemical changes to a peptide-based linker part of a fluorescent probe could be used to fine-tune affinity and/ or selectivity at a given receptor. This is because the linker is in contact with receptor regions able to engage in molecular recognition[159]. This hypothesis was tested further in our laboratories by Vernall *et al.* on the adenosine receptor (AR) A_1 and A_3 subtypes using the non-selective antagonist xanthine amine congener (XAC-**12**) as the orthosteric ligand[119]. The adenosine subtypes A_1 and A_3-ARs have generated increasing interest as drug targets due to their implication in biological process and pathologies[163]. Vernall *et al.* worked on the peptide-modified adenosine receptor ligands and was able to convert a non-selective A_1 and A_3-ARs antagonist into subtype selective probes of higher affinity by introducing amino acids as part of the linker. They successfully demonstrated the peptide linker contribution; it enhanced ligand binding affinity when compared to the endogenous ligand, and imbued selectivity towards the A_3AR subtype. Additionally, the

dipeptide-linked fluorescent probe showed improved imaging properties with strongly defined membrane binding and low intracellular uptake. The lead modified congener SAR studies were compared to the final conjugate. These had suggested that the BODIPY dye might have possible favorable interactions with diverse amino acid residues on the receptor considering existing knowledge of the orthosteric binding pocket filled by the ligand[119]. Therefore it was thought suitable to use the dipeptide linker strategy as the template on which this project on β-adrenoceptor ligands would be based.

1.6 Research Aims

Designing GPCR fluorescent ligands is a complex process which requires careful consideration as previously explained in section 1.5 (fluorescent ligand design). Previously described linkers vary from aliphatic chains (C2-C8) to polymers such as polyethyleneglycol (PEG). Baker *et al.* noted that the linker size and chemical properties had an impact on the overall pharmacology, selectivity and affinity[130, 131, 157]. Previous propranolol-based ligand displayed high affinity, however their confocal image showed significant non-specific intracellular uptake that happened after 30 minutes with fluorescent probe diffusion into the cell cytosol (Figure 1-18).

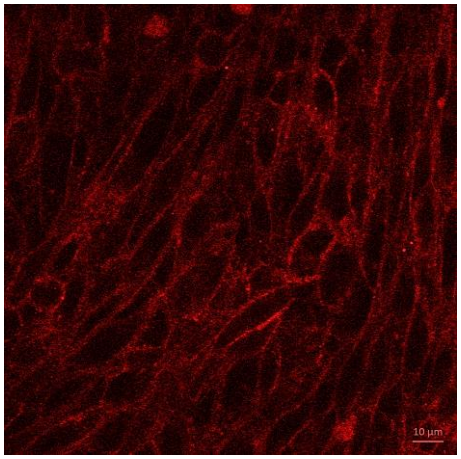

Figure 1-18| Confocal visualization of 10nM PEG-propranolol (**23**) binding to CHO cells stably expressing the human β_2-AR. Cell imaging was undertaken in the continued presence of the fluorescent probe.

Work carried out by Vernall and colleagues on peptide-modified fluorescent adenosine receptor ligands have shown that the peptide linker contributed in enhancing the ligand binding affinity and imaging properties when compared to the parent ligand as illustrated in Figure 1-15[119]. Therefore it was suitable for us to use this as the template premise upon which this β-adrenoceptor project would be based.

The aim of our project was to design, synthesise and pharmacologically validate a library of dipeptide-linked propranolol derivatives for human β_1 and β_2–adrenoceptors as a drug discovery tool. The idea was to take a single orthosteric ligand, and through manipulation of the linker, imbue receptor subtype selectivity into a range of fluorescent ligands. This provides a time- and cost-saving ability to devise one synthetic route to a series of subtype selective ligands[2, 6]. Additionally, novel ligands would be pharmacologically characterized through a series of assays at the target receptors.

2 DESIGN AND SYNTHESIS OF DIPEPTIDE-LINKED FLUORESCENT LIGANDS

2.1 Propranolol

A retrosynthetic analysis was undertaken in order to design an appropriate synthetic route for the first series of propranolol-based fluorescent ligands and this is illustrated in Scheme 2.1.

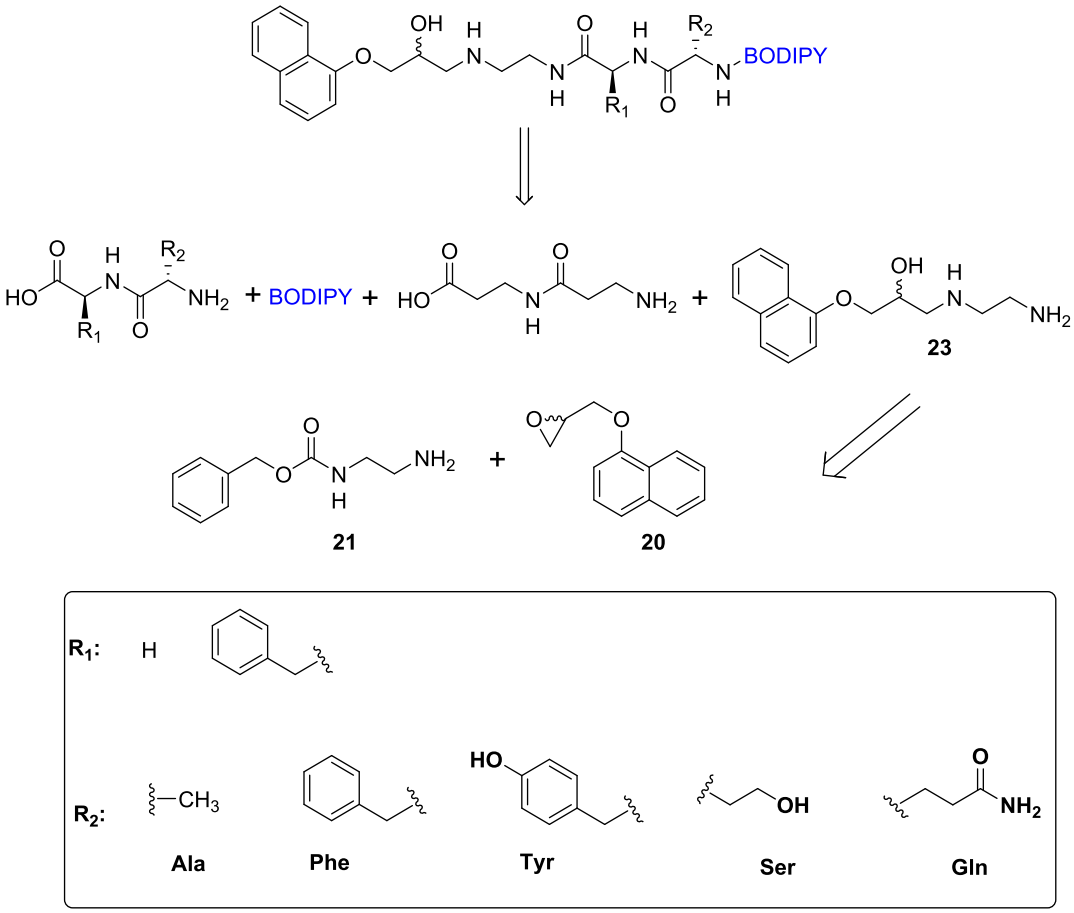

Scheme 2-1| Retrosynthetic route for the synthesis of fluorescent probes and dipeptide linkers.

Propranolol was initially selected as the orthosteric binding moiety to explore as it fulfilled criteria set out by Vernall *et al* for the adenosine receptor; e.g. a receptor ligand which itself displayed little subtype selectivity. Therefore provided an ideal template on which to explore whether peptide-based linkers could be designed to imbue selectivity to the final fluorescent conjugate, by the nature of their side-chain interactions outside of the orthosteric binding pocket.

The desired final conjugates could be obtained *via* simple acylation of a library of propranolol-peptide congeners using commercially available fluorophore active esters. The propranolol peptide congeners could themselves be synthesised in an expeditious fashion starting with commercially available naphth-1-ol *via* a series of peptide coupling steps following initial construction of the aryloxypropanolamine pharmacophore using well-established literature methodology[2].

2.1.1 Chemistry

2.1.1.1 Ligand and dipeptide linkers synthesis

A series of reactions were undertaken in order to synthesize the first tranche of fluorescent ligands and these are illustrated in Scheme 2-1. The commercially available 1-naphthol was therefore alkylated with racemic epichlorohydrin in DMF with sodium hydride to afford 92% of compound **20**[2, 157].

The formation of **20** was monitored *via* liquid chromatography tandem to mass spectroscopy (LC-MS), which showed a single peak at 2.26 minutes corresponding to the desired product molecular ion mass of 201.02. The ^{1}H-NMR data showed

peaks which integrate for 3 protons in total at 2.86-2.84 ppm (dd, J=2.7/2.7Hz, 1H, epoxide CH_2), 2.97-2.95 ppm (t, J= 4.8Hz, 1H, epoxide CH_2), 3.44-3.44 ppm (m, 1H, epoxide CH) characteristic of the epoxide; the ^{13}C-NMR spectrum showed the characteristic epoxide peak at 44.96 and δ 43.41 ppm.

In order to avoid side reactions during synthesis of the dipeptide-linked fluorescent ligands, the amine had to be mono-protected with a suitable protecting group; either the *tert*-butyloxycarbonyl group (Boc) or carboxybenzyl (Cbz) group could be utilised. The main advantage of the Cbz group is its stability under basic or acidic conditions and its removal by hydrogenation, making it suitable for the series of reactions for this project. The mono-benzyl carbamate (Cbz) protected ethylenediamine was synthesized from benzyl chloroformate and 1,2-diaminoethane in chloroform to yield **21** (82%). The desired product formation was monitored *via* LC-MS; the spectrum showed a single peak at 0.42 minutes with the ion mass of 195.5 after stirring for 18h.

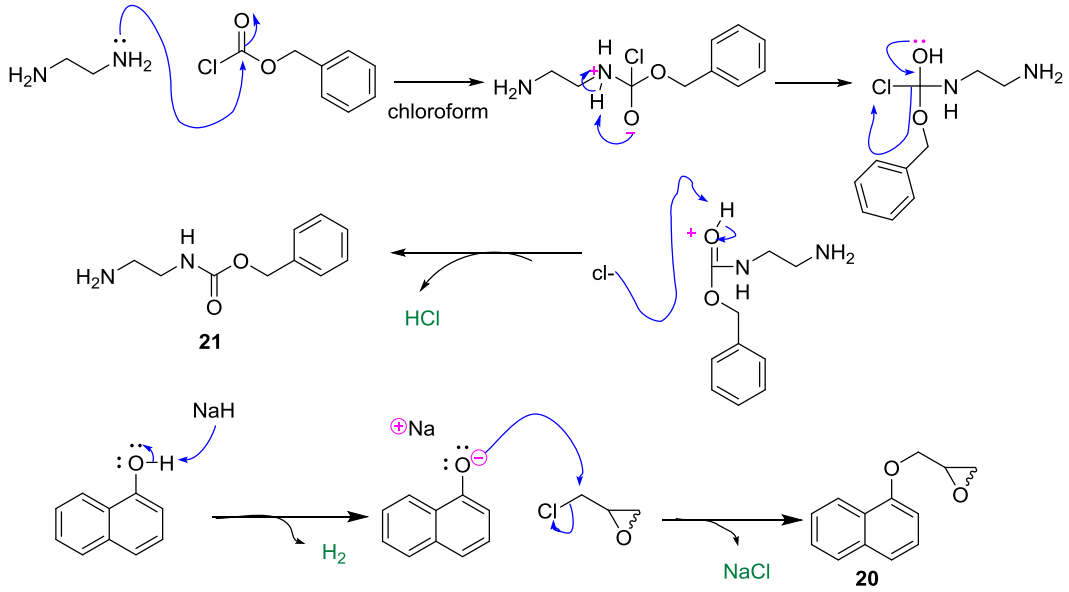

Scheme 2-2| A proposed mechanism for the synthesis of the Cbz protected amine **21** and the epoxide **20**.

The aryloxypropanolamine core (**22**) was then completed *via* nucleophilic ring opening of epoxide **20** with the mono-protected ethylenediamine synthon **21** in hexafluoropropan-2-ol (HFIP) at ambient temperature to yield 82% of **22** as an off-white solid. HFIP was previously used to open epoxide[164, 165]. Das *et al.*[166] claimed that reactions were particularly successful for aromatic amines such as anilines but unsuccessful with aliphatic amines[166]. In our lab, HFIP was revisited as a solvent for the nucleophilic epoxide opening reaction[1]. In our hands, the results showed a successful outcome with aliphatic amine at room temperature. Given that the reaction was conducted at room temperature, there was a reduction in the formation of *bis*-adduct (as illustrated in Scheme 2-3).

The reaction was monitored *via* LC-MS and after 12 h the spectrum showed 4 peaks (Table 2-1). The reaction was left a further 44 h to stir at ambient temperature in order to bring it to completion. At this juncture the major peak displayed in the LC-MS trace corresponded to the desired product at 2.27 minutes with the ion mass of 395 and the minor peak was attributed to the *bis*-adduct shown in Scheme 2-3. The proposed mechanism of this reaction is illustrated in Scheme 2-3.

Retention time (min.)	Ion mass (m/z, Da)	Residue
0.55	195.24	Amine (compound **21**)
2.27	395.00	Compound **22**
2.61	596.30	*Bis*-adduct
2.86	200.24	Epoxide (compound **20**)

Table 2-1| Compound **22** synthesis products present on the LC-MS spectrum.

The reaction proceeds *via* an S_N2 type mechanism, with the amine nucleophile attacking the methylene carbon on the epoxide followed by proton transfer to yield the final amino alcohol.

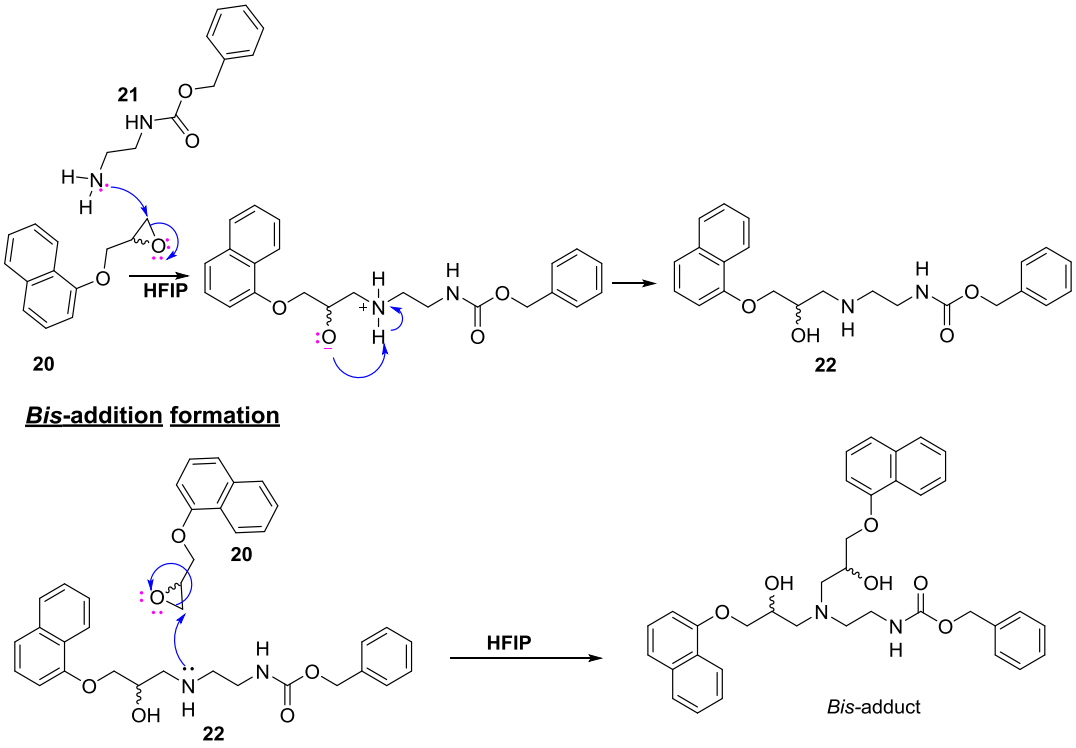

Scheme 2-3| A proposed mechanism for reaction between **20** and **21** to yield **22**.

It was noted that for compound **22**, the secondary amine can act as a nucleophile, reacting again with the epoxide to yield a bis-adduct. Selectivity was achieved using an excess of the amine (4 equivalents) in order to successfully synthesise the desired product. The Cbz protecting group was removed by hydrogenolysis using 10% palladium-on-carbon and hydrogen to afford compound **23**[167], which was used

without further purification (Scheme 2-4); NMR and LC-MS confirmed that the reaction was successful. A changed in product mass was observed, as it decreased from 395 Da to the desired 260.15 Da. The ^{13}C-NMR spectrum showed the absence of the carbamate carbon signal, whilst the ^{1}H-NMR showed a loss of signal in the aromatic region and the doublet of doublet between 4.16-4.12 ppm.

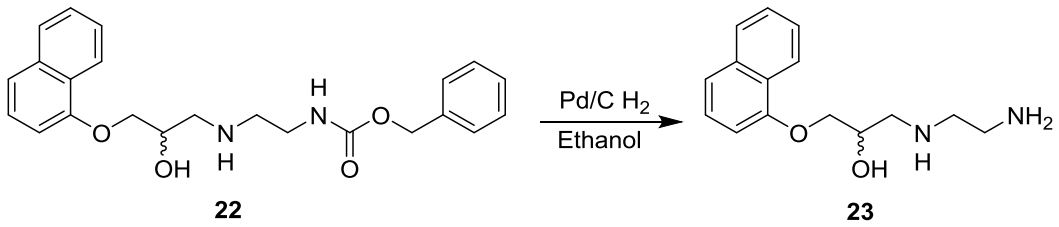

Scheme 2-4| Schematic of the hydrogenation of **22** to yield **23**.

2.1.1.2 Amino acid activation and coupling

Work previously described by Vernall *et al.* showed improvement in fluorescent ligand affinity when polar and non-polar amino acid residues (glycine, alanine, tyrosine, phenylalanine, glutamine and serine) were used as part of a dipeptide linker region of the conjugates[119]. Glycine was used to explore the requirements of the second amino acid for optimum binding because it contained no side-chain. The idea was to lock that residue in place and then switch the glycine residue for side-chain modified variants to see if further improvements could be achieved. Propranolol-gly was then coupled to each of the other amino acids respectively to create a mini library of five molecules, precursors ready to be coupled to the commercially available fluorophore succinimide ester (BODIPY 630/650-X or BODIPY FL).

Various protecting groups for the primary amine of an amino acid are available depending on the synthetic requirements. The Boc protecting group is suitable for liquid phase peptide synthesis while Fmoc works best with solid phase peptide synthesis[168]. The Boc group is stable under basic conditions and is removed under acidic conditions, where a range of acids can be used e.g. hydrochloric acid (HCl) or trifluoroactetic acid (TFA)[169]. For these reasons, Boc was selected for our synthesis. The core molecule was then coupled to either *t*ert-butyl carbamate (Boc)-glycine, Boc-phenylalanine or Boc-βalanine in the presence of *N,N,N',N'*-tetramethyl-*O*-(1*H*-benzotriazol-1-yl)uronium hexafluorophosphate (HBTU) and *N,N*-diisopropylethylamine (DIPEA) in DMF to afford compounds **24**-**26** and (80 - 75%)[170]. The proposed mechanism for this reaction is illustrated in Scheme 2-5.

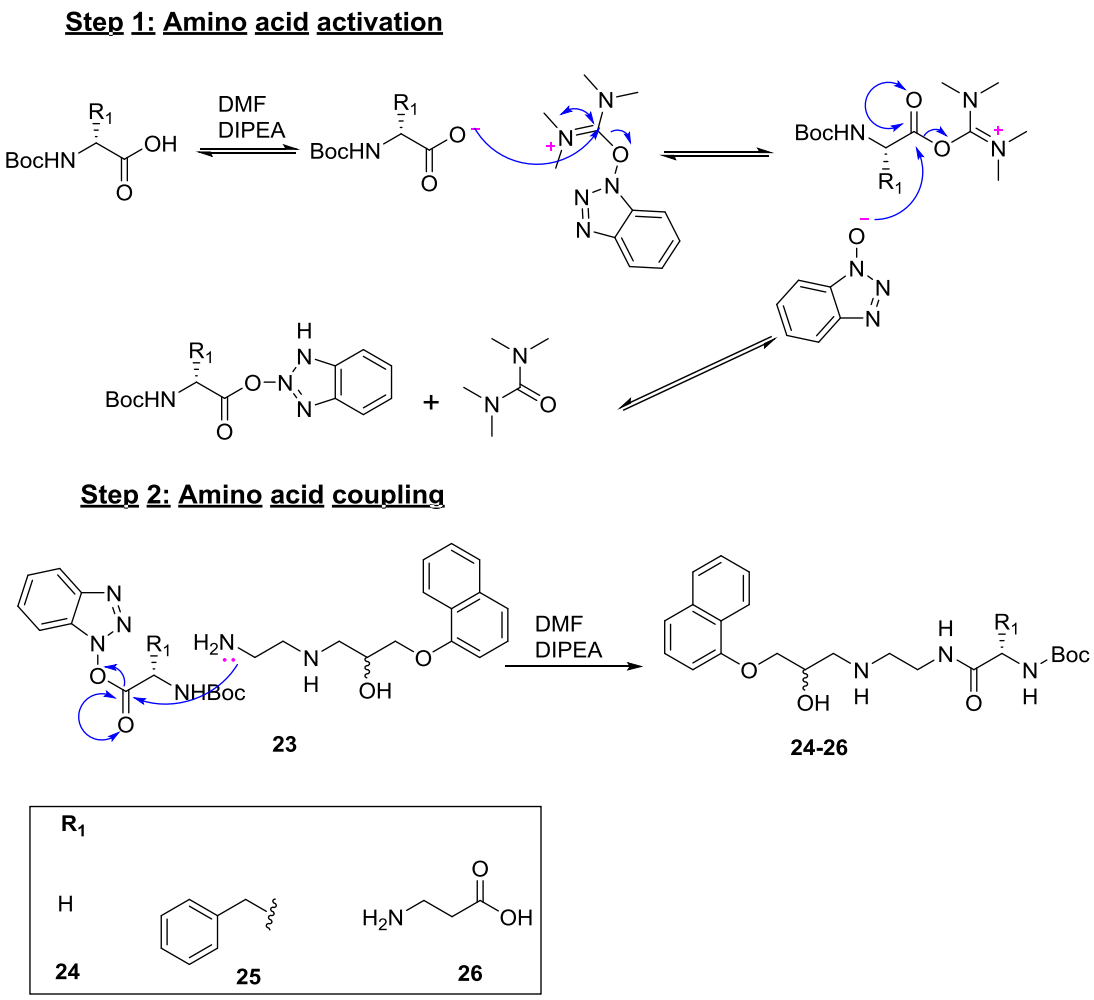

Scheme 2-5| The activation and coupling of Boc-Gly-OH with aryloxypropanolamine core **23** to afford **24-26**.

The activation of Boc-Gly-OH is a fast process, which takes place within minutes of stirring at room temperature[171]. The reaction was left overnight to ensure that it goes to completion.

2.1.1.3 Boc deprotection and secondary amino acid coupling

The Boc protecting group was removed *via* acidolysis, using anhydrouds 4N hydrochloric acid in 1,4-dioxane as illustrated in

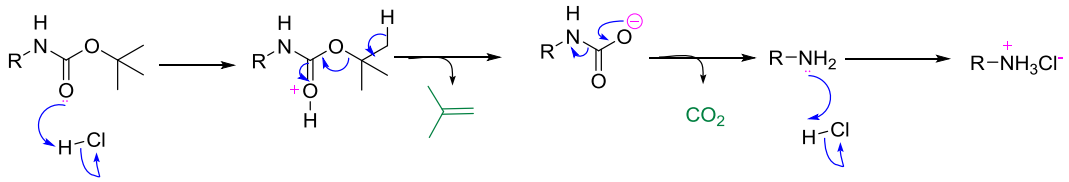

Scheme 2-6 to yield compounds **27- 29**[172].

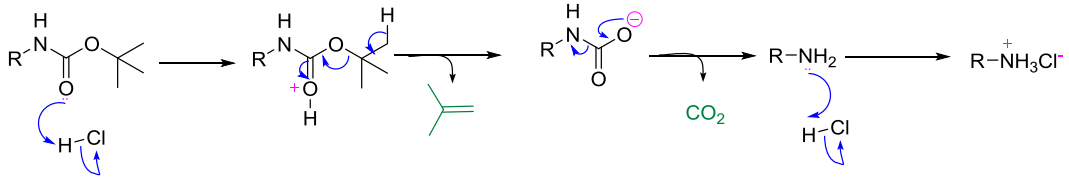

Scheme 2-6| A mechanism for Boc removal with 4N solution of HCl in dioxane to yield the HCl salt.

The reaction was straightforward with quantitative yield. The products were dried *in vacuo* and used in the following reactions without further purification. The hydrochloride amine salts **27- 29** (as seen in scheme 2-7 and scheme 2-8) were subsequently coupled to the second *N*-Boc protected amino acid residue; alanine (Ala), phenylalanine (Phe), tyrosine (Tyr), serine (Ser), glutamine (Gln) and beta-alanine (β-ala), in the same fashion as previously described, to yield seven distinct congeners (**30a-e**) illustrated in Scheme 2-7 and Scheme 2-5.

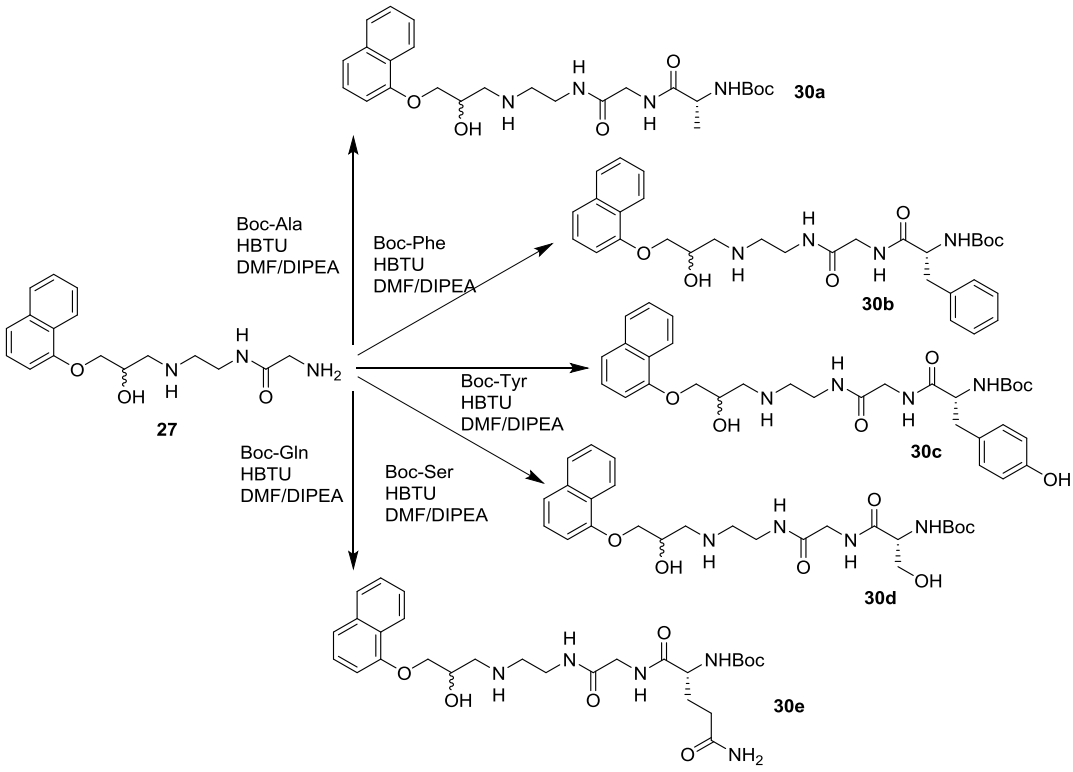

Scheme 2-7| Second amino acids coupling with compound **27** to yield the 5 amine congeners.

The reaction between compound **27** and the amino acid residues tyrosine, serine and glutamine had to be repeated with a range of conditions. There was a need to improve on the amino acid equivalents in order to avoid side reactions such as the amino acid residues coupling with the secondary amine on the pharmacophore (**27**). The reaction was then attempted with increasing temperature to 40 °C in order to boost the kinetic energy and lower the activation barrier, however this did not affect the rate of reaction given and no change in yield was observed. It appears that the side chains might have been preventing successful reactions. Ideally, nucleophilic amino acids should be protected with a protecting group to prevent side reactions. However, protecting groups will introduce steric hindrance, which might negatively

influence the activation and coupling of amino acid residues with glycine primary amine. The protection of compound **27** secondary amine with a benzyl group would aid not only with the overall yield but also facilitate purification of the dipeptide-linked compounds on the silica column.

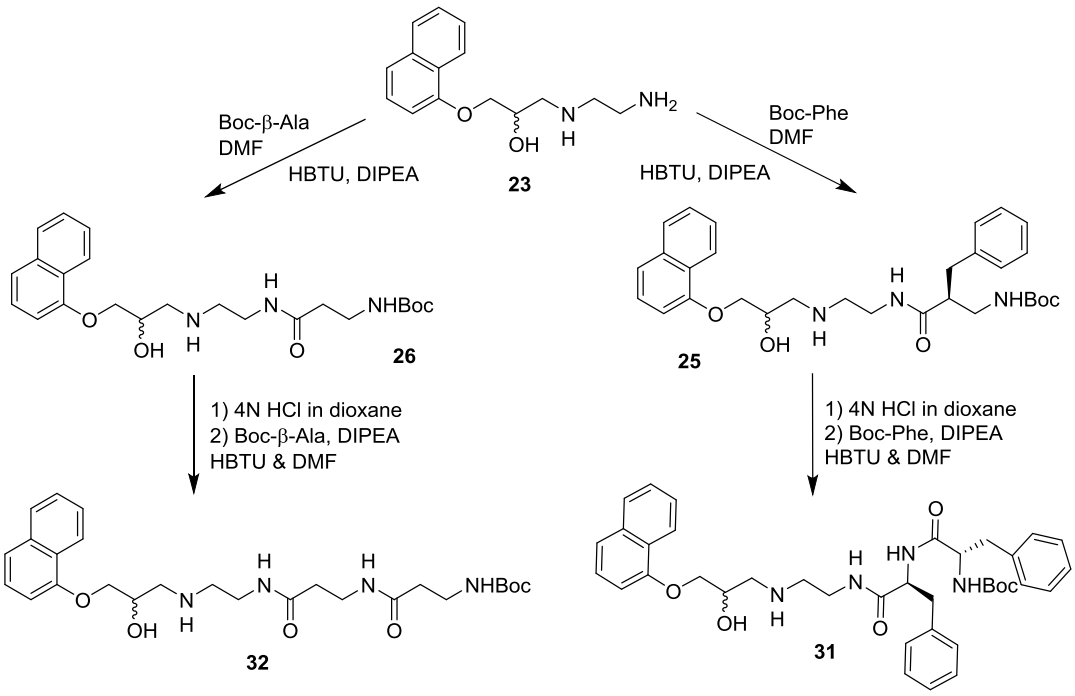

Scheme 2-8| Amine congeners with the same amino acid residues in the dipeptide linkers.

Propranolol-β.Ala-β.Ala (**32)** coupled to BY-X-630/650 is a good example of a dipeptide fluorescent probe made by CellAura (CA200645)[71]. In our laboratory, the beta-alanine-linked fluorescent probe was extensively characterised, however it lacks selectivity between the human β_1- and β_2-AR. This provided a good template for us to test other amino acids with different residues. Boc-Phe was favoured on the basis of its aromatic side chain. It was important to investigate whether an aromatic side chain would increase binding potential by forming π-π stacking with

residues in the binding site when compared to the use of either aliphatic or hydrophilic residues as secondary amino acids for the synthesis of the dipeptide linkers.

Step 1: Secondary amino acid deprotection

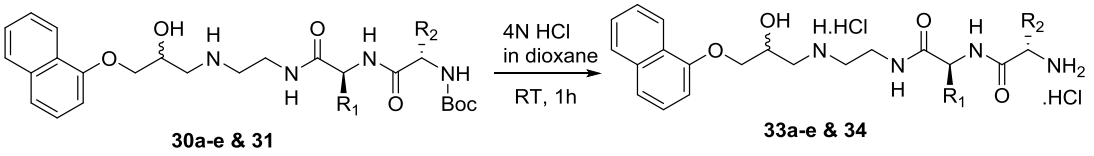

30a-e & 31 **33a-e & 34**

Step 2: Acetylation

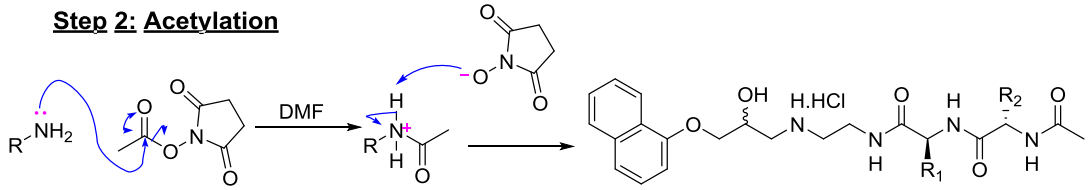

36a-e & 37

	R_1	R_2
30, 33 & 36	H	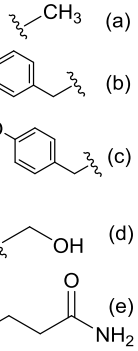 (a) (b) (c) (d) (e)
31, 34 & 37		

Scheme 2-9| Step 1 shows the amino acid deprotection; Step 2 shows the acetylation mechanism to yield the acetylated compounds.

Subsequently, the Boc protecting group for each of the seven intermediates (**30a-e**, **31** and **32**) was removed *via* acidolysis as previously described to yield seven amine

congeners ready to be coupled to the fluorophore active ester (either BY-X-630/650, BYFL or BYFL-X) to in turn yield the first tranche of fluorescent probes.

Beta-blocker SAR studies for the beta-adrenergic receptor showed the secondary amine in the phenylethanolamine side chain ending (orthosteric head group) is essential in molecular binding [173]. It is crucial that the primary amine remains the point of acetylation under reaction conditions. The kinetics of the reaction depends on the reactivity and concentration of both the acetylating reagent and the amine[174].

While synthesising the acetylated ligands, pre-activated *N*-hydroxysuccinimidyl (NHS) was used because it selectively acetylates primary amines given that there are 2-10 equivalences of primary amine to 1 NHS. Amine reactivity varies according to basicity and class (aromatic or aliphatic). Primary amines are moderately basic and react readily with NHS to afford carboxamides. The amine congeners were acetylated (as illustrated in

Scheme **2-9**, step 2) in order to tease out the fluorophore contribution on the dipeptide-linked propranolol derivatives. The acetylated congener syntheses were confirmed *via* proton and carbon NMR studies. The key characteristic was the presence of a singlet at 1.36 ppm that integrated for 3 protons corresponding to the methyl chemical shift, and the ^{13}C-NMR showed an extra peak at 174 ppm, which corresponded to a carbonyl chemical shift. Additionally, the ^{1}H- NMR showed the absence of a singlet at 1.6 ppm that integrated to 2 protons corresponding to NH_2 chemical shift and the presence of a singlet at 8.58 ppm corresponding to an amide chemical shift.

The acetylated congeners are novel molecules in their own right. They were also therefore regarded as important cost-effective test compounds with which to ascertain whether certain amino acid sequences are favoured or deleterious for subsequent fluorescent ligand generation.

2.1.1.4 Fluorescent ligand synthesis

Following the final Boc deprotection, amine congeners were coupled to the commercially available active ester fluorophores BODIPY-X-630/650-OSu (BY630) and BODIPY-FL (BYFL) to yield the first tranche of fluorescent ligands (**38a-e**, **39** and **40** for red ligands, **41a**,**b** & **d**, **42** and **43** & **44** green ligands) as illustrated in Scheme 2-10[2, 6, 119, 131, 157]. The novel fluorescent compounds were isolated and purified using preparative reverse-phase high performance liquid chromatography (HPLC); their final purity was confirmed using analytical HPLC with dual wavelength detection with the compound identity subsequently confirmed by HRMS (TOF ES^+). The purities of all compounds subsequently tested in biological systems were determined as being greater than 95%.

The synthesis of the dipeptide-linked fluorescent ligands represents a new generation of β-adrenoceptor fluorescent probes. They might hopefully display high efficacy compared to previous propranolol-based β-adrenoceptor fluorescent ligands[2]. The fluorescent ligands synthesised would ideally meet the photophysical, pharmacological and physicochemical characteristics required in order to study GPCRs in recombinants cells and in whole cell assays[119].

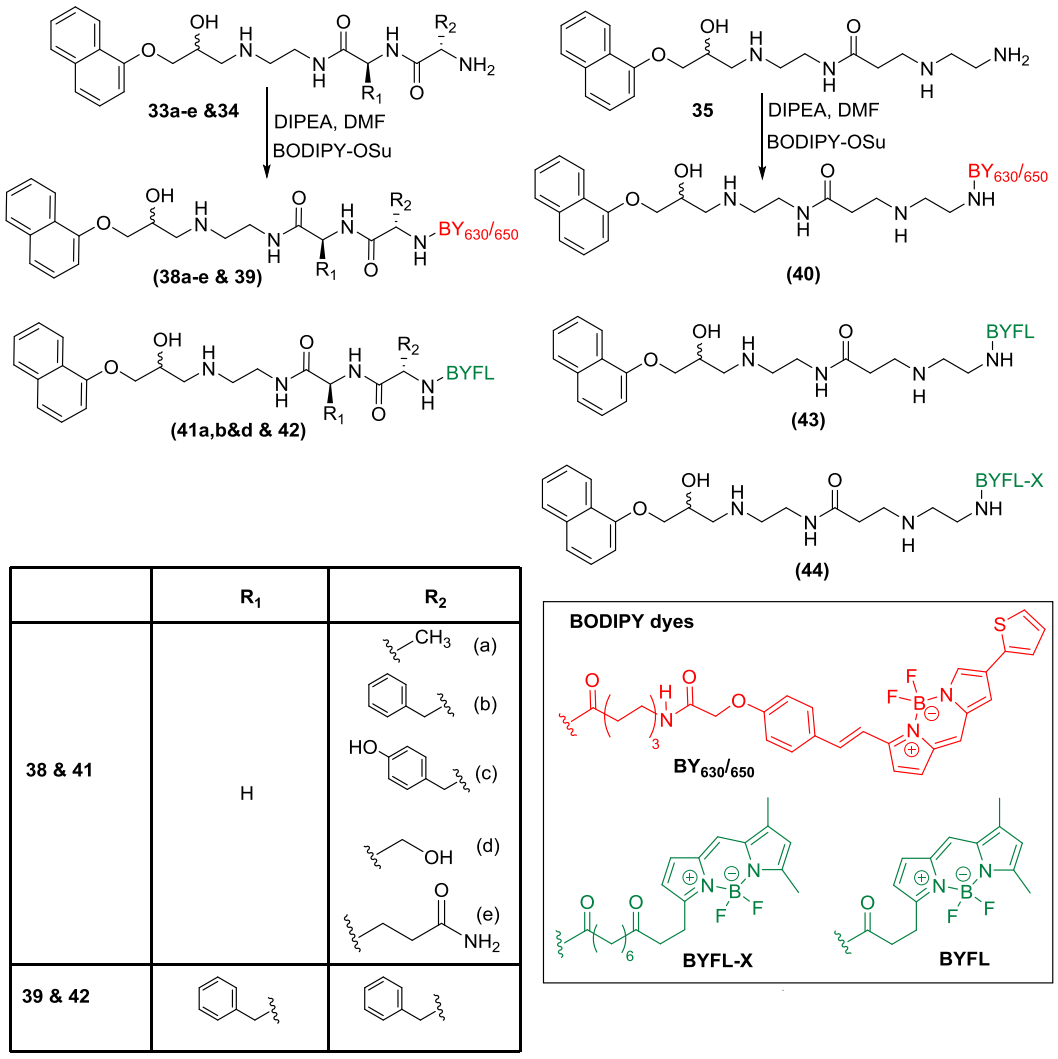

Scheme 2-10| BODIPY-OSu coupling with the amine congeners to yield the first tranche of fluorescent ligands.

2.1.2 Pharmacology

The pharmacological characterization of the novel acetylated ligands and fluorescent ligands was carried out in β_1 & β_2-ARs CHO CRE-SPAP cells and Nluc-β_1 & β_2-ARs HEK cells. Human Embryonic Kidney 293 (HEK 293) cells were tagged at the receptor *N*-terminus with nanoluc (Nluc) stably expressing either human adrenoceptor subtype (Nluc-β_1 & β_2-ARs), which were used for the whole

cell and saturation binding assays. For imaging purposes, both CHOK1 and HEK 293 cells stably expressing either the human β_1- or β_2 AR were used.

In order to assess the activity of the synthesised dipeptide-linked acetylated and fluorescent ligands at β_1 and β_2 adrenoceptors, several assays were employed.

2.1.2.1 Acetylated congeners

2.1.2.1.1 Functional Reporter Gene studies: CRE-SPAP Assay

The CRE-SPAP assay showed encouraging results. All acetylated congeners were able to antagonize the cimaterol-mediated agonist response at the human β_1 & β_2-ARs in CHO CRE-SPAP cells (Table 2-2).

Compounds	Linker	β_1 pA_2	n	β_2 pA_2	n	β_2 vs β_1
Propranolol.HCl		7.79±0.05	5	8.62±0.09	5	7
36a	Gly-Ala	8.10±0. 10	6	8.41±0.11	5	2
36b	Gly-Phe	7.58±0.07	5	8.58±0.24	6	10*
36c	Gly-Tyr	7.60±0.15	10	8.89±0.16	10	20*
36d	Gly-Ser	7.69±0.05	5	7.92±0.03	5	2
36e	Gly-Gln	7.65±0.12	5	7.27±0.08	5	0.4
37	Phe-Phe	6.99±0.12	5	8. 53±0.10	5	35*

Table 2-2| Acetylated congener pA_2 values from antagonism of cimaterol-stimulated CRE reporter gene responses at the human β-adrenoceptors. $^{\alpha}pA_2$ values were obtained from the shift in cimaterol concentration response curves produced by the acetylated congeners in CHO cells expressing human β_1 and β_2-ARs . Values are mean ± SEM for n separate experiments. *P<0.005, unpaired Student t-test for difference in values obtained at the β_1- and β_2- ARs.

The pA_2 is a measure of the affinity of an antagonist for the receptor; it is effectively the negative log of the K_D[175]. The results classify the six acetylated compounds into

two groups. The first group shows no significant difference in selectivity ($p>0.005$, with unpaired Student t-test) between β_2-AR and β_1-AR for compounds **36a**, **d** and **e**. Fortunately, in the second group, compounds **36b-c** & **37** displayed significant selectivity for β_2-AR versus β_1-AR, especially **37**, which was 35-fold more selective for β_2-AR versus β_1-AR (Table 2-2). In order to confirm the reporter gene findings, two acetylated conjugates (**36a** and **37**) were chosen for the radioligand displacement binding screening with [^{3}H]-CGP12177. The chosen acetylated ligands **36a** and **37** represent the two extremes from the results; **36a** displayed no significant difference in selectivity between β_2-AR and β_1-AR whereas **37** is 35-fold selective for β_2-AR versus β_1-AR.

2.1.2.1.2 [^{3}H]-CGP12177 Whole Cell Binding

In order to carry out the radioligand assay, two different cell lines were screened (β_1 & β_2-ARs CRE-SPAP CHO and Nluc HEK 293). The mean receptor expression level was the same as literature values quoted by Soave *et al.* for β_1-NL[176], Stoddart *et al.* for β_2-NL[71] and Baker *et al*. for CHOK1 cells[177]. The aim of saturation binding was to obtain [^{3}H]-CGP1277 K_D and the maximal receptor occupancy at equilibrium in CHO and Nluc cells.

	β_1-AR				**β_2-AR**			
Compound	pK_D CHO	n	pK_D HEK	n	pK_D CHO	n	pK_D HEK	n
[^{3}H]-CGP12177	9.05±0.04	6	8.62±0.06	6	9.15±0.04	6	8.89±0.06	5

Table 2-3| [^{3}H]-CGP12177 binding affinities at human β_1-AR and β_2-AR stably expressed in CRE-SPAP CHO and Nluc HEK 293 cells. Data are mean ± SEM of pK_D values obtained in n separate experiments.

The results highlight a slight difference in binding between the β_1 & β_2-ARs regardless of cell type, which are significant according to the unpaired Student t-test ($p<0.004$). The K_D values indicating the affinity of [^{3}H]-CGP12177 was determined in the saturation binding assays is shown in

Table 2-3. The pK_D, defined as $-\log_{10}K_D$, is an important measure for the comparison of ligand affinity and selectivity [178]. A series of experiments were conducted to compare affinity values between different assays and cell lines, with the purpose of affirming the reporter gene data.

2.1.2.1.3 Competition binding assays (CHO and Nluc-HEK 293)

Binding affinity of a competing ligand can be determined from the IC_{50} values following correction for the presence of the radioactive ligand using the Cheng-Prusoff equation ($\mathbf{K_i = \frac{IC_{50}}{1+(L/K_D)}}$). The competition binding assay provides a measure of the ability of acetylated ligands to compete with radioligand for the receptor binding site. The selected acetylated ligands were able to displace [^{3}H]-CGP12177 specific binding at the human β_1 & β_2-ARs expressed in both CHO CRE-SPAP and Nluc cells. Given that the half-maximal inhibitory concentration (IC_{50}) of a compound may vary between experiments depending on radioligand concentration, it is important to correct for these variations by the conversion of the IC_{50} value into a constant, K_i. Subsequently, we calculated the respective pK_i values indicating the affinity of compounds **36a** and **37** from the corresponding IC_{50} values using the Cheng-Prusoff equation (equation 4)[179]. The values obtained for both cell

lines (Table 2-4) are comparable with the reporter gene assay data as shown in Table 2-2.

		β_1-AR		β_2-AR	
Ligands	Linker	pK_D CHO	pK_D HEK	pK_D CHO	pK_D HEK
36a	Gly-Ala	7.93±0.06	7.80±0.04	8.25±0.13	8.28±0.09
37	Phe-Phe	6.83±0.09	6.52±0.05	8.32±0.17	8.16±0.13

Table 2-4| Acetylated congener binding affinities at human β_1-AR and β_2-AR stably expressed in CRE-SPAP CHO and Nluc cells. The pK_D values were obtained using the Cheng-Prusoff correction. The concentration of [^{3}H] CGP12177 was 2.8nM. Data are mean ± SEM of values obtained in n separate experiments for CHO (n=5) and HEK (n=6).

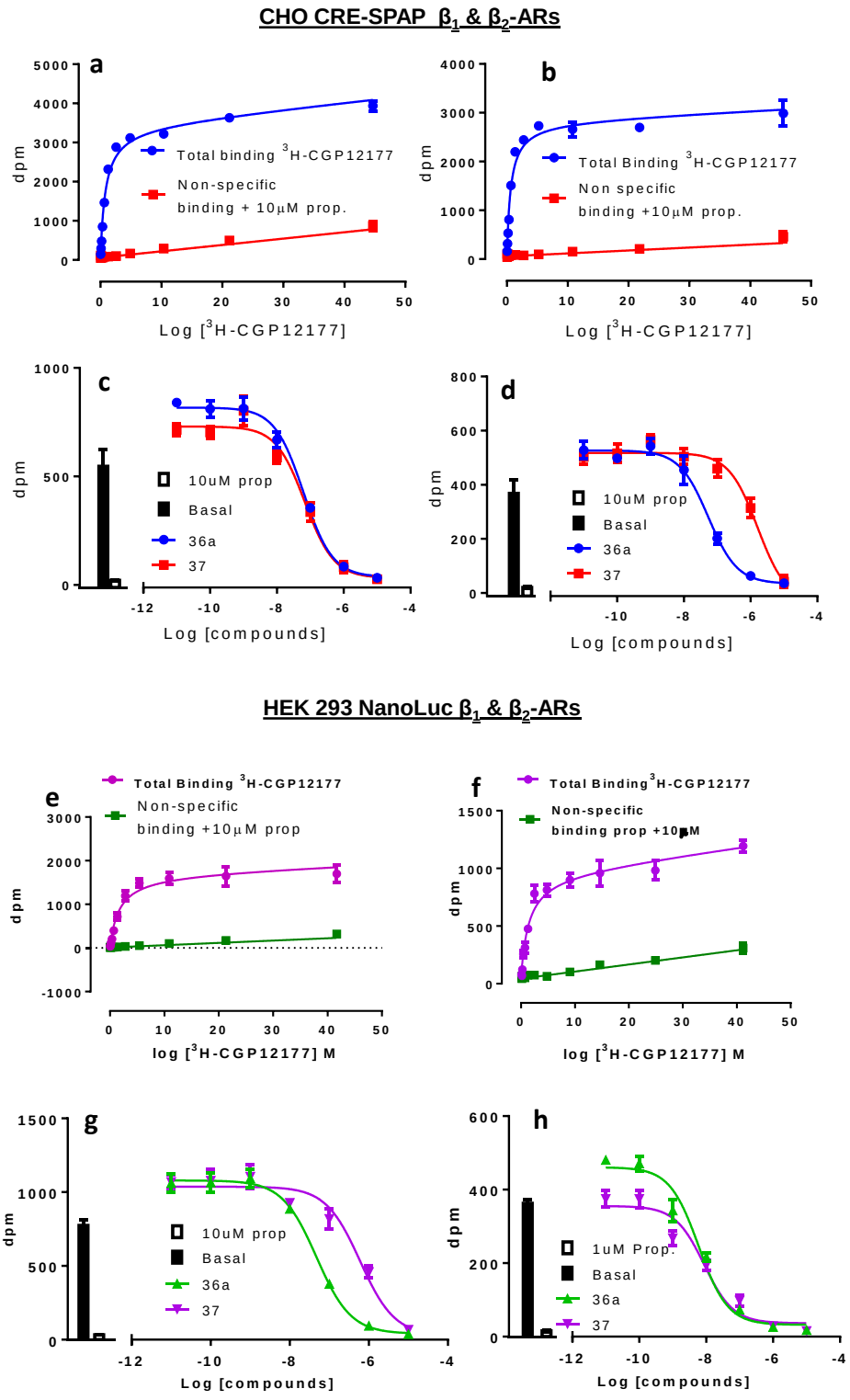

Figure 2-1| Radioligand saturation binding graphs for [^{3}H]-CGP12177 at CHO β_1 ARs (a) and β_2-ARs (b) and Nluc saturation at β_1 ARs (e) and β_2-ARs (f). [^{3}H]-CGP12177 displacement binding with compounds 36a & 41 at β_1 & β_2-ARs (c, g & d, h) with CHO and Nluc cells respectively. Data are mean ± SEM of pK_D values obtained in n separate

experiments. The graphs are representative of (a-f) six and (g-h) five separate experiments. The concentration of [^{3}H]-CGP 12177 in the displacement binding experiments was 4.68nM.

2.1.2.2 Fluorescent ligands

2.1.2.2.1 Reporter gene assay: CRE-SPAP assay

To check whether this novel series of fluorescent ligands were efficacious and able to antagonize agonist-stimulated responses at the β-adrenoceptor subtypes (β_1 & β_2-ARs), we initially evaluated their capacity to attenuate functional activity in CRE-SPAP CHO cells.

ID		β_1		β_2		β_2/β_1
	Linkers	pA_2	n	pA_2	n	
		BY630/650-X				
38a	Gly-Ala	7.66±0.23	5	8.57±0.08	5	8
38b	Gly-Phe	6.62±0.24	6	7.70±0.14	5	12
38c	Gly-Tyr	7.42±0.22	7	7.92±0.26	7	3
38d	Gly-Ser	7.69±0.14	5	8.44±0.27	5	7
38e	Gly-Gln	7.52±0.14	5	8.19±0.32	6	5
39	Phe-Phe	<6.0	8	6.94±0.06	7	-
40	β-Ala-β-Ala	8.84±0.12	5	9.96±0.15	5	13
Ref.	PEG-8	7.74±0.11	3	8.90±0.06	3	11
		BYFL				
41a	Gly-Ala	7.31±0.14	5	9.16±0.10	6	71*
41b	Gly-Phe	<6.0	5	7.33±0.10	5	-
41d	Gly-Ser	7.05±0.09	7	8.90±0.07	9	71*
42	Phe-Phe	<6.0	8	6.27±0.10	8	-
43	β-Ala-β-Ala	7.99±0.09	6	9.02±0.06	6	11
		BYFL-X				
44	β-Ala-β-Ala	8.43 ±0.24	6	9.56±0.11	6	13

Table 2-5| Fluorescent ligand pA_2 values from antagonism of cimaterol-mediated enhancement of CRE reporter gene responses at the human β-adrenoceptors[α]. [α]pA_2 values were obtained from the shift in cimaterol-concentration response curves produced by the acetylated congeners in CHO cells expressing the human β_1 and β_2-ARs. Values are mean ± SEM obtained from n separate experiments. *p <0.01, Student unpaired t-test for difference in values obtained at the β_1 and β_2-ARs. No shift in the concentration-response curve to cimaterol in the presence of competing compound (1μM) is represented by pA_2<6.0.

The SPAP assay showed encouraging results given that all fluorescent ligands were able to antagonize the cimaterol-mediated agonist response at the human β_1 & β_2-ARs (Table 2-5) as seen with the acetylated ligands. Table 2-5 shows that all thirteen fluorescent ligands tested gave affinity values which varied from 6.27 to 9.96 at β_2-AR while **41a** & **d** attracted particular attention; they had the highest pA_2 values for β_2-AR (9.16±0.10 and 8.90±0.07 respectively) within the propranolol-gly series. Compound **40** displayed the highest affinity across the table for β_2-AR. Of the six BY630 compounds (**38a-e, 43 & 40**), compounds **38b** and **40** showed more than 10-fold selectivity for β_2 over β_1-AR, while compound **40** displayed the highest selectivity for β_1-AR, 10-fold greater than the reference ligand CellAura® PEG-8-propranolol. A Student's unpaired T-test showed no significant difference in affinity values between both receptor subtypes for compounds **38a, c-e.** However, compounds **38b** and **40** showed significant difference in pA_2 value between β_2 and β_1-ARs where the degree of confidence was p<0.01. Furthermore, compound **43** was modestly selective for β_2-AR (pA_2 = 6.94±0.06) versus β_1-AR (pA_2<6.0).

In parallel, the newly synthesized BYFL ligands showed higher affinity than their BY630 counterparts within the propranolol-gly series. Compounds **41a** and **41d**

displayed the highest affinity for β_2-AR with 71-fold selectivity at β_2-AR compared to β_1-AR (Table 2-5).

Compounds **41b** and **42** showed low affinity for β_1-AR (pA_2<6.0) and modest selectivity for β_2-AR. Beta alanine-linked dipeptides displayed no difference in selectivity between the red (**40)**, and green (**43** and **44)** ligands. Compound **42** displayed a modest affinity (6.27±0.10) at β_2-AR with a partial agonist profile at higher concentrations (≥1000 nM) even under conditions of maximal stimulation by cimaterol (Figure 2a and b). Compound **42** is a clear example which emphasizes that novel fluorescent probes should be treated as a new entity in their own right, because they might display different profiles from their parent molecules. This compound provided a further example of how subtle changes in the structural nature of the linker can exert a significant impact on the pharmacology of the final conjugate.

Figure 2-2c shows that the partial agonist effect of compound **42** at high concentration is not antagonized by high concentration of propranolol hydrochloride (10 μM). Interestingly, compound **42** is potentially binding to an alternative site to the classic catecholamine site; therefore there is a need for further investigation. This effect is clearly driven by the synergic effect between the green fluorophore (BYFL) and the linker because the equivalent red ligand **39** has no partial agonist effect. Moreover, the partial agonist action was confirmed with further CRE-SPAP experiments as shown in Figure 2-2 (a, b, d & f). The results illustrated in Figure 2-2c imply the partial agonism effect is not mediated by the β_2 ligand binding site, because this effect is not inhibited by the unlabeled propranolol at 1 or 10 μM. The intriguing question remains concerning the mode of action of the compound,

whether it be binding to an allosteric binding site, acting as a bitopic ligand, exhibiting cooperative binding [65, 180, 181] or it is an non-specific effect.

Further experiments were conducted in order to investigate the alternative site hypothesis. Figure 2-2d shows the partial agonist actions of CGP12177 and **42** and the dose response curve for propranolol hydrochloride and **39**. The alternative binding site hypothesis is supported by data shown in Figure 2-2e and f; CGP12177 is a partial agonist at β_2-AR by inhibiting cimaterol response at different concentrations without further stimulation, suggesting that there is competition for the catecholamine binding site (Figure 2-2).

However, compound **42** showed a different profile to CGP12177 as it inhibited cimaterol action then stimulated a response [Figure 2-2(f)]. This is very interesting because current opinion is that β_2-AR has only one orthosteric-binding site with an unknown allosteric or alternative site. The results presented here suggest a mode of action which is consistent with the presence of yet undescribed allosteric binding pocket[65, 182]. It might be that **42** is acting as a classic partial agonist at low concentrations (i.e. below 1 μM and has a non-specific effect at 10 μM concentrations). Further experiments such as radioligand binding were conducted in order to obtain a full characterization profile of the ligand.

It is worth noting that the results showed a significant fluorophore-receptor interaction as the affinity values are lower at β_1-AR for the BYFL ligands when compared to their corresponding BY630 fluorescent ligands. It is interesting to see the lack of selectivity generated between different amino acid residues on the receptor subtypes when tagged with BY630 compared to BYFL. Whilst designing

the linker, the aim was to introduce amino acid residues to potentially increase receptor affinity and hence enhance selectivity.

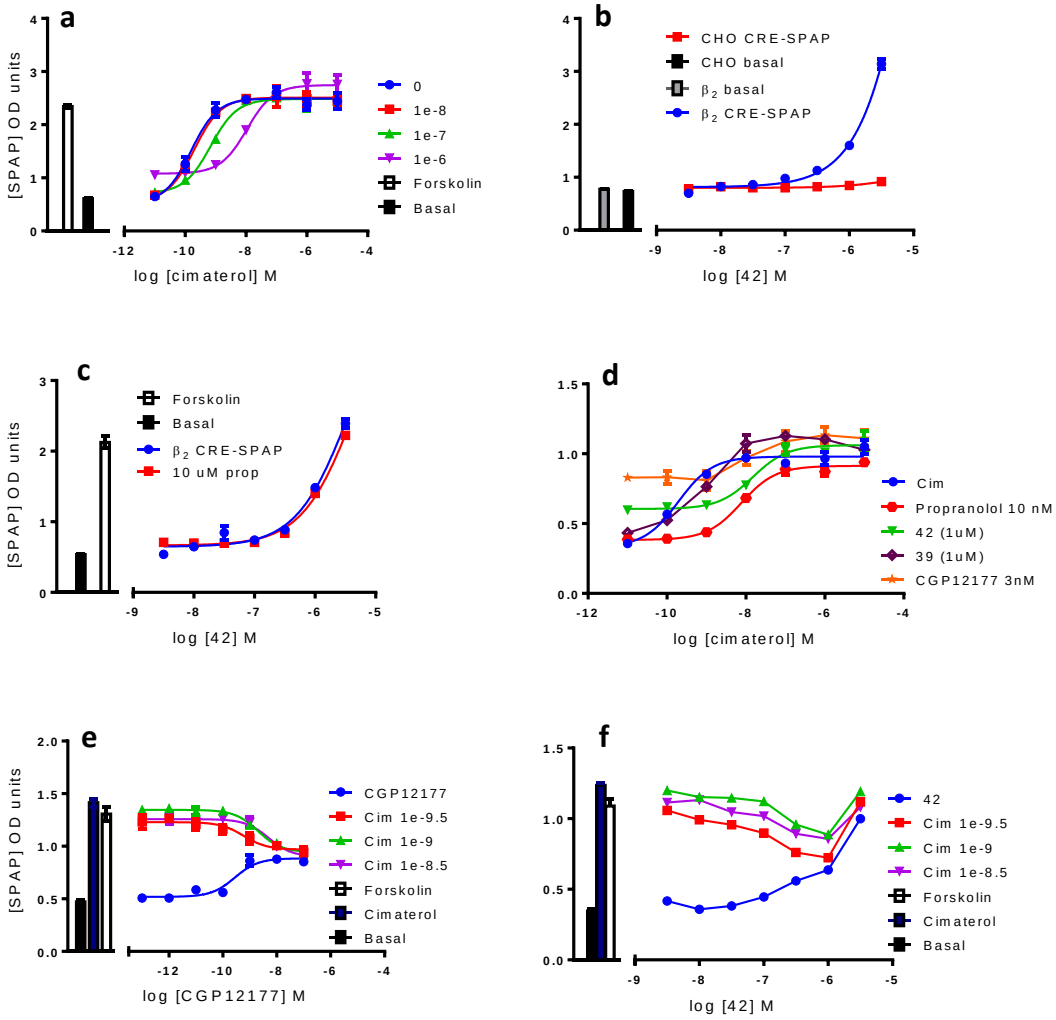

Figure 2-2| Propranolol-Phe-Phe-FL (**42**) CRE-SPAP results at β_2-AR. **(**a) CRE-SPAP production in the presence of 10, 100, and 1000 nM (**42**) following cimaterol stimulation. (b) Partial agonist response of compound 42 leading to the production of CRE-SPAP in β_2-AR and non-transfected CHO in the absence of cimaterol stimulation. (c) Partial agonist response of **42** leading to the production of CRE-SPAP in β_2-AR in the presence and absence of 1000 nM propranolol. (d) A summary of graphs showing partial agonist response of compound **42** (green) and CGP12177 (Orange); and the dose response curve for propranolol (red) and compound **39**. (e) Binding site competition experiment between CGP12177 and cimaterol and (f) Binding site competition between **42** and cimaterol. Data points are mean ± SEM of triplicate determinations. The graphs are representative of (a) eight, (b) five, (c) nine, (e & f) four separate experiments.

The novel fluorescent ligands **41a** & **d** showed 71-fold selectivity toward β_2 (pA_2 9.16±0.10 and 8.90±0.07, respectively) when compared to β_1 (Table 2-5). Of even greater significance, the BYFL fluorophore drives the compound selectivity profile closer to 100-fold in the SPAP assay. Compounds **41a** & **d** lead us closer to the project goal and objectives, which is to synthesis subtype-selective fluorescent ligands. The results in Table 2-5 show promising indications as to the affinity of various probes to the receptor subtypes, therefore binding assays were used in order to consolidate this data.

2.1.2.2.2 NanoBRET

For the studies described here, the in-house NanoBRET™ assay was initially utilised to quantify the binding interaction between the thirteen synthesized fluorescent ligands at β_1 and β_2-ARs in Nluc HEK 293 cells. The saturation data confirmed the observed concentration-dependent ligand-binding BRET signal in cells expressing Nluc-β_1AR and Nluc-β_2AR, which was fully inhibited by a high concentration (10 μM) of unlabeled propranolol as reported by Stoddart [71]. The assay showed a high level of reproducibility and reliability, the pK_D values for the cellAura® PEG-8-propranolol were comparable to those previously obtained by Baker *et* al[2] in CHO cells.

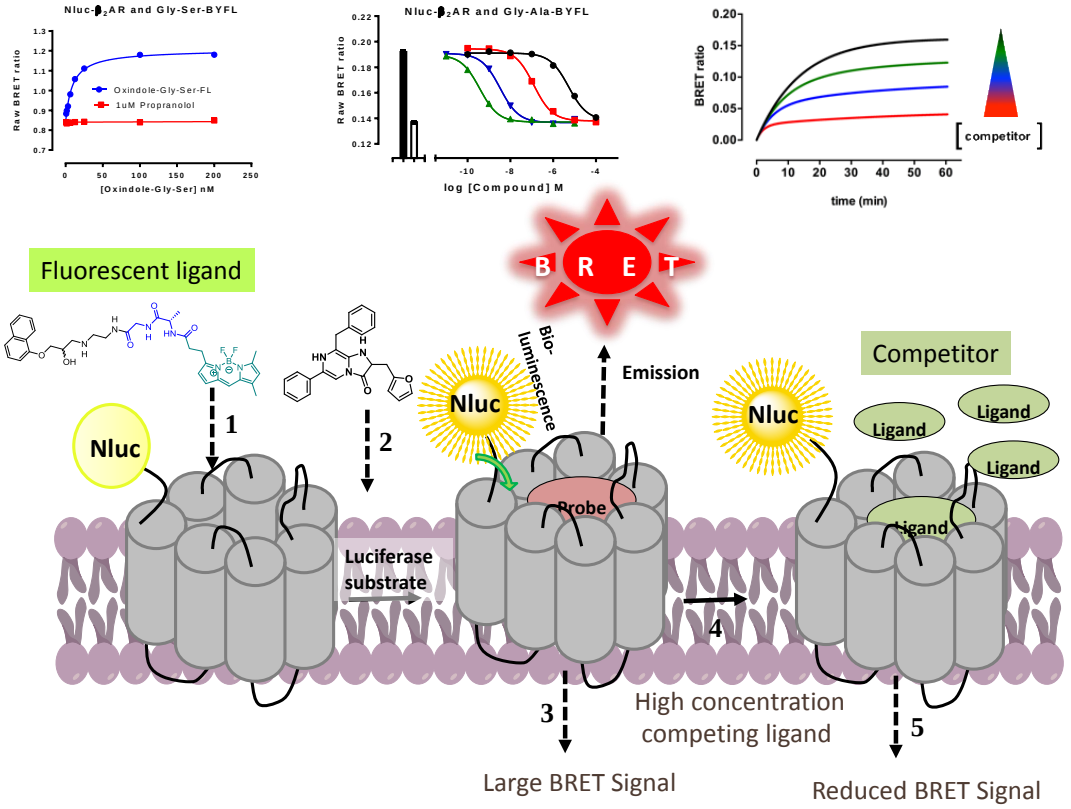

Figure 2-3| Illustration of the NanoBRET technology mode of action. (1) The fluorescent probe binds to the receptor of choice tagged with the Nluc protein. (2) On the addition of the substrate furimazine, Nluc catalyses the breakdown of furimazine to bioluminescence light that in turn excites the fluorophore at its excitation wavelength. (3) This produces a large BRET signal that can be measured using a bioluminescence plate reader such as the BMG-Pherastar FS. (4-5) In the presence of a high concentration of non-fluorescent competing inhibitor, eg: propranolol, the BRET ratio is reduced[71].

2.1.2.2.3 Saturation binding

The novel fluorescent probes were validated using the NanoBRET assay. This allows the ligand affinity constant K_D and the B_{max} to be calculated, in the same fashion as for the radioligand assay. A ligand binding with a K_D of 1 nM or less is said to have high affinity for its receptor whereas a ligand with a K_D of 1 µM has low affinity. The saturation binding assay can provide indications of receptor affinity and density.

ID		β_1		β_2		β_2/β_1
	Linkers	pK_D	n	pK_D	n	
		BY630/650-X				
38a	Gly-Ala	6.68±0.08	7	6.96±0.12	7	2
38b	Gly-Phe	6.42±0.27	5	6.37±0.10	5	1
38c	Gly-Tyr	6.60±0.06	7	6.61±0.09	7	1
38d	Gly-Ser	6.62±0.06	7	7.18±0.07	7	4
38e	Gly-Gln	6.99±0.06	7	7.64±0.05	9	4
39	Phe-Phe	<6.0	8	<6.0	7	-
40	β-Ala-β-Ala	7.44±0.08	7	7.57±0.11	7	1
Ref.	PEG 8	7.17±0.09	8	7.57±0.023	8	3
		BYFL				
41a	Gly-Ala	6.65±0.09	6	8.59±0.16	7	87*
41b	Gly-Phe	<6.0	6	6.92±0.08	8	-
41d	Gly-Ser	6.32±0.20	8	7.74±0.03	8	26*
42	Phe-Phe	<6.0	8	6.97±0.04	8	-
43	β-Ala-β-Ala	7.33±0.09	7	7.70±0.11	6	2
		BYFL-X				
44	β-Ala-β-Ala	7.67 ±0.08	7	8.02±0.11	6	5

Table 2-6| Fluorescent ligand pK_D values obtained *via* saturation binding. Nluc- β_1 and β_2-AR cells were treated with increasing fluorescent ligand concentration and incubated for 2h. After the addition of furimazine, the BRET ratio was measured. The pK_D values were obtained using Prism software (GraphPad Prism 6) by simultaneously fitting the total and non-specific saturation binding curves using the one site-total and nonspecific binding equation. Values are mean ± SEM for n separate experiments. *p <0.01, student unpaired t-test for difference in values obtained at the β_1 and β_2-ARs.

All fluorescent ligands gave a saturable signal at β_2 AR with a very low level of non-specific binding across the chosen concentration range (as illustrated in Figure 2-4). The unpaired student t-test was performed in order to validate the significance in receptor selectivity across the table; the results showed two compounds **41 a** & **d** that display a significant difference in selectivity between Nluc-β_1AR and Nluc-

β_2AR. Specific binding was observed with both fluorophores (BY630 and BYFL), which was inhibited by unlabeled propranolol (Figure 2-4).

It is worth highlighting that BYFL compounds displayed a lower signal-to-noise ratio due to the large degree of donor background emission present in the BRET acceptor channel. However, this did not affect the ratio between the bioluminescence and the fluorescent ligand. The data illustrated in Table 2-6 indicates that most of the BY630 ligands displayed no significant selectivity between the subtype β_2 versus β_1-AR, which is in accordance with the SPAP assay data. Compounds **41a** & **d** displayed the highest selectivity for β_2-AR, while compounds **41b**, **43** and **42** show no affinity toward β_1-AR versus β_2-AR.

Though the beta-ala-beta-ala amine was coupled to three distinct fluorophores (BY630, FL and X-FL), the pK_D data showed no significant difference between the respectively labelled ligands **40**, **43** and **44**. This might imply that the fluorophore composition has no effect on the final conjugate pharmacology for the chosen assay. The saturation assay also highlights that compound **43** does not bind to either β_2-AR or β_1-AR, which is in general agreement with SPAP data (see Table 2-5). Though the affinity values obtained using the SPAP assay are slightly higher than those of the saturation data, the difference in the affinity value can be attributed to differences in constructs (Nluc and CRE-SPAP) and cell types (CRE-SPAP CHO and Nluc-HEK 293) [65]. To obtain more definitive data, the logical approach was to perform whole cell binding experiments using radioligands.

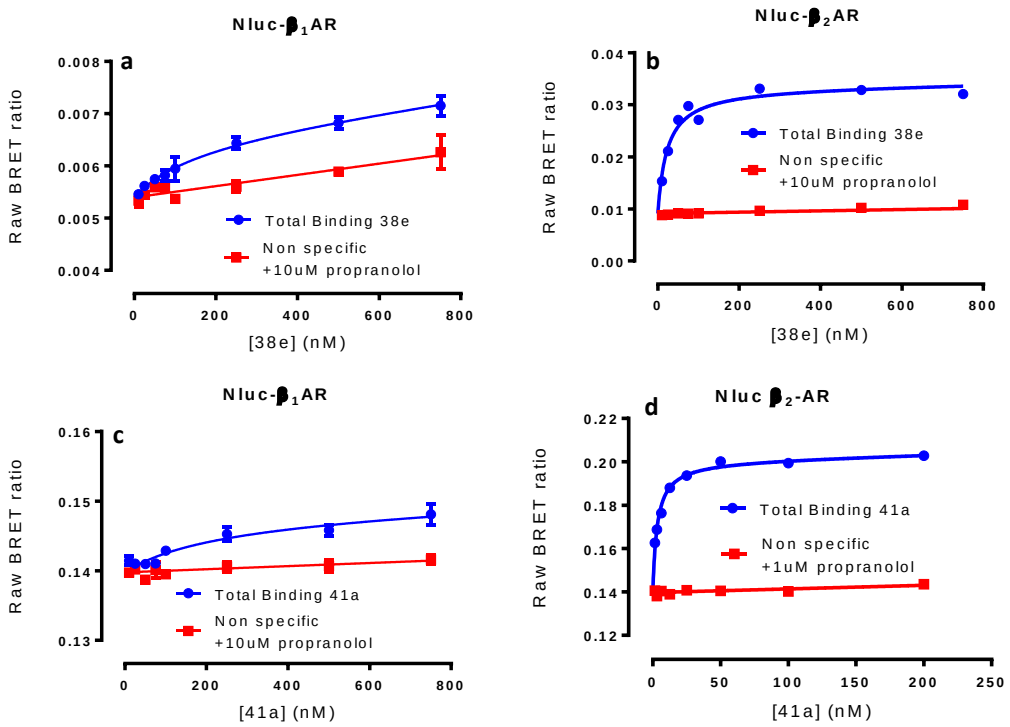

Figure 2-4| Fluorescent ligands saturation binding graphs. NanoBRET signal at Nluc-β_1AR and β_2AR treated with increasing concentrations of compounds **38e** (a & b) and **41a** (c & e) with nonspecific binding established with 10 µM propranolol. BRET was measured after furimazine addition and a 5 minutes equilibration period inside the PHERAstar FS plate reader. The graphs are representative separates experiments of (a & d) seven (b) nine, and (c) six separates experiments.

2.1.2.2.4 Competition binding

To further characterize the four chosen fluorescent ligands with the highest affinity at β_2-AR from saturation binding data, the next step was to perform some competition experiments (Figure 2-5). The Cheng-Prusoff correction was used to calculate the apparent pKi value for unlabelled ligands (CGP20712A, cimaterol, propranolol and ICI118544) treated with 10 nM fluorescent ligand **38e** (a), **41a** (b), **41d** (c) and **40** (d).

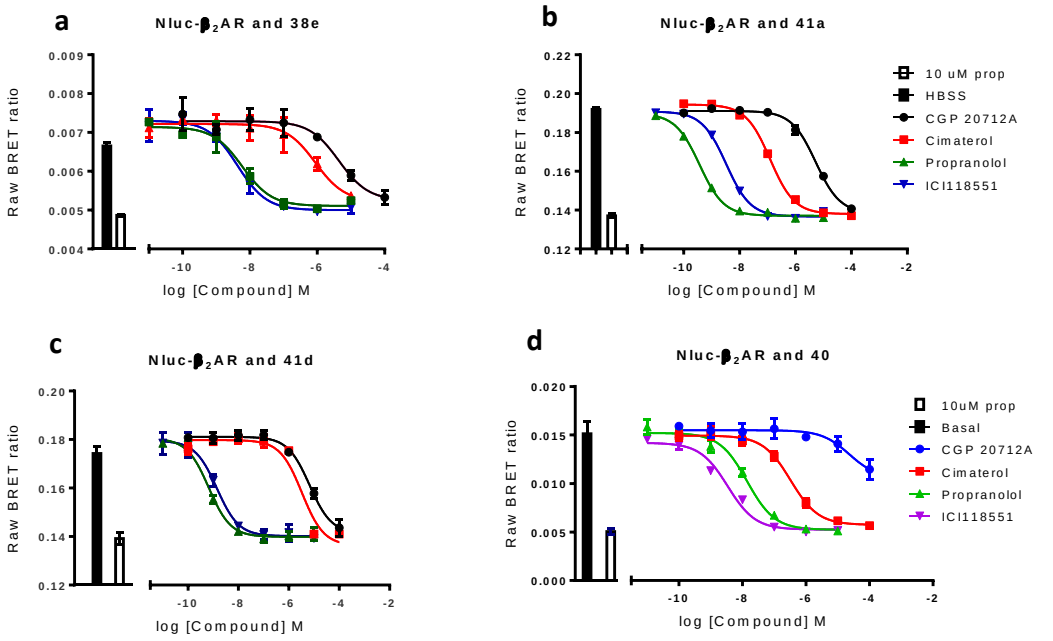

	10nM 38e		10nM 41a		10nM 41d		10nM 40		[^{3}H]-CGP12177 in CHO cells	
Ligands	pKi	n	pKi	n	pKi	n	pKi	n	pK_D	n
CGP20712a	5.08±0.13	5	5.58±0.09	7	5.53±0.28	5	4.84±0.08	5	6.11±0.05	4
Cimaterol	6.21±0.17	5	6.46±0.17	7	6.12±0.12	5	6.36±0.37	6	7.26±0.09	9
Propranolol	8.85±0.15	5	9.13±0.19	7	8.76±0.20	5	8.08±0.09	6	9.08±0.06	8
ICI118551	8. 89±0.10	5	8.98±0.13	7	8.92±0.12	5	8.57±0.11	6	9.26±0.03	12

Figure 2-5| Displacement binding of (a) **38e**, (b) **41a**, (c) **41d** and (d) **40** at the Nluc β_2-AR. The Cheng-Prusoff correction was used to calculate the apparent pK_i value for unlabelled ligands. BRET signal at Nluc-β_2 with increasing concentration of CGP20712A, cimaterol, propranolol and ICI118544 treated with 10 nM fluorescent ligand. Data points are ± SEM of triplicate determinations. The graphs are representative of n separate experiments. The reference data was performed using whole cell radioligand binding in CHO cells expressing the β_2-AR by Baker[4, 67].

However, Figure 2-5 also shows that **38e** (a) demonstrated a pK_i for CGP20712a which was 10-fold lower than the reference value of 6.11 previously obtained with radioligand binding studies. Across the table illustrated in Figure 2-5 all fluorescent ligands show the same trend for cimaterol. It is important to point out the fact that CGP20712a is a selective β_1-AR antagonist whereas cimaterol is a non-selective

agonist at β-AR[183]. The reference values were obtained by whole cell radioligand binding with different constructs (CRE-SPAP in CHO cells) instead of the Nluc-tagged receptors in HEK cells which were used for these experiments.

The fluorescent probes **38e** (a), **41a** (b), **41d** (c) and **40** (d) were also used as tracers for the elucidation of acetylated ligand pK_i value at the Nluc β_2-AR. Results were comparable for **38e** (a), **41a** (b) and **41d** (c) with SPAP assay obtained with CHO cells. However, probe **40** showed a pK_i for **36a** (Gly-Ala ac) that was 10-fold lower than the reference value of 8.41±0.11 previously obtained with functional assay (SPAP) studies (see section 2.1.2.2.1). The difference in affinity might reflect the differences between CHO and HEK 293 cells.

It is possible that the difference in ligand affinity is due to the fluorophore type or binding mode. This could explain the left shift in affinity observed with competing ligands. This hypothesis of binding mode might be further investigated *via* molecular modelling.

	β_2-AR					
	38e	**41a**	**41d**	**40**	**SPAP CHO**	
Linkers	pKi	pKi	pKi	pKi	pA_2	n
Gly-Ala	7.70±0.08	8.04±0.22	7.96±0.07	6.97±0.28	8.41±0.11	5
Gly-Phe	8.53±0.18	8.88±0.20	8.87±0.15	7.84±0.27	8.58±0.24	6
Gly-Tyr	8.63±0.13	9.23±0.24	8.88±0.19	7.78±0.13	8.89±0.16	10
Phe-Phe	7.63±0.12	8.29±0.16	8.09±0.12	7.17±0.06	8.53±0.10	5

Figure 2-6| Displacement binding of a fixed concentration (10nM) of **38e**, **40** and **41a** and **d** at the Nluc β_2-AR by acetylated ligands. Data points are ± SEM of triplicate determinations representative of (**38e** and **41d**) five, (**41a**) seven and (**40**) eight separate experiments.

Given that the green shifted fluorescent ligands used for this pilot study have low affinity for the β_1-AR, the competition experiment was repeated using compounds **38e** with known ligands and novel acetylated ligands.

At first glance, the graphs representing the displacement of known ligands show visible shifts with minimal errors when compared to the acetylated ligands graphs. The results illustrated in Figure 2-7 show that when compound **38e** was the tracer for the competition experiment with known ligands (CGP20712a, cimaterol, propranolol and ICI 118544), the pK_i values indicating the affinity for cimaterol is 10-fold lower at β_1-AR when compared to the reference. This difference in affinity value between the CHO cells in whole cell binding data was also seen in β_2-AR for cimaterol where the pK_i is 10-fold lower than its reference value. This raised some questions regarding the observed difference in affinity obtained using the two assays, such as whether this could be attributed to the cell type or binding mode of the ligands.

A series of competition binding experiments involving compounds **38e** with the acetylated ligands (**36a-c** and **41**) was performed to explore the low affinity question. The results showed that acetylated ligand (**41**) is 100-fold less selective at β_1-AR for **38e** as a tracer compared to β_2-AR (Figure 2-7). The acetylated ligands pK_i values correlation with SPAP data within the experimental error margin. To help address these questions, we ran parallel radioligand competition experiments using both CRE-SPAP CHO and Nluc HEK cell types in order to address the differences in affinity obtained by the SPAP and the Nluc binding assays.

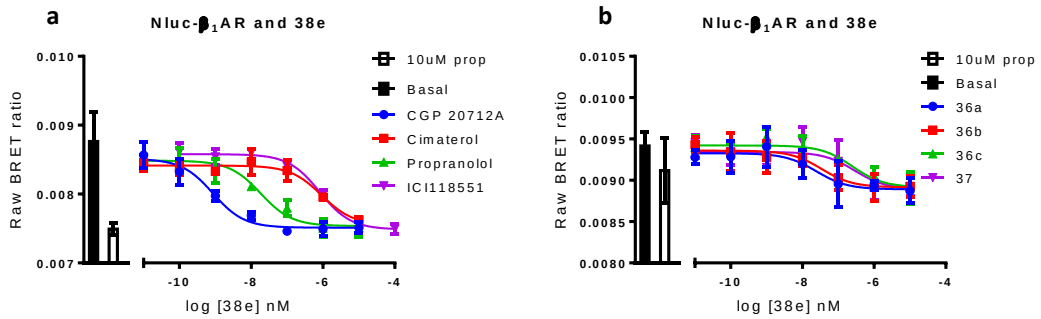

	100nM 38e		[^{3}H]-CGP12177 in CHO cells			100nM 38e		CRE- SPAP (CHO)	
Ligands	**pK_i**	**n**	**pK_i**	**n**	**Acetylated Ligands**	**pK_i**	**n**	**pA_2**	**n**
CGP20712a	8.47±0.23	6	8.82±0.03	10	36a	7.68±0.39	5	8.25±0.09	6
Cimaterol	5.75±0.40	6	6.57±0.06	11	36b	7.14±0.23	5	7.41±0.17	5
Propranolol	8.08±0.18	6	8.17±0.08	5	36c	7.18±0.30	5	7.58±0.18	10
ICI 118551	7.06±0.26	6	6.53±0.02	4	37	6.41±0.31	4	8.54±0.10	5

Figure 2-7| Displacement binding of **38e** at the Nluc β_1-AR. The Cheng-Prusoff correction was used to calculate the apparent pK_i value for unlabelled ligands. BRET signal at Nluc-β_1 with increasing concentration of CGP20712A, cimaterol, propranolol, ICI118544 and acetylated ligands treated with 100nM of fluorescent ligand above. Data points are mean ± SEM of triplicate determinations. The graphs are representative of n separate experiments. The reference data was obtained by Baker *et al.* using whole cell radioligand binding assay in CHO cells expressing the human β_1-AR[4, 67].

2.1.2.2.5 Radioligand Binding Assay

The binding affinity for novel fluorescent probes was determined by competitive displacement of the radioligand, [^{3}H]-CGP 12177 from CHO and Nluc cells expressing either β_1- or β_2-adrenoceptors.

ID	β_1-AR				β_2-AR			
	pK_i HEK	n	pK_i CHO	n	pK_i HEK	n	pK_i CHO	n
BY630/650-X								
38a	6.44 ±0.11	6	7.13±0.13	6	7.53±0.16	9	8.03±0.01	6
38b	6.18 ±0.11	6	6.91± 0.11	6	7.02±0.03	5	7.40 ±0.05	6
38c	6.54 ±0.07	6	7.15 ±0.04	6	7.35±0.05	7	7.80±0.05	6
38d	7.11 ±0.08	6	7.43±0.06	6	7.65±0.12	9	8.32±0.01	6
38e	6.81 ±0.04	6	7.39 ±0.08	6	7.42±0.09	7	8.12 ±0.04	6
39	5.92 ±0.07	6	6.33±0.11	5	6.24±0.13	6	7.11±0.20	5
40	7.34 ±0.05	6	8.60 ±0.12	5	8.38±0.13	7	8.94 ±0.09	6
Ref.	6.58 ±0.12	6	7.93±0.16	5	7.97±0.11	7	9.27±0.15	5
BYFL								
41a	6.41 ±0.10	6	6.77 ±0.16	6	8.60±0.11	6	8.37 ±0.10	6
41b	6.03 ±0.05	6	6.15±0.13	5	7.25±0.05	7	7.52±0.13	6
41d	6.40 ±0.04	6	6.91±0.19	6	8.43± 011	6	8.64 ±0.13	6
42	6.40 ±0.08	6	6.80 ±0.12	6	6.79±0.05	6	7.60±0.07	6
43	7.02 ±0.02	6	7.44±0.07	6	8.26±0.08	6	9.08±0.25	6
BYFLX								
44	7.41 ±0.11	6	7.92±0.04	6	9.01±0.22	7	9.26±0.05	6

Table 2-7| Whole cell competition binding for CHO CRE-SPAP and Nluc β_1& β_2-ARs. The Cheng-Prusoff correction was used to calculate the apparent pK_i value for fluorescent ligands. Data are mean ± SEM of pK_i values obtained in n separate experiments.

The results obtained from the whole cell radioligand binding assay are shown in Table **2-7** and compare results obtained in both Nluc HEK and CRE SPAP CHO

cell lines. There is a good correlation between pK_i values obtained for the fluorescent ligands for β_1 & β_2-AR (R^2 = 0.86). However, comparison of results for the two cell lines revealed differences in data obtained for certain compounds such as **40, 41a** & **d** and the reference PEG-8-propranolol. These are the same compounds for which the Nluc and CRE-SPAP assays gave dissimilar results for pK_D regardless of the receptor subtype. However, there is a significant difference in affinity between the SPAP and radioligands data for **41a** (p=0.03) and **39** (p=0.04), the general trend being that SPAP affinity values are higher than those of the cell binding data. Interestingly, the opposite trend is seen with the same compounds for the saturation binding data compared to the radioligand data. Overall, the results strongly suggest that the difference between data obtained using the CHO CRE SPAP assay and the Nluc HEK 293 saturation binding assay was largely due to cell type. Also, the radioligand data, particularly for β_2-AR closely match the Nluc fluorescent ligands saturation binding data when experiments are performed in the same cellular environments (Figure 1-8).

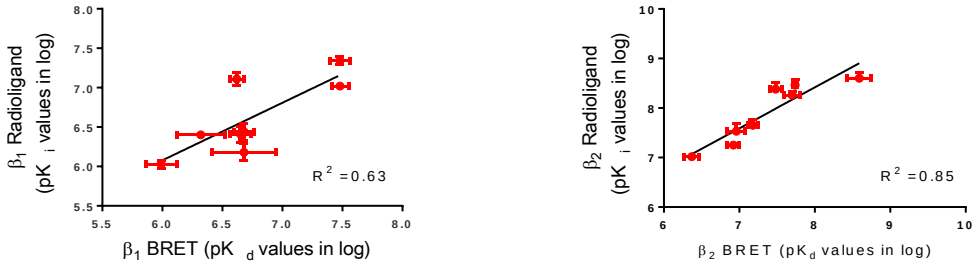

Figure 2-8| Correlation graphs of saturation binding and displacement binding of [^{3}H]-CGP12177 by the BY-630 and BY-FL fluorescent probes in HEK cells expressing either Nluc-β_1 or β_2-AR. Values are mean ± SEM of n (5-9) separate experiments. The Cheng-Prusoff correction was used to calculate the apparent pK_i value for each fluorescent ligand.

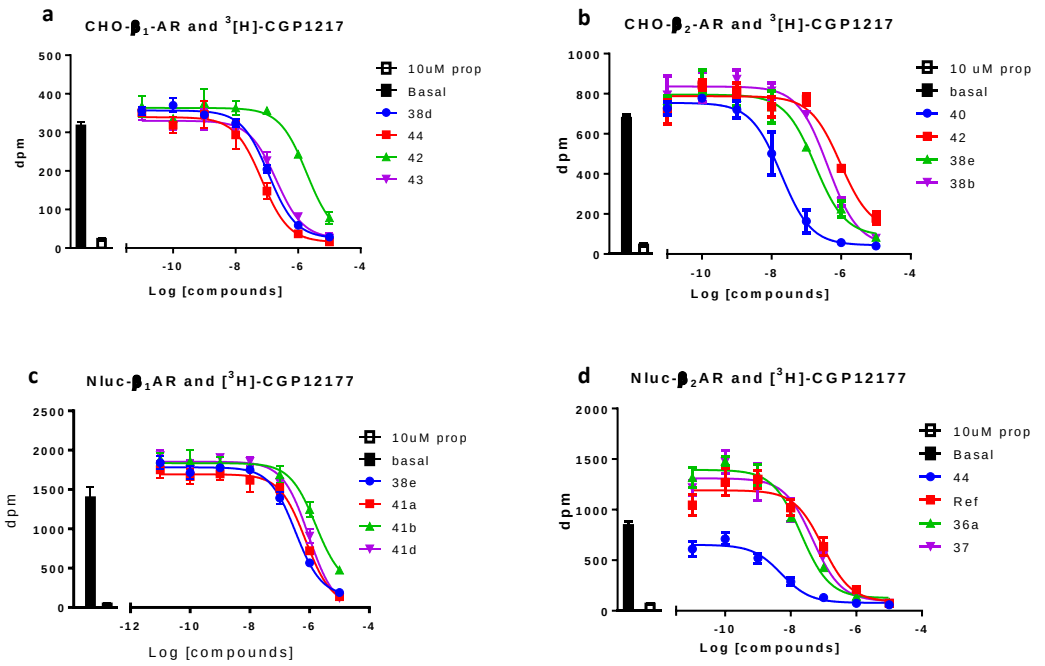

Figure 2-9| Displacement binding of [^{3}H]-CGP12177 in CRE-SPAP CHO and Nluc HEK cells expressing human β_1 & β_2-ARs. The Cheng-Prusoff correction was used to calculate the apparent pK_i value for fluorescent ligands. Data points are mean ± SEM of values obtained in n separate experiments. The graphs are representative of (a & c) six (b &) seven separates experiments

The data represented in Figure 2-9 show the inhibition of the binding of [^{3}H]-CGP12177 to CRE-SPAP CHO and Nluc cells expressing the human β_1 & β_2-ARs by the range of fluorescent ligands. Figure 2-9 (b & d) showed a competitive model of binding whereas β_1-AR data display less competition regardless of the cell type.

2.1.2.2.6 Confocal Imaging

Confocal imaging was used to study the dipeptide-linked fluorescent ligands, which allowed the visualisation of receptor localisation and pharmacology[140]. It is imperative that the fluorescent probes are suitable for imaging in biological

experiments, especially in live-cell imaging assays. A key prerequisite of a good fluorescent ligand is its ability to selectively bind to the target of choice with low intracellular uptake. Previously synthesised propranolol-based fluorescent ligands had issues with their imaging properties. They were very selective, however, they diffused readily into the cell cytosol within a timeframe of 30 minutes after their addition and imaging. First, the red emitting fluorescent ligands (**38a-e**) were imaged using the CRE-SPAP CHO cells. Compounds **38a-c** were chosen to illustrate the fluorescent probes' ability to visualise membrane binding at human β_1 and β_2-ARs in CHO CRE-SPAP cells. Membrane localisation observed was specific as it was prevented by pre-incubating the cells with non-fluorescently labelled propranolol (Figure 2-10).

A lower level of intracellular fluorescence was observed in cells expressing β_2-AR or β_1-AR. The β_1 adrenoceptor image showed an increased cytoplasmic signal, the fluorescent ligand (**38a-c**) appearing to have diffused through the membrane. It was clearly visualized that the fluorescent ligand had formed granules that were not seen at the β_2–AR. Both unspecific binding and granules were observed with all fluorescent ligands when binding at the β_1 adrenoceptor. The granules might be attributed to insolubility of the fluorescent ligands, precipitating out of solution during the incubation period, or to receptor internalisation.

In order to investigate the solubility or internalisation hypothesis, an alternative cell line, HEK 293 cell line expressing the human β_2-AR, was utilised. Selected ligands (**38d**, **40**, **41d** and **43)** were utilised for this part of the experiment.

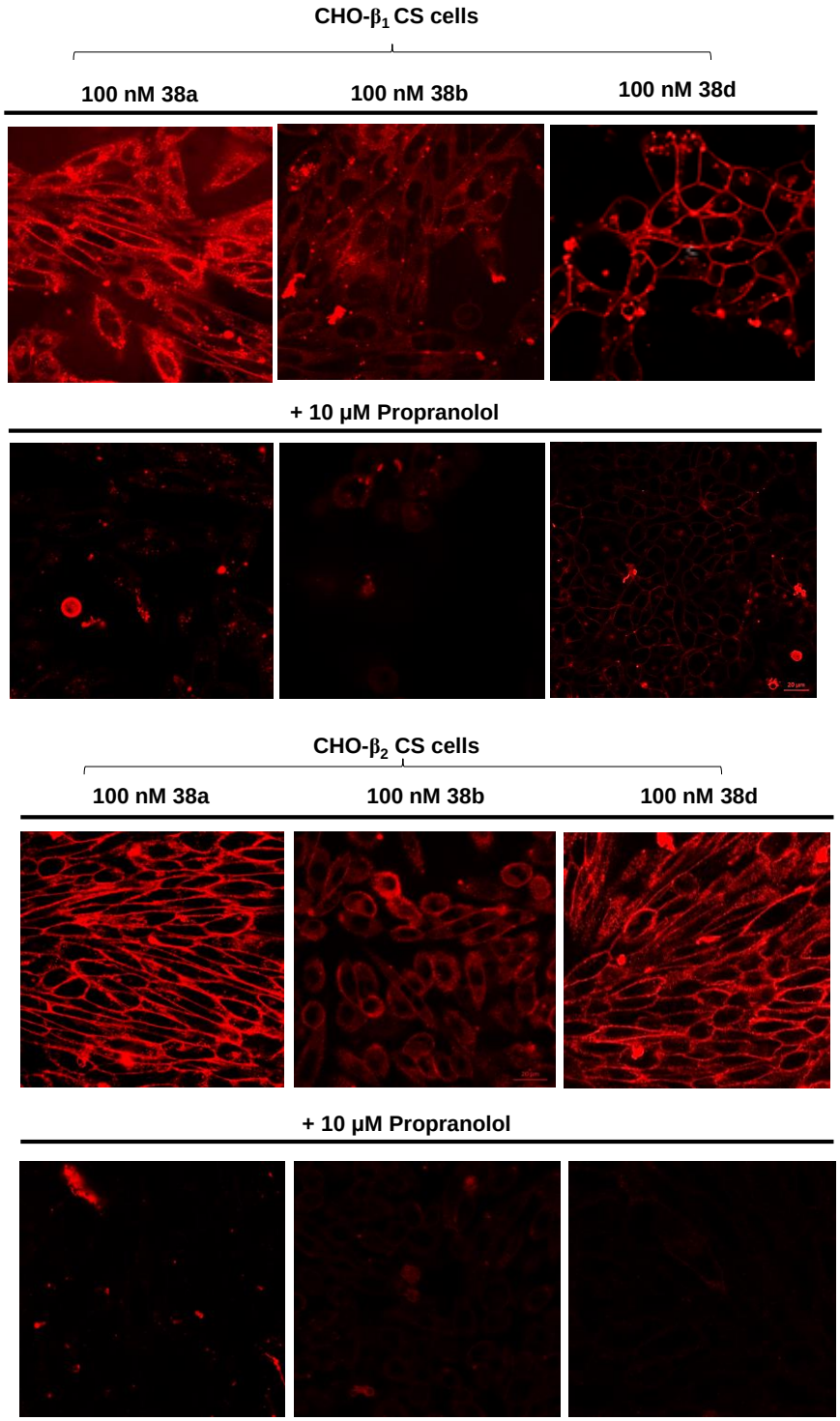

Figure 2-10| Live cell confocal images of 38a-c binding to the CHO-CS expressing human β_1 and β_2-ARs. Top panel, β_1 and β_2-AR CHO CRE-SPAP cells were incubated with (100 nM) **38a-c** and the bottom panel cells were pre-treated with the unlabelled propranolol for 30 minutes prior to the addition of **38a-c** for 60 minutes. Cells imaging was carried out in the continued presence of fluorescent ligands.

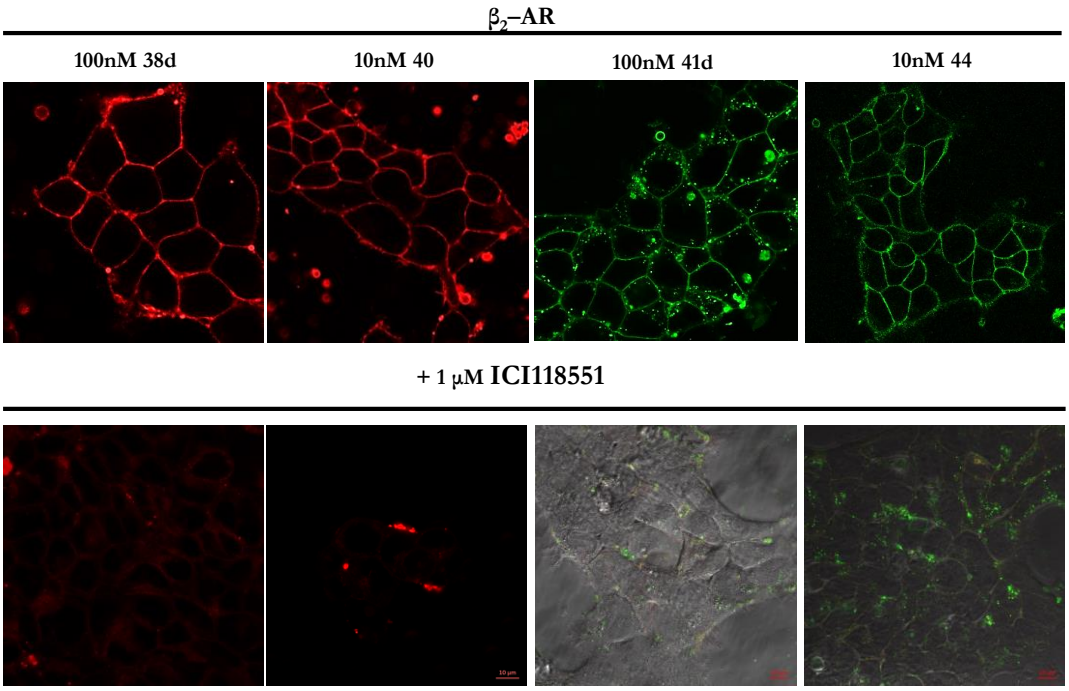

Figure 2-11| Live cell Confocal images of compounds **38d** & **40** and **41d** & **44** binding to HEK 293 expressing human β_2-AR. Top panel, cells were incubated with probes only and specific membrane localisation was observed. Bottom panel; cells were incubated with 1uM ICI 118544 to displace fluorescent ligand membrane binding. Cell imaging was carried out in the continued presence of fluorescent ligands. Scale bar = 20μm.

An ideal fluorescent probe would be selective, sensitive and show a low intracellular uptake[184]. Previous work in our laboratory by Vernall and colleagues focused on the development of dipeptide-linked fluorescent ligands for investigation of adenosine receptors. The results showed improved imaging properties and higher affinities and reduced plasma membrane intake[158]. This peptidic linker approach was in turn adopted for the adrenoceptor in order to improve the imaging properties of previous fluorescent ligands by Baker and colleagues[2]. A series of red- and green-shifted fluorescent probes were imaged at the β_2-ARs in HEK 293 cells.

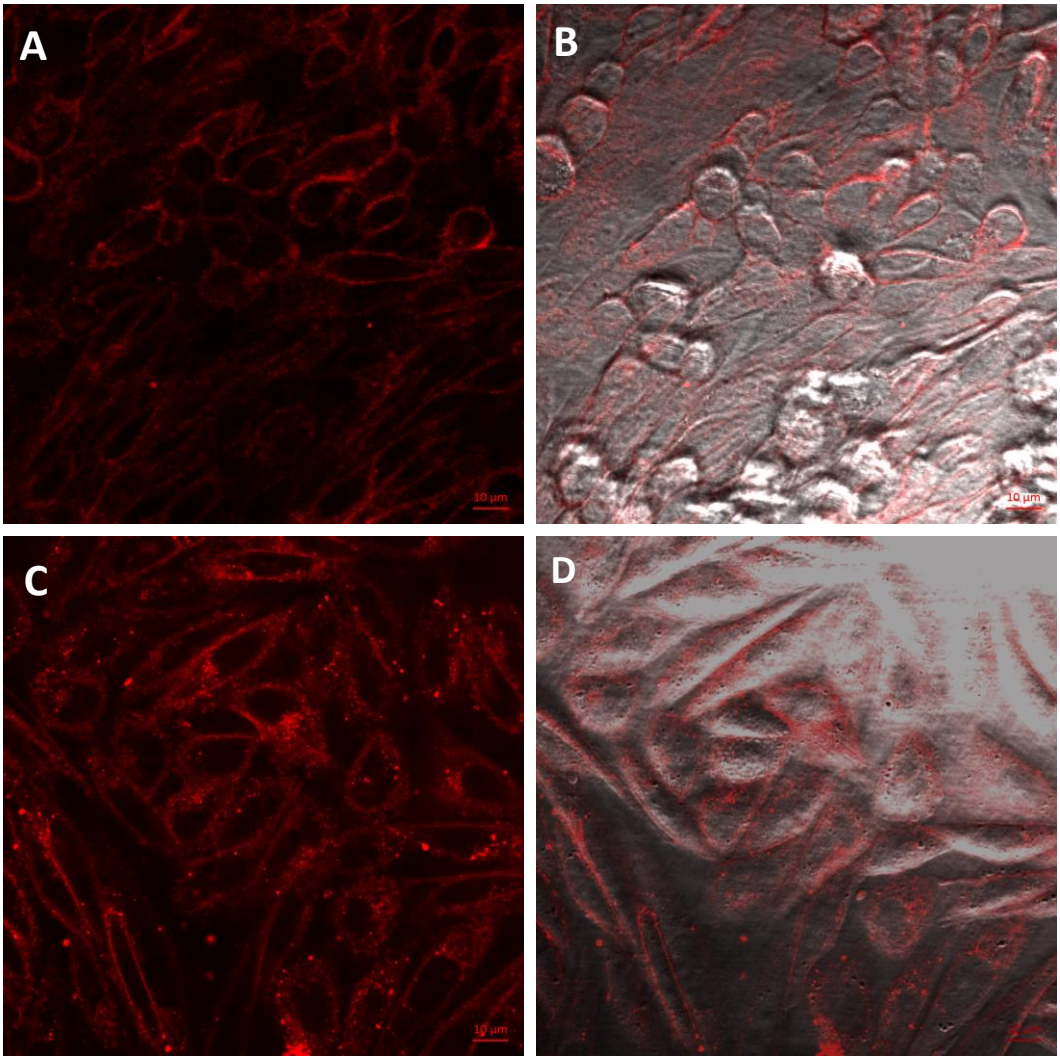

Figure 2-12|Live cell confocal imaging of PEG-8-propranolol (**15**) and compound **38e**. Cells were incubated with 10nM PEG-8-propranolol (a & b) and 100nM **38e** (c & d). The imaged window for PEG-8-Propranolol is 30 minutes whereas c& d showed an imaging window of 143 minutes after the addition of the fluorescent probe.

Green-emitting fluorescent compounds **41d** and **43** and their red counterparts **38d** and **40** showed selectivity for β_2-AR. Membrane localisation observed was specific for all compounds as it was inhibited by ICI118544 (10µM). Also levels of intracellular fluorescence for all compounds were low (Figure 2-11). However, it would appear that the chosen fluorescent ligands formed granules. They might be

suggestive of receptor internalization. Internalization of GPCRs occurs in response to activation of the receptor resulting in a redistribution of receptors away from the plasma membrane and towards endosomes[185, 186]. The results show an improvement in the imaging window to approximately 143 minutes after the addition of fluorescent ligands, compared this to PEG-8-propranolol BY630/650, which has a very short imaging window of approximately 30 minutes before the fluorescent probe diffuses into the cytosol (Figure 2-12). Also, the peptidic linkers have improved specific membrane binding that is inhibited by unlabeled propranolol or IC I118544.

2.2 Oxindole

An alternative core, the hydroxyindolin-2-one moiety was synthesised using the most selective dipeptide linkers' combination (Gly-Ala and Gly-Ser) from the naphthol series. The hydroxyindolin-2-one (oxindole) moiety was chosen because of its potential to be more potent and efficacious when compared to the naphthalene moiety.

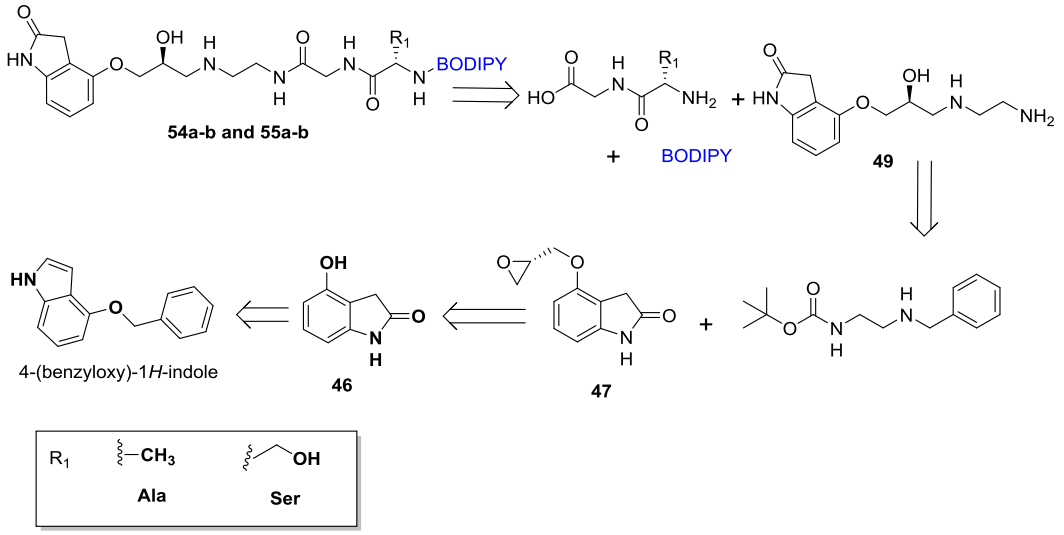

Scheme 2-11| Retrosynthetic route towards hydroxyindonlin-2-none moiety fluorescent ligands.

Both moieties may interact with the human β_2-adrenoceptors amino acid residues in the binding pockets. There might be a π-π interaction between the aromatic rings (naphthalene and oxindole) with Phe^{290} and hydrogen bonding interactions with Asn^{312} and Asp^{113}. Extra interaction include hydrogen bonding with Ser^{203} which might be exclusive to the oxindole moiety. The aim was to generate a series of fluorescent ligand that could selectively bind to either the high (β_{1H}-AR) or low (β_{1L}-AR) affinity binding sites of the β_1-AR adrenoceptor as it is for the [^{3}H]CGP 12177

[68]. Research has shown that β_{1L}-AR mediates the acute cardio-stimulant effects of some clinically relevant β-blockers (such as propranolol, pindolol and many others) while a high-affinity site (β_{1H}-AR) mediates blockade of the effects of catecholamines[187, 188]. The concept of two binding site may contribute to the design of highly specific drugs for treatment of heart failure and asthma[189]. Understanding the pharmacology of the 2nd low affinity binding site will help in terms of drug discovery and delivery process. Ongoing research in our lab on the non-fluorescent oxindole-base compounds are showing promising results regarding the two site binding hypothesis. The development of highly potent and selective fluorescent ligands that are able to interact with distinct β_1-AR binding site might be beneficial for drug design and discovery program. This will provide further details into β_{1L}-AR binding site roles in normal physiology parameters and their therapeutic implications in disease state[190].

Four fluorescent ligands were synthesised in the same manner as previously described (see section 2, for the design and synthesis of propranolol fluorescent ligands).

2.2.1 Chemistry

2.2.1.1 Fluorescent ligand synthesis.

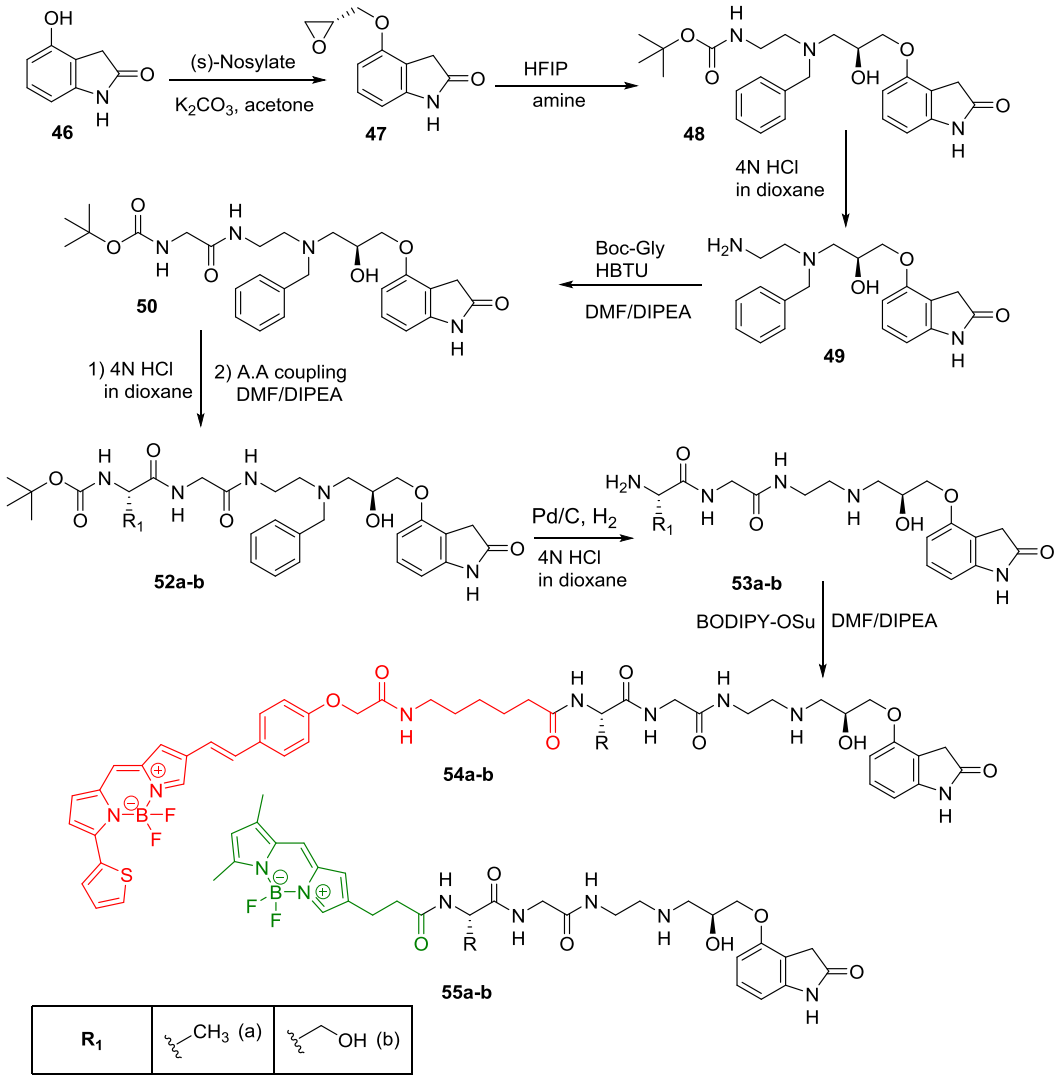

Scheme 2-12| Synthetic route for dipeptide-linked fluorescent ligand synthesis.

A series of reactions were undertaken in order to synthesize the second tranche of fluorescent ligands (illustrated in Scheme 2-12). A solution of 4-benzyloxyindole in *tert*-butanol was reacted with *N*-bromosuccinimide (NBS) in an electrophilic

substitution reaction to form a bromo-intermediate that quickly hydrolyses to the desired product **45** in the presence of water or weak acid[191, 192].

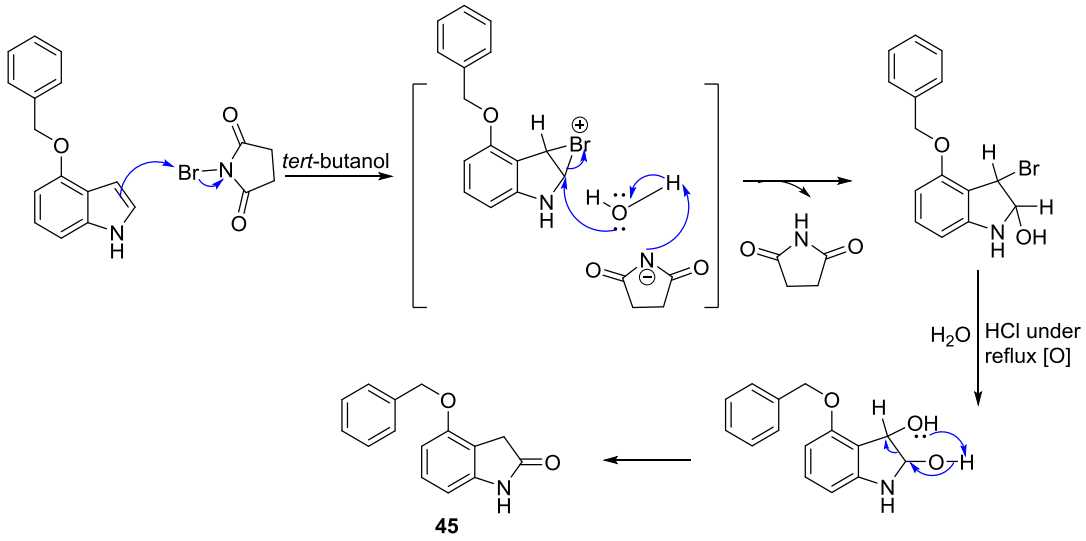

Scheme 2-13| Mechanism of a 4-alkoxy indole bromination and oxidation into a 2-oxindole (**45**).

The reaction was monitored *via* LC-MS, which showed one main peak and a minor peak. The main peak at 2.66 min, with a mass of 240 Da, corresponded to the desired product, the 2-oxindole. Whereas the minor peak, with a mass of 302 Da, was attributed to a bromo intermediate (bromination that occurred elsewhere on the aromatic ring). The formation of the oxindole was confirmed *via* infrared spectroscopy. The infrared spectra showed a very strong peak at 1679.24 cm^{-1} which confirms the presence of the carbonyl group. The ^{1}H- NMR showed loss of a proton at 7 ppm corresponding to the indole CH and singlet at 10 ppm corresponding to the NH chemical shift. The ^{13}C-NMR showed the appearance of a chemical shift at 179 ppm that can be attributed to the carbonyl present in the 2-oxindole.

The benzyl protecting group was removed *via* hydrogenolysis to yield compound **46**. The racemic epichlorohydrin was used in many attempts, however the reaction remain unsuccessful. Epichlorohydrin was reacted either under microwave radiation or at room temperature with various conditions; however, there was a full conversion to the *bis*-adduct (as illustrated in Scheme 2-14) therefore the chiral pure (*S*)-(+)-glycidyl nosylate was used. Previous high affinity propranolol-based fluorescent ligands by Baker *et al*.[2] were synthesized with the *S* enantiomers. Nosylate was the ideal alkylating agent compared to tosylate or mesylate because maintain the stereochemistry (97:3)[193]. In parallel, the epoxide **47** was synthesised from **46** and (*S*)-(+)-glycidyl nosylate in acetone with potassium carbonate as a base[194].

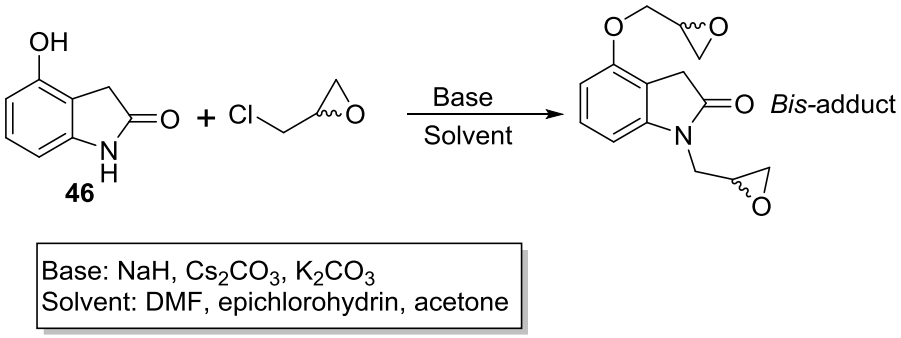

Scheme 2-14| The attempted synthesis of the epoxide **447**.

Compound **48** was synthesised from its precursors, **47** and the commercially available *tert*-butyl (2-(benzylamino)ethyl)carbamate, in hexafluoropropan-2-ol (HFIP) *via* nucleophilic epoxide ring-opening at 90°C for 20 minutes under microwave radiation. The benzyl protecting group was removed by hydrogenolysis using 10% palladium-on-carbon and hydrogen in MeOH to afford compound **49**.

The core molecule was then coupled to the *tert*-butyl carbamate (Boc) glycine in the presence of *N,N,N',N'*-tetramethyl-O-(1H-benzotriazol-1-yl)uronium hexafluorophosphate (HBTU) and *N,N*-diisopropylethylamine (DIPEA) in DMF to afford compound **48**. The ^{1}H- NMR confirmed that no coupling was seen on the oxindole NH given that NH chemical shift was still visible in the NMR spectrum at 10 ppm. Then, the Boc protecting group was removed using 4N HCl in dioxane to afford the amine salt intermediate. This was followed by coupling of the respective *N-Boc* protected amino acids; alanine (Ala) or serine (Ser) in the same fashion as previously described to yield two distinct congeners. Following the final Boc deprotection, as previously described, the amine congeners were coupled to the commercially available fluorophores, (BODIPY-X-630/650-OSu) and (BODIPY-FL-OSu) illustrated in Scheme 2-12 to yield the second tranche of fluorescent ligands (**54a-b** red and **55a-b** green). The novel fluorescent compounds were isolated and purified as previously stated with the propranolol-based ligands.

2.2.2 Pharmacology

After the novel oxindole fluorescent probes were synthesised, they were initially characterised with a NanoBRET saturation assay. As previously discussed, the K_D values from the NanoBRET saturation assay were comparable to the radioligand binding assays data in the same cellular environment. Results showed that most of the compounds had a greater affinity for β_2-AR than β_1-AR (Figure 2-13). Compounds **54a** and **55b** displayed the highest affinity for β_2-AR and **54b** and **55a-b** do not bind to β_1-AR (Table 2-8). This trend was also apparent in the propranolol

derived fluorescent ligands. From these preliminary study, it can be summarised that amino acid residues Gly-Ala and Gly-Ser in conjunction with the BYFL fluorophore do not favour ligand binding at the β_1-AR, hence driving the selectivity toward β_2-AR instead. The logical step is to tease out the orthosteric head effect on the binding to the adrenoceptor with respect to the bioluminescence assay, NanoBRET.

Linker			**β_1-AR**				**β_2-AR**	
	Oxindole	n	Propranolol	n	Oxindole	n	Propranolol	n
				BY630/650				
Gly-Ala	7.15±0.14	9	6.68±0.08	7	7.88±0.10	7	6.62±0.06	7
Gly-Ser	<6	9	6.62±0.06	7	7.29±0.29	7	7.18±0.07	7
				BYFL				
Gly-Ala	<6	9	6.65±0.09	6	<6	7	8.59±0.16	7
Gly-Ser	<6	9	6.32±0.20	8	7.44±0.14	7	7.74±0.03	8

Table 2-8|NanoBRET saturation pK_D values between the orthosteric heads: naphthol and oxindolol. Data are mean ± SEM of n separate experiments**.** Nluc- β_1 and β_2-AR cells were treated with increasing fluorescent ligand concentration and incubated for 2h. After the addition of furimazine, the BRET ratio was measured. The pK_D values were obtained using Prism software (GraphPad Prism 6) by simultaneously fitting the total and non-specific saturation binding curves using the one site-total and nonspecific binding equation. Values are mean ± SEM for n separate experiments.

Table 2-8 data clarifies some observations regarding the ligand moieties:

- Naphthalene moiety shows moderate affinity for β_1-AR compared to the indolin-2-none (oxindole), which show no affinity for β_1-AR except for **54a**.
- Fluorescent ligands have similar affinity for β_2-AR regardless the orthosteric moiety except for the oxindole-Gly-Ala FL that does not bind to this receptor as well.

This interesting observation regarding the dipeptide linker synergy with the BYFL fluorophore is favouring the naphthol moiety instead of the oxindole. In regards to the effect of the linker on ligand-binding, Jacobson and others have suggested that upon ligand binding, the linker creates contact with receptor regions that enable the fluorescent conjugate to engage in molecular recognition with the receptor of interest[159]. The results in Table 2-8 clearly highlight the difference in the orthosteric moiety rather than the linker amino acid residues impact on the final conjugate within the NanoBRET assay. Also, the data may be highlighting the importance of the aromatic hydrophobic interaction for the binding to occur in the β_2-AR binding pocket with residues such as Phe[290]. When comparing the linker Gly-Ala coupled to BY630/650, regardless of the ligand moieties, it does not imbue subtype selectivity between the β_1 and β_2-ARs. Given that the alanine side chain is a methyl group; it might be that the probes are not engaging in specific molecular recognition when in contact with the receptor.

Intriguing that the same linker (Gly-Ala) coupled to the BYFL fluorophore has a subtype selectivity that is greater than two-fold between the β_1 and β_2-ARs in propranolol has an adverse effect on the oxindole moiety. Compound **55a** does not binds to either β_1 or β_2-ARs in the Nanoluc®-tagged cell lines. It might be that the ligand is not binding to the receptor because of the Nanoluc® construct. This was seen with compound **39 (**propranolol-Phe-Phe-BY630/650), which did not bind to the β_2-AR in the NanoBRET assay, while it had a moderate affinity for the β_2-AR ($pA_2 = 6.94 \pm 0.06$) in the functional assay, SPAP. Given that the BRET assay is a

proximity assay, it might be possible that the fluorophore is not in close proximity with the luciferase donor, Nanoluc® therefore the BRET signal is reduced.

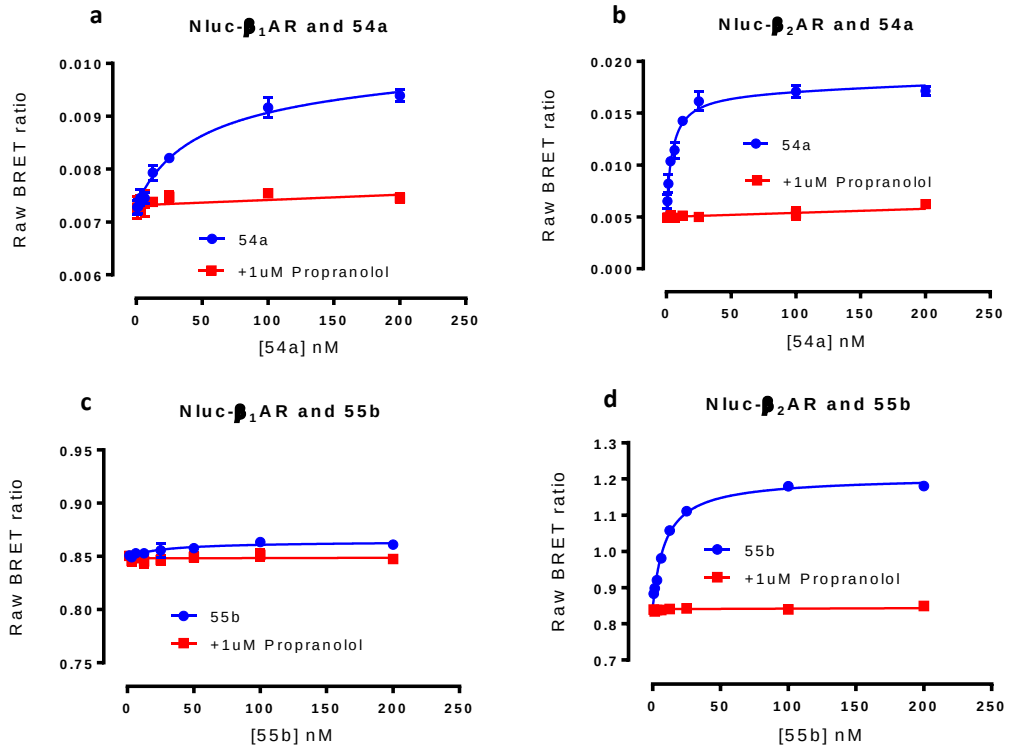

Figure 2-13| Saturation binding for oxindole fluorescent ligands at either human β_1-AR or β_2-AR tagged with an *N*-terminal Nluc tag (a-d). The single experiments are representative of (a & c) nine and (b & d) seven separates experiments.

3 CONCLUSION AND FUTURE WORK

3.1 Summary

A series of β-adrenoceptors dipeptide-linked fluorescent and acetylated ligands were successfully synthesised. The novel dipeptide-linked fluorescent ligands were characterised with functional assays, binding assays and confocal microscopy techniques. The seventeen ligands displayed a range of binding affinities primarily favouring β_2-AR over β_1-AR. They displayed different physiochemical properties with linker chemistry varying from dipeptides with glycine given that it contained no side-chain to explore the requirements of the second amino acid for optimum binding (e.g. Gly-Ser) **38e** to ones with the same amino acid repeated in the linker (e.g. Phe-Phe) **42**. The amine congeners have been coupled to three distinct BODIPY fluorophores (BY630/650-X, BYFL and BYFL-X). The novel probes have been used as imaging tools in CHO and HEK 293 cells stably expressing the human β_1 and β_2-ARs.

The fluorescent ligands were made of three entities: the orthosteric binding moiety, the fluorophore and the linker which joined the two components together. The idea was to ensure that all regions of the fluorescent ligand contribute to the overall conjugate's physiochemical and pharmacological properties[160]. Jacobson *et al.*[159] have previously suggested purposely engineering the fluorescent ligand linker in order to introduce useful groups, which may improve the overall ligand selectivity and affinity[159]. Vernall *et al.*[158] then conclusively demonstrated that the linker's physiochemical properties can influence the overall selectivity and affinity of a fluorescent ligand and its imaging properties. The use of a carefully engineered

dipeptide linker, designed on the basis of SAR considerations, converted a non-selective adenosine receptor antagonist into an A_3-selective high affinity fluorescent probe[158].

Previously synthesised propranolol-base fluorescent ligands did not meet all the requirements of a good fluorescent probe. Confocal microscopy studies showed that the fluorescent probe had a very short imaging window. Approximately 30 minutes after the probe addition, probe diffusion inside the cell cytosol from the cell membrane was observed. Therefore the dipeptide linker was introduced in order to improve on propranolol-based ligands imaging properties.

3.1.1 Propranolol

In this study, manipulation of ligands by the introduction of a dipeptide linker resulted in the generation of some promising compounds. The results were compared and contrasted between either cell types (HEK 293 and CHO) or assay utilized.

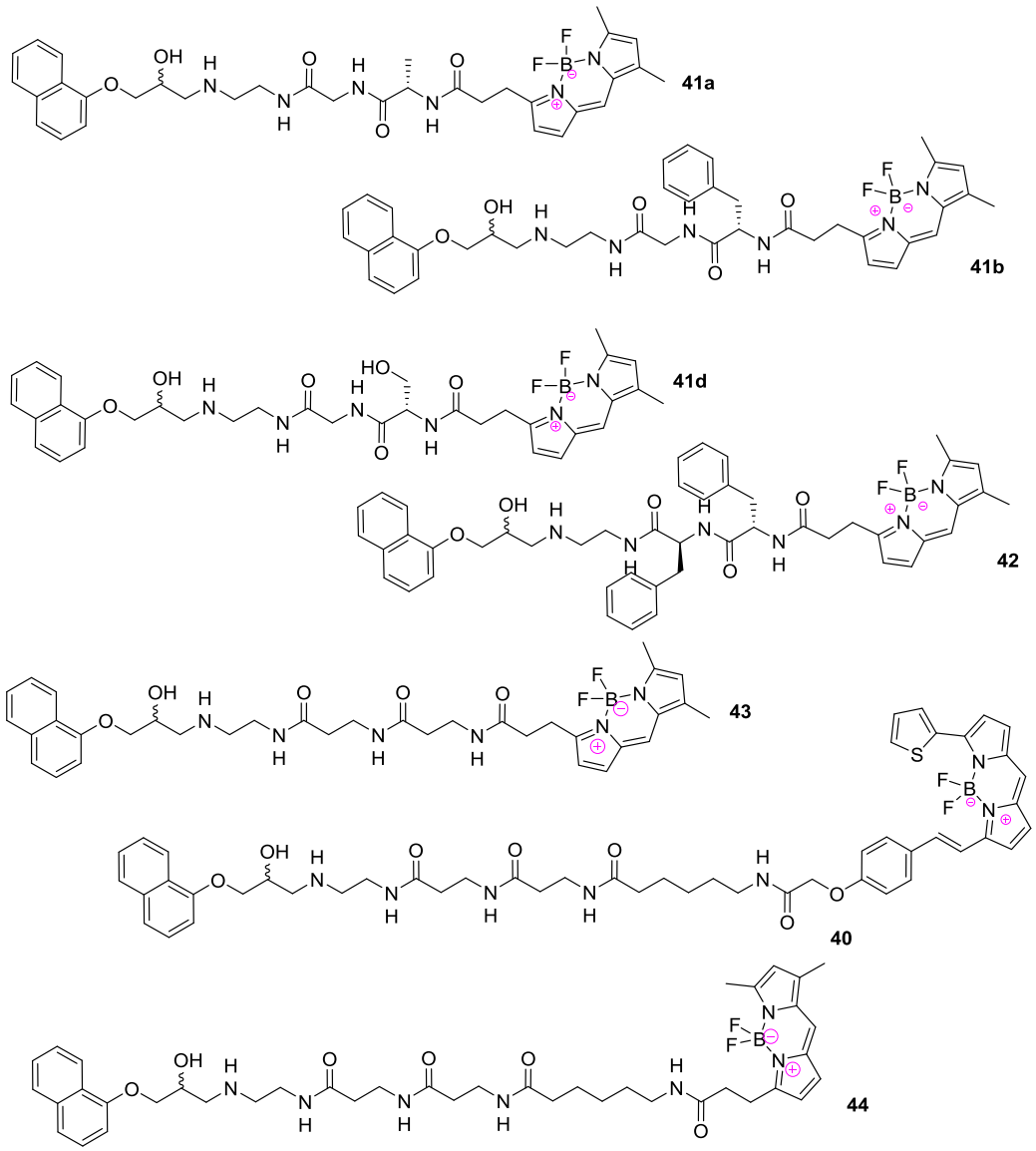

Figure 3-1| Selected propranolol-based fluorescent probes that displayed interesting pharmacological profile at the β-AR.

3.1.1.1 SPAP in CHO vs NanoBRET in HEK 293

In general, affinity values obtained in functional SPAP assays were approximately 10-fold higher than those obtained in direct BRET ligand-binding studies; except for the reference compound PEG-propranolol BY630/650 (**Ref.**) and propranolol-

gly-ala-FL (**41a**), which show the inverse trend. In both assays, compounds **41a** and **41d** displayed more selectivity for β_2-AR (100-fold) when compared to β_1-AR. The difference in affinity between the functional assay SPAP and NanoBRET is most likely to be cell type related (CHO versus HEK 293 cells). Furthermore, compounds **39** (Phe-Phe-BY630/650), **41b** (Gly-Phe-FL) and **42** (Phe-Phe-FL), did not bind to β_1-AR in either assays. Meanwhile, compound **42** shows moderate selectivity for β_2-AR versus β_1-AR with partial agonist action that is not mediated by β_2-AR in SPAP assay.

3.1.1.2 NanoBRET vs radioligand binding in HEK 293

There was a good correlation between the NanoBRET and displacement data from the radioligand assay for β_2-AR (R^2=0.85) compared to β_1-AR (R^2=0.63). The reference ligand PEG-8-propranolol showed no difference between the two assays. Radioligand results showed that compounds **41a** and **41d** displayed the highest affinity for β_2-AR (155- and 115-fold selectivity), which was confirmed both the NanoBRET and SPAP assays. For the beta alanine ligands, compound **44** was the most potent at β_2-AR; it is 40-fold more selective at β_2-AR compared to 17- (**43**) or 11-fold (**44**). In general radioligand data and saturation data are comparable within experimental error.

3.1.1.3 Radioligand binding: CHO vs HEK 293 cells

There was a good correlation between the data regardless of the cell lines used [β_1 and β_2-AR (R^2=0.86)]. However, compound **44** showed a significant difference in affinity, it was 18-fold higher for β_1-AR in CHO cell than in HEK 293 cells. This cell type difference was also highlighted when performing the NanoBRET displacement assay, using **40** as a tracer for known ligands cimaterol, propranolol, ICI18551 and CGP20712a. There was an average of 10-fold decrease in affinity for all unlabelled ligands.

3.1.1.4 Live cell imaging

Dipeptide-linked propranolol derivatives were designed and synthesized in order to improve the imaging time of previous ligands synthesized by Baker *et al*[2]. The PEG-8-linked propranolol showed good affinity and selectivity toward β_2-AR (pK_D =7.4 and 9.4) but had a short imaging time of approximately 30 minutes; and readily diffuses into the cytosol from the cell membrane. Peptide linkers (as shown with the adenosine ligands) promoted better membrane binding and lower levels of non-specific binding and cellular uptake. This was the goal for the beta-adrenoceptor ligands. Although the majority of synthesized fluorescent probes were non-selective, they showed varying degrees of specific membrane-binding which was displaced by either propranolol or ICI18551. Encouragingly, this project has produced novel dipeptide-linked fluorescent ligands that can be used as imaging tools in order to characterize β-adrenoceptor in recombinant cells and maybe progress to primary cells.

3.1.2 Oxindole

The dipeptide-linked oxindole fluorescent ligands were synthesised in order to determine possible interaction of the orthosteric head with the receptor in order to improve the fluorescent ligand affinity and selectivity for a specific β-AR subtypes. The preliminary results of the bioluminescence assay, NanoBRET, showed that none of the ligands bound to β_1-AR except for compound **54a**. It also showed that **55a** does not bind to either β_1 or β_2-ARs. Given that these results are preliminary, further studies such as functional assays, imaging and radioligand binding are required in order to fully characterise the oxindole dipetide-linked fluorescent ligands.

3.2 Future Work

A range of red and green emitting fluorescent ligands have been synthesised and pharmacologically characterised using various assays. Future work needs to further explore the screening assays for the oxindole dipeptide-linked fluorescent ligands (**54a-b** and **55a-b**) in order to fully characterise and understand their pharmacological profile, as previously performed with propranolol-derived fluorescent ligands.

There is a need to further scrutinize the effects of compounds **42** and **40**. Compound **42** showed an interesting profile in terms of its partial agonist effect on β_2-AR binding, which was not inhibited by propranolol. This might imply a novel alternative binding pocket at β_2-AR. The alternative binding pocket hypothesis

could be investigated with kinetic and dimerization studies. There was a possibility that **42** is binding to an orthosteric pocket of a dimerised receptor or it is displaying a new pharmacology, which might imply that there is an alternative binding site at the β_2-AR.

Additionally, compound **40** displayed discrepancy between two different cell lines (CHO CRE SPAP and HEK 293 Nluc) when used as a tracer ligand for Nanoluc® displacement assay and in radioligand binding experiments. This needs further investigation in terms of negative cooperativity[195]. The remaining 11 propranolol derived probes (red and green ligands) can be investigated as outlined below.

3.2.1 Molecular Modelling

Previous pharmacological data have shown that most fluorescent ligands displayed no significance in selectivity between the β-AR subtypes (β_1 and β_2). This lack of selectivity was somewhat expected since the same orthosteric head was used and it was hoped that the introduction of a dipeptide linker might lead to β-AR subtype selectivity. Given that the assays utilised in this project have provided the empirical data on a suite of fluorescent probes such as affinity values in functional and binding assays; it is currently possible to explore whether molecular modelling can be used as a tool to rationalise the modest selectivity seen. And if so, then there is the opportunity to use this model to help design even more selective ligands which could then find application in primary cells that potentially express multiple beta-adrenoceptor subtypes.

3.2.2 Combinatorial Chemistry

Given that only seven amino acid residues were used as part of the dipeptide linkers, there is perhaps potential for optimisation of the linker. There are 22 proteinogenic (naturally occurring in protein) and synthetic amino acids residues[196] that can be incorporated as part of the linker though they have to be chosen carefully to avoid side reaction when conducting the chemistry. Combinatorial chemistry is ideal to address the lack of diversity on the linker chemistry and accelerate the synthesis process. It may provide support with the dipeptide linker synthesis by allowing various combinations of the amino acid residue to be used and hence yield a library that creates the best combination needed for subtype selectivity in β-AR[197]. In order for the combinatorial chemistry to be implemented, the protecting group strategy had to be optimised.

3.2.3 Extending Linker Size

When designing and synthesising fluorescent ligands, the choice of linker chemistry and size is very important. It has been proven in the case of adenosine receptors and β-AR that linker length impacts on the overall pharmacology of the final conjugate[131, 198]. Given that the majority of dipeptide linkers have not imparted significant subtype selectivity between β_1 and β_2–ARs; the obvious alternative to the dipeptide-linker might be extension of the linker size to tri- or tetrapeptides. In the quest for subtype selectivity, molecular modelling might again help with amino acid selection. As it would propose possible interactions (ligand-protein) that can be

formed between the amino acids in the binding pocket and the fluorescent ligand linker, and hence could make predictions on the fluorescent probes' biological activities[199].

This project has confirmed that subtle changes in the linker, such as introducing amino acid an integral part of the linker make-up, has potential benefit in the overall pharmacological of the final conjugate as seen in the adenosine project.

3.2.4 Working with human primary cells

For decades, recombinant cell lines have played a key role in research for the investigation of cell function and processes. However they do not accurately represent cellular processes because when generated, they often differ genetically and phenotypically from their primary cells (tissue of origin) due to cellular transformation (changes in expression profile)[200]. In contrast, primary cells maintain many of the important markers and functions seen in vivo[201]. Screening the novel dipeptide-linked fluorescent probes with human cardiomyocytes or pulmonary epithelia cells will provide higher quality research data and subsequently a better understanding of complex cellular processes in beta adrenoceptor pharmacology.

4 EXPERIMENTAL

4.1 General Chemistry

4.1.1 Synthesis

4.1.1.1 Materials

Chemicals and solvents were purchased from standard suppliers and used without further purification. BODIPY-630/650-X-SE (BY-630/650) and BODIPYFL (BY-FL) were purchased from Molecular Probes (Invitrogen, United Kingdom). Thin layer chromatography (TLC) plates were supplied by Merck Kieselgel; flash column chromatography (FCC) cartridges were supplied by Biotage (Cardiff, Wales). Standard and deuterated solvents were purchased from Fisher (England), VWR (England) and Sigma-Aldrich Company Ltd (England).

4.1.1.2 Techniques

Unless otherwise stated, reactions were carried out at room temperature. Reactions were monitored by LC-MS and TLC on commercially available pre-coated aluminium and silica backed plates (Merck Kieselgel 60 F254). General staining was carried out with Ninhydrin (solution in ethanol), $KMnO_4$ or phosphomolybdic acid (PMA). Visualisation was performed by examination under UV light (254 and 366 nm). All organic extracts after aqueous work-up procedures were dried over Na_2SO_4 before gravity filtering and evaporation to dryness. Organic solvents were evaporated *in vacuo* at $\leq$ 40°C (water bath temperature) using a Büchi rotary evapotator. Flash chromatography was performed using an Isolera, FlashMaster III.

Analytical LC-MS were performed on a Shimadzu UFLCXR system coupled to an Applied Biosystems API2000. The column by default used was Phenomenex Gemini-NX 3µm-110A C18, 50x2mm with the flow rate 0.5ml/min. UV detection was recorded at 220 (channel2) and 254nm (channel1). The short gradient: Pre-equilibration run for one min at 5% B; then method run: 5 to 98% solvent B in 2min, 98% B for 2min, 98 to 10% B in 0.5min then 10% for one min. Solvent A: 0.1% formic acid in water; solvent B: 0.1% formic acid in MeCN (system 1).

System 2: YMC reverse-phase C8 column (150 x 4.6 mm) with a flow rate of 1.00 mL/min and the UV detection at 254nm. Samples were run using a linear gradient 5% - 95% solvent B over 35 minutes. Solvent A: 0.1% formic acid in water; solvent B: 0.1% formic acid in MeCN

System 3: YMC reverse-phase C8 column (150 x 10 mm) with a flow rate of 4.00 mL/min and the UV detection at 254nm. Samples were run using a linear gradient 5% - 95% solvent B over 25 minutes. Solvent A: 0.1% formic acid in water; solvent B: 0.1% formic acid in MeCN

System 4: Phenomenex Gemini reverse-phase C18 column (100 x 10 mm), using a flow rate of 4 mL/min and UV detection at 254 nm. Samples were run using a linear gradient 5% - 95% solvent B for 25 minutes. Solvent A: 0.1% formic acid in water; solvent B: 0.1% formic acid in MeCN.

Preparative HPLC was performed using a Phenomenex Luna reverse-phase C8 column (150 x 30 mm), a flow rate of 20.00 mL/min and UV detection at 254 nm. Samples were run in a linear gradient 5% - 95% solvent B for 19 minutes. Solvent

A: 0.1% formic acid in water; solvent B: 0.1% formic acid in MeCN. Analytical RP-HPLC was used to confirm that all final products were >95% pure using (system 5).

High-resolution mass spectrum (HRMS) - time of flight, electrospray (TOF ES +/-) were recorded on a Waters 2795 separation module/micromass LCT platform. Melting points (Mp) were recorded on a Reichert 7905 apparatus or Perkin Elmer Pyris 1 differential scanning calorimeter and were uncorrected. Proton nuclear magnetic resonance (^{1}H NMR) spectrum were recorded on a Bruker-AV 400 at 400.13 MHz and the ^{13}C NMR spectrum were recorded at 101.62 MHz. Chemical shifts (δ) are recorded in parts per million (ppm) with reference to the chemical shift of the deuterated solvent or an internal tetramethylsilane (TMS) standard. Coupling constants (*J*) are recorded in Hz and the significant multiplicities described by singlet (s), doublet (d), triplet (t), quadruplet (q), broad (br), multiplet (m), doublet of doublets (dd), doublet of triplets (dt).

4.1.1.3 General Procedures

A: Hydrogenation

To a solution of benzyl/Cbz protected compound (1 equiv.) in 20 mL of ethanol and ethyl acetate mixture (7:3) was added 10% Pd/C (10 equiv.) and was stirred at room temperature. The mixture was degassed using 2 cycles of vacuum then nitrogen flush and placed under an atmosphere of hydrogen *via* a balloon. The suspension was stirred at room temperature for 18h then filtered on a celite pad under reduced pressure. The celite was washed (x 4) with methanol and the combined filtrate solution was evaporated in vacuo to afford the titled compounds. The product was used without further purification.

B: Amino acid activation and coupling

Boc-Amino acid (1 equiv.), HBTU (1 equiv.) and DIPEA (7 equiv.) was dissolved in DMF and was stirred for 30 minutes. The amino acid solution was then added to the amine solution (1 equiv.) in DMF (5 mL). The solution was then stirred at room temperature for 18 h. The solvent was evaporated *in vacuo* and the residue dissolved in saturated NH_4Cl (50 mL) and extracted with EtOAc (3x50 mL). The combined organic extracts were washed with saturated NaCl (2x50 mL) and dried over anhydrous Na_2SO_4. The organic extracts were concentrated under reduced pressure to yield the desired product. The crude product was purified *via* silica gel flash chromatography employing a gradient of 0 to 10% 1N NH_3 in MeOH/DCM as eluent to afford the title compound.

C: Boc deprotection

To a solution of the Boc-protected compounds in dichloromethane (1 mL) was added 4N HCl in dioxane (1 mL), and the mixture was stirred for 1 h. The solvent was removed under reduced pressure to give the intermediate product as the hydrochloride salt in quantitative yield, which was then used without further purification.

D: Amine acetylation with succinic anhydride

A solution of amine dihydrochloride (1 equiv.) in DMF with DIPEA (2 equiv.) was stirred for 5 minutes at room temperature. To the above solution, *N*-acetoxysuccinimide was immediately transferred into the mixture and the reaction was stirred for 12h. The excess solvent was removed under reduced pressure, and

the residue was purified by semi-preparative RP-HPLC to afford the desired products. All six acetylated congeners were observed to elute as single and symmetrical peaks at the retention time $R_{t;}$ and their purities were further analyzed by performing a second analytical HPLC (system 2). The eluted clear solution was ion-exchanged with Amberlyst a-21-ion exchange resins and freeze-dried to afford white amorphous solids. The identities of all the compounds were further analyzed by HRMS (TOF ES^+). The compounds tested in biological systems were of ≥95% purity.

E: Fluorescent ligand coupling

A solution of amine dihydrochloride (2 equiv.), DIPEA (4 equiv.), and the fluorophore-SE (1 equiv.) was stirred in DMF (1 mL) with the exclusion of light for 12 h. The solvent was removed under reduced pressure, and the residue was purified by semi-preparative RP-HPLC. All fluorescent probes were observed to elute as single and symmetrical peaks at the retention time R_t and their purities were further analyzed by performing a second analytical HPLC by system 2, 3 and 4. The Amberlyst a-21-ion exchange resins were stirred for 20 minutes in MeOH and the excess solvent was decanted (x3); and the fluorescent compounds were also dissolved in MeOH. The eluted blue solution was ion-exchanged with Amberlyst a-21-ion exchange resins and freeze-dried to afford blue amorphous solids. The identities of all the compounds were further analyzed by HRMS (TOF ES^+). The compounds tested in biological systems were of ≥ 95% purity.

4.1.2 Propranolol

(±)-2-((naphthalen-1-yloxy)methyl)oxirane (20)

NaH (60% in mineral oil) (1.66 g, 69.36 mmol, 2 equiv.) was dispersed in anhydrous DMF (35 mL) under an atmosphere of nitrogen at room temperature. To this vigorously stirred suspension was added a solution of 1-naphthol (5.00 g, 34.68 mmol) in anhydrous DMF (35 mL). The resulting pale green suspension was stirred at room temperature for 30 min. Epichlorohydrin (9.51 mL, 121.38 mmol, 35 equiv.) was added drop-wise into the solution and stirred overnight at ambient temperature. The mixture was quenched cautiously with methanol (50 mL) and partitioned between a large excess of water (100 mL). The aqueous slurry was extracted with EtOAc (3x 50 mL). The combined organic extracts were washed with aqueous 2M NaOH (50 mL) and dried over anhydrous $MgSO_4$ and the organic extracts were concentrated under reduced pressure1-3. The crude product was further purified by flash column chromatography (eluent EtOAc/ petroleum ether 1:9) to afford the titled compound as a colourless oil (6 g, 86 %).

^{1}H NMR ($CDCl_3$): δ 2.87(1H, dd, J=2.7/2.7Hz), 2.98 (1H, t, J= 4.8Hz), 3.51-3.43 (1H, m), 4.16 (1H, dd, J=5.6/5.6Hz), 4.41 (1H, dd, J=3.1/3.12Hz), 6.82-6.80 (1H, m), 7.39-7.34 (1H, m), 7.53-7.43 (3H, m), 7.83-7.79 (1H, m), 8.37-8.30 (1H, m).

^{13}C NMR ($CDCl_3$): δ 44.96, 50.41, 69.16, 105.15, 121.04, 122.18, 125.44, 125.83, 126.66, 127.60, 128.29, 134.71, 154.

LC-MS: 2.86 min, m/z: theo. 200.24; meas. [MH^+] 201.3 (system 1)

Benzyl 2-aminoethylcarbamate (21)

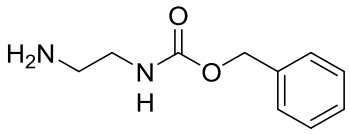

A solution of benzyl chloroformate (4.99 mL, 35.00 mmol, 1 equiv.) in $CHCl_3$ (20 mL) was added drop-wise (3 h) to a stirred solution of 1,2-diaminoethane (10.52 mL, 175.00 mmol, 5 equiv.) in $CHCl_3$ (50 mL) at 0°C. The reaction mixture was cooled to room temperature and stirred for 18 h. The reaction mixture was concentrated, and the residue partitioned between EtOAc (50 mL) and H_2O (20 mL). The organic layer was washed with H_2O (3x 50 mL), and the combined aqueous phases were discarded. The organic layer was washed with 2M HCl (aq) (3x 50 mL), and the aqueous layers were combined, adjusted to pH 12 (solid NaOH), and saturated with NaCl (solid). Following extraction with EtOAc (3x 50 mL), the combined organic fractions were washed with brine (2x 50 mL), dried, and evaporated to yield the title compound as a clear oil (5.6 g, 82 %), which were used without further purification[157].

^{1}H NMR ($CDCl_3$): δ 2.78-2.75 (2H, t, J=5.8Hz), 3.21-3.16 (2H, m), 5.06 (2H, s), 5.42- (1H, s), 7.35-7.26 (5H, m).

^{13}C NMR ($CDCl_3$): δ 41.73, 43.82, 66.73, 128.08, 128.09, 128.10, 128.52, 128.51, 136.62, 156.71.

LC-MS: 0.44 min, m/z: theo.194.11; meas. [MH^+] 195.26 (system 1)

(±)-Benzyl 2-(2-hydroxy-3-(naphthalen-1-yloxy)propylamino)ethylcarbamate (22).

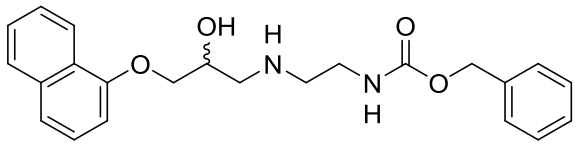

Epoxide **24** (1.00 g, 5 mmol) and Cbz protected diamine **25** (3.97 g, 20.44 mmol, 4 equiv.) were dissolved in HFIP (20 mL) and stirred at room temperature for 44 h[166]. The solvent was evaporated under reduced pressure and the crude material was purified by flash column chromatography on silica employing a gradient from 0 to 15% 1N NH_3 in MeOH and DCM as eluent to afford the title compound as an off-white solid (1.96 g, 83%).

^{1}H NMR ($CDCl_3$): δ 2.95-2.80 (6H, m), 3.21 (2H, d, *J*=5.1Hz), 4.17 (2H, dd, *J*=5.6/5.6Hz), 4.21 (1H, s), 5.09 (2H, s), 5.41 (1H, s), 6.81 (2H, d, *J*=7.6Hz), 7.37-7.27 (5H, m), 7.51-7.41 (3H, m), 7.81-7.79 (1H, m), 8.25-8.23 (1H, m).

^{13}C NMR ($CDCl_3$): δ 49.31, 51.91, 66.90, 66.94, 68.67, 70.63, 88.20, 104.99, 120.7, 121.71, 125.43, 125.65, 125.83, 126.50, 127.70, 128.15, 128.20, 128.26, 128.28, 130.49, 134.71, 154.18 , 156.73.

MP: 119.6 °C- 121.1°C.

LC-MS: 2.27 min, m/z: theo. 394.42; meas. [MH^+] 395.1 (system 1)

(±)-1-(2-aminoethylamino)-3-(naphthalen-1-yloxy)propan-2-ol (**23**).

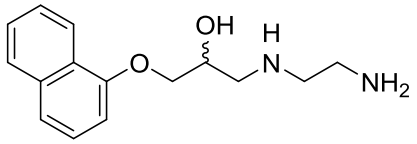

Compound **27** was synthesized *via* general procedure A to afford the title compound as a transparent oil (0.80 g, 72.8%).

^{1}H NMR ($CDCl_3$): δ 2.95-2.80 (6H, m), 3.21-3.16 (2H, d, *J*=5.1Hz), 4.19 (2H, dd, *J*=5.6/5.6Hz), 4.18 (1H, s), 5.09 (2H, s), 5.41 (2H, s), 6.79 (2H, d, *J*=7.6Hz), 7.51-7.41 (3H, m), 7.81-7.79 (1H, m), 8.25-8.23 (1H, m).

^{13}C NMR ($CDCl_3$): δ 41.73, 43.82, 51.79, 68.42, 70.42, 106.99, 122.75, 124.13, 124.74, 125.08, 125.43, 125.83, 126.50, 127.57, 154.71.

LC-MS: 0.55 min, m/z: theo. 260.15; meas. [MH^+] 261.3 (system 1).

(±)-*Tert*-butyl-(2-((2-((2-hydroxy-3-(naphthalen-1-yloxy)propyl)amino)ethyl)amino)-2-oxoethyl)carbamate (**24**).

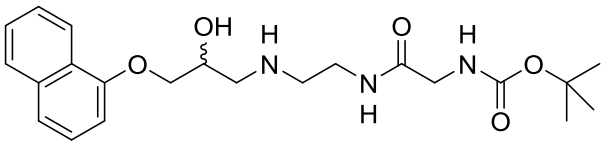

Compound **28** was synthesized *via* general procedure B to afford the title compound as a transparent oil (0.97 g, 87%).

^{1}H NMR ($CDCl_3$): δ 1.50 (9H, s), 2.95-2.80 (6H, m), 3.18 (2H, d, *J*=5.1Hz), 4.14 (2H, dd, *J*=5.6/5.6Hz), 4.18 (1H, s), 5.09 (2H, s), 5.41 (2H, s), 6.80-6.78 (2H, d, *J*=7.6Hz), 7.51-7.41 (3H, m), 7.81-7.79 (1H, m), 8.25-8.23 (1H, m).

^{13}C NMR ($CDCl_3$): δ 30.30, 30.32, 30.34, 41.73, 45.75, 50.50, 53.79, 68.42, 70.42, 80.30, 104.99, 120.7, 121.45, 121.49, 125.81, 125.84, 125.86, 126.50, 127.57, 135.61, 154.18, 156.73, 164.73.

LC-MS: 2.42 min, m/z: theo. 417.50; meas. [MH^+] 418.5 (system 1)

***Tert*-butyl ((2*S*)-1-((2-((2-hydroxy-3-(naphthalen-1-yloxy)propyl)amino)ethyl)amino)-1-oxo-3-phenylpropan-2-yl)carbamate (25).**

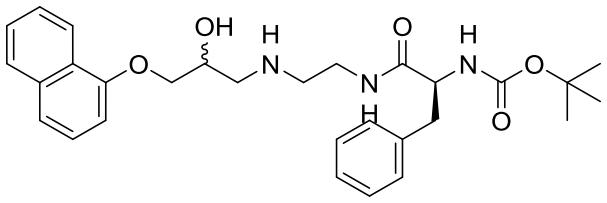

Compound **29** was synthesized *via* general procedure B to afford the title compound as a transparent oil (0.110 g, 80%).

^{1}H NMR (CD_3OD): δ 1.34 (9H, s), 3.28-2.80 (2H, m), 2.88-2.67 (6H, m), 3.67 (2H, d, *J*=5.3Hz), 4.06 (1H, m), 4.03-3.99 (1H, m), 4.16-4.09 (3H, m), 4.85 (1H, s), 6.83-6.79 (2H, d, *J*=7.4Hz), 7. 24-7.14 (4H, m), 7.33-7.31 (3H, m), 7.42-7.36 (3H, m), 7.77-7.75 (1H, m), 8.18-8.15 (1H, m).

^{13}C NMR (CD_3OD): δ 27.32 (3), 37.22, 38.08, 53.56, 56.55 (2), 59.27, 68.05, 68.42, 68.13, 70.14, 70.19, 104.50 (2), 119.95, 121.79, 124.71, 125.61, 125.95, 126.28, 126.76, 127.01, 127.99, 128.89, 138.91, 154.42, 172.69.

LC-MS: 2.49 min, m/z: theo. 507.53; meas. [MH^+] 508.5 (system 1)

(±)-*Tert*-butyl (3-((2-((2-hydroxy-3-(naphthalen-1-yloxy)propyl)amino)ethyl)amino)-3-oxopropyl)carbamate (26)

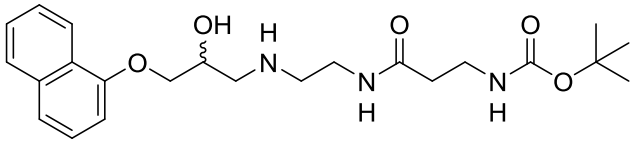

Compound **30** was synthesized *via* general procedure B to afford the title compound as a transparent oil (0.200 g, 50%).

^{1}H NMR (CD_3OD): δ 1.40 (9H, s), 2.88-2.67 (3H, m), 3.92-3.78 (4H, m), 4.06 (2H, m), 4.03 (1H, s), 4.20-4.11 (2H, m), 5.35 (1H, s), 6.83-6.79 (2H, d, *J*=7.4Hz), 7. 24 (1H, m), 7.33 (1H, s), 7.42-7.36 (1H, m), 7.64-7.62 (3H, m), 8.12 (1H, s), 820-8.25 (1H, m), 8.30-8.27 (1H, m).

^{13}C NMR (CD_3OD): δ 28.42(3), 38.12, 39.13, 42. 65, 50.50, 52.72, 68.05, 68.42, 69.89, 70.79, 104.50, 119.95, 125.36, 127.01, 127.99, 128.89, 135.74 (2), 154.12, 154.96, 174.59. **LC-MS:** 2.27 min, m/z: theo. 431.52; meas. [MH^+] 432.5 (system 1)

(±)-2-amino-*N*-(2-((2-hydroxy-3-(naphthalen-1-yloxy)propyl)amino)ethyl)acetamide dihydrochloride (27)

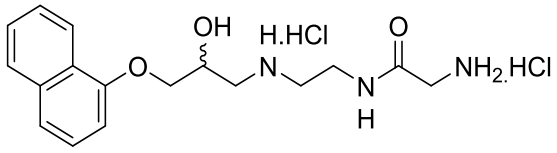

This compound was synthesised *via* protocol C to yield an orange solid (0.80 g, 86%), which was dried and used without further purification.

^{1}H NMR (DMSO-d$_6$): δ 2.85-2.50 (4H, m), 3.14-3.01 (4H, m), 4.09 (1H, s), 4.16-4.06 (3H, m), 4.28-4.16 (2H, m), 5.09 (2H, s), 5.41 (1H, s), 6.80-6.78 (2H, d, J=7.6Hz), 7.35-7.30 (2H, m), 7.44-7.36 (3H, m), 7.681 (1H, s), 7.79-7.74 (2H, m), 8.27-8.21 (2H, m)

^{13}C NMR (DMSO-d$_6$): δ 38.60, 44.40, 44.78, 50.82, 68.25, 70.56, 104.82, 120.7, 121.71, 122.50, 125.07, 125.21, 126.50, 127.57, 134.38, 154.21, 171.03.

LC-MS: 2.66 min, m/z: theo. 319.52; meas. [MH$^+$] 318.3 (system1)

(2*S*)-2-amino-N-(2-((2-hydroxy-3-(naphthalen-1-yloxy)propyl)amino)ethyl)-3-phenylpropanamide dihydrochloride (28)

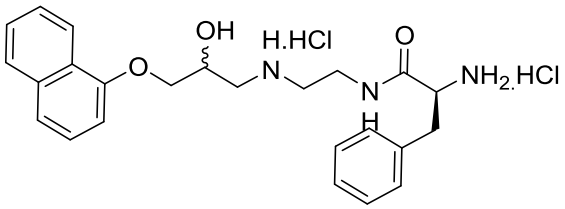

Compound **32** was synthesized *via* general procedure B to afford the title compound as a transparent oil (0.100 g, 85%).

^{1}H NMR (DMSO-d$_6$): δ 2.83-2.49 (4H, m), 3.45-3.20 (5H, m), 3.95 (1H, s), 4.20-4.00 (4H, m), 5.41 (1H, s), 6.23 (1H, m), 7.21 (4H, s), 7.25 (1H, m), 7.44-7.36 (4H, m), 7.97-7.85 (2H, m), 8.55 (1H, m), 8.98 (1H, s)

^{13}C NMR (DMSO-d$_6$): δ 39.75, 40.87, 50.12, 53.52, 55.95, 70.22, 71.44, 109.02, 119.53, 124.87, 126.31 (2), 127.41 (3), 128.41 (2), 129.11 (2), 135.10 (2), 136.78 (1), 156.33(1), 169.01 (1)

LC-MS: 2.03 min, m/z: theo. 407.50; meas. [MH$^+$] 408.50 (system1)

(±)-3-amino-*N*-(2-((2-hydroxy-3-(naphthalen-1-yloxy)propyl)amino)ethyl)propanamide dihydrochloride (29)

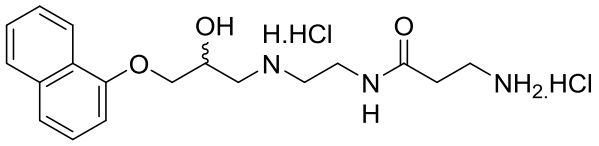

Compound **33** was synthesized *via* general procedure B to afford the title compound as a transparent oil (0.260 g, 67%).

^{1}H NMR (DMSO-d$_6$): δ 1.80 (2H, s), 2.84-2.60 (6H, m), 2.95 (2H, m), 3.70 (2H, m), 4.12 (1H, s), 4.22-4.10 (3H, m), 6.32 (2H, m), 7.55 (1H, m), 7.65 (3H, m), 8.10 (1H, s), 8.13 (1H, m), 8.35 (1H, m)

^{13}C NMR (DMSO-d$_6$): δ 38.22, 41.61, 41.70, 51.42, 55,53, 75.56, 82.09, 110.71, 121.41, 124.83, 126.04, 126.42, 127.50, 127.57, 128.61, 136.41, 156.21, 177.03.

LC-MS: 2.11, m/z: theo. 331.42; meas. [MH$^+$] 332.4 (system1)

***Tert*-butyl ((2*S*)-1-((2-((2-((2-hydroxy-3-(naphthalen-1-yloxy)propyl)amino)ethyl)amino)-2-oxoethyl)amino)-1-oxopropan-2-yl)carbamate** (**30a**).

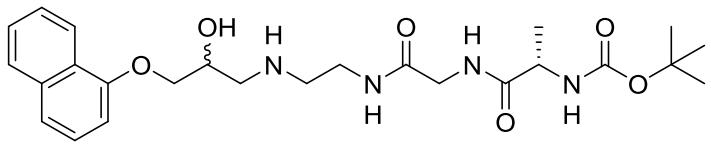

Compound **30a** was synthesized *via* general procedure B to afford the title compound as a yellow oil (0.67 g, 83%).

^{1}H NMR (CDCl$_3$): δ 1.45 (9H, s), 2.97-2.50 (4H, m), 3.87-3.79 (2H, m), 3.99-3.89 (2H, m), 4.18-4.00 (3H, m), 4.28-4.16 (2H, m), 5.28 (1H, s), 5.32 (1H, s), 6.80-6.78 (2H, d, *J*=7.5Hz), 7.35-7.30 (2H, m), 7.36-7.40 (1H, m), 7.44-7.36 (3H, m), 7.681 (1H, s), 7.80-7.66 (2H, m), 8.25-8.19 (1H, m,).

^{13}C NMR (CDCl$_3$): δ 17.82, 27.43, 27.50, 27.52, 43.42, 51.79, 54.43, 66.73, 67.07, 67.77, 69.58, 107.82, 120.40, 121.68, 125.11, 125.45, 126.27, 127.40, 127.49, 129.38, 134.71, 154.18, 157.73, 164.53, 171.44.

LC-MS: 2.17 min, m/z: theo. 448.2; meas. [MH$^+$] 449.3 (system 1)

***Tert*-butyl ((2*S*)-1-((2-((2-((2-hydroxy-3-(naphthalen-1-yloxy)propyl)amino)ethyl)amino)-2-oxoethyl)amino)-1-oxo-3-phenylpropan-2-yl)carbamate (30b).**

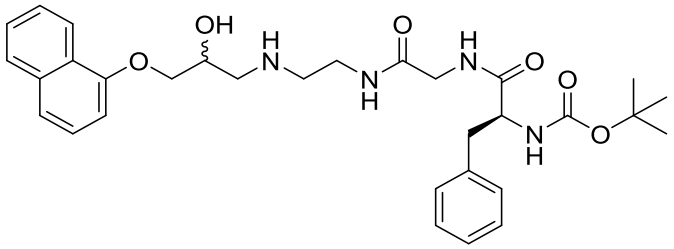

Compound **30b** was synthesized *via* general procedure B to afford the title compound as an orange oil (0.110g, 50%).

^{1}H NMR ($CDCl_3$): δ 1.41 (9H, s), 2.97-2.50 (4H, m), 3.49-3.70 (2H, m), 3.85-3.80 (2H, m), 3.99-3.90 (2H, m), 4.20-4.07 (3H, m), 4.25-4.14 (2H, m), 5.24 (1H, s), 5.36 (1H, s), 6.78-6.65 (3H, m), 6.83-6.80 (2H, m), 7.08-6.99 (2H, m) 7.37-7.33 (2H, m), 7.40-7.44 (1H, m), 7.58-7.42 (3H, m), 7.68 (1H, s), 7.80-7.72 (2H, m), 8.27-8.22 (1H, m).

^{13}C NMR ($CDCl_3$): δ 27.43, 27.49, 27.51, 40.42, 43.42, 51.79, 54.43, 66.73, 67.10, 68.41, 69.58, 106.92, 119.20, 121.62, 121.68, 125.10, 125.13, 125.69, 126.34, 127.21, 127.26, 127.40, 127.60, 128.81, 128.88, 129.38, 134.71, 154.18, 157.73, 164.53, 169.40.

LC-MS: 2.41 min, m/z: theo. 564.2; meas. [MH^+] 565.4 (system 1)

***Tert*-butyl ((2*S*)-1-((2-((2-((2-hydroxy-3-(naphthalen-1-yloxy)propyl)amino)ethyl)amino)-2-oxoethyl)amino)-3-(4-hydroxyphenyl)-1-oxopropan-2-yl)carbamate (30c).**

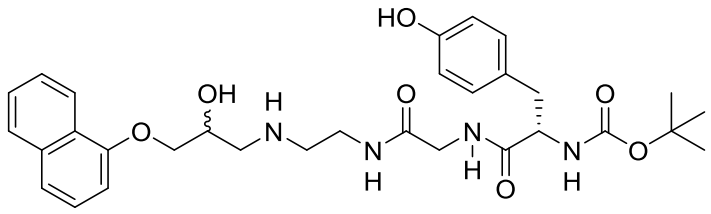

Compound **30c** was synthesized *via* general procedure B to afford the title compound as a yellow oil (0.850 g, 53%).

^{1}H NMR ($CDCl_3$): δ 1.53 (18H, s), 2.97-2.50 (4H, m), 3.87-3.79 (2H , m), 3.99-3.89 (2H, m), 4.18-4.00 (3H, m), 4.28-4.16 (2H, m), 5.26 (1H, s), 5.35 (1H, s,), 6.75-6.62 (3H, m), 6.80-6.78 (2H, d, *J*=7.5Hz), 7.07-6.97 (2H, m), 7.35-7.30 (2H, m), 7.36-7.40 (1H, m), 7.44-7.36 (3H, m), 7.681 (1H, s), 7.81-7.68 (2H, m), 8.25-8.19 (1H, m).

^{13}C NMR ($CDCl_3$): δ 26.49, 26.52, 26.54, 28.09, 28.12, 28.14, 30.82, 43.42, 51.79, 54.43, 66.73, 67.07, 67.77, 69.58, 109.22, 120.60, 121.68, 121.73, 123.40, 123.44, 125.25, 125.34, 126.11, 126.40, 126.27, 127.40, 129.38, 129.43, 133.51, 133.54, 134.71, 134.74, 154.18, 159.43, 169.27, 170.30.

LC-MS: 3.14 min, m/z: theo. 580.67; meas. [MH^+] 581.3 (system 1)

***Tert*-butyl ((2*S*)-3-hydroxy-1-((2-((2-((2-hydroxy-3-(naphthalen-1-yloxy)propyl)amino)ethyl)amino)-2-oxoethyl)amino)-1-oxopropan-2-yl)carbamate (30d).**

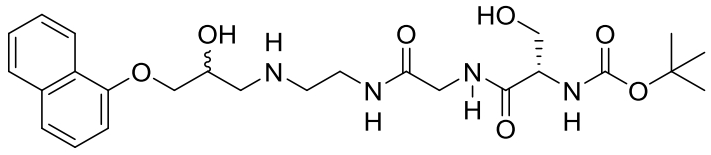

Compound **30d** was synthesized *via* general procedure B to afford the title compound as a transparent oil (0.151 g, 50%).

^{1}H NMR ($CDCl_3$): δ 1.43 (9H, s), 2.99-2.53 (4H, m), 3.50-3.69 (2H, m), 3.87-3.79 (2H , m), 3.99-3.89 (2H, m), 4.00-4.16 (2H, m), 4.18-4.00 (3H, m), 4.28-4.16 (2H, m), 5.25 (1H, s), 5.32 (1H, s), 6.75-6.62 (3H, m), 6.80-6.78 (2H, m), 7.07-6.97 (2H, m) 7.35-7.30 (2H, m), 7.44-7.36 (3H, m), 7.681 (1H, s), 7.80-7.66 (2H, m), 8.28-8.23 (2H, m).

^{13}C NMR ($CDCl_3$): δ 28.45, 28.50, 28.52, 40.42, 43.42, 51.79, 54.43, 60.87, 67.07, 67.80, 75.93, 85.45, 107.82, 119.20, 121.68, 125.11, 126.27, 127.40, 128.71, 129.38, 134.73, 154.18, 159.82, 164.53, 169.40.

LC-MS: 2.27 min, m/z: theo. 504.5; meas. [MH^+] 505.58 (system 1)

***Tert*-butyl ((2*S*)-5-amino-1-((2-((2-((2-hydroxy-3-(naphthalen-1-yloxy)propyl)amino)ethyl)amino)-2-oxoethyl)amino)-1,5-dioxopentan-2-yl)carbamate (30e).**

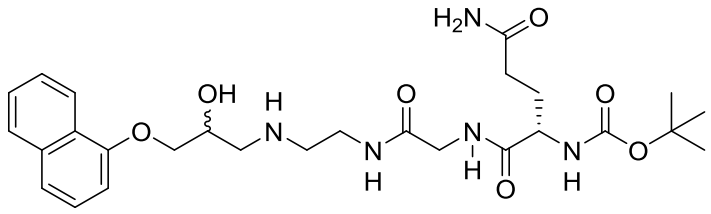

Compound **30e** was synthesized *via* general procedure B to afford the title compound as a transparent oil (0.439 g, 60%).

^{1}H NMR ($CDCl_3$): δ 1.41 (9H, s), 2.35-2.20 (4H, m), 2.97-2.50 (4H, m), 3.99-3.89 (2H, m), 4.28-4.16 (2H, m), 5.28 (1H, s), 5.82 (1H, s), 6.75-6.62 (1H, m), 6.80-6.78 (1H, m), 7.10-6.97 (1H, m), 7.25-7.07 (15H, m), 7.35-7.30 (1H, m), 7.36-7.40 (1H, m), 7.44-7.36 (1H, m), 7.681 (1H, s), 7.80-7.66 (2H, m), 8.18-8.15 (1H, m), 8.25-8.19 (1H, m).

^{13}C NMR ($CDCl_3$): δ 27.49, 27.52, 27.54, 41.12, 45.30, 51.79, 53.41, 66.73, 67.07, 67.77, 69.58, 78.39, 79.93, 107.62, 107.82, 119.20, 120.82, 121.68, 125.10, 126.15, 126.17, 126.22, 126.52, 126.60, 127.36, 127.40, 127.43, 127.91, 128.05, 128.13, 128.42, 129.38, 131.60, 132.75, 133.50, 133.68, 133.89, 134.76, 134.89, 143.66, 143.69, 145.84, 154.18, 157.73, 164.53, 169.40, 171.05.

LC-MS: 3.12 min, m/z: theo. 545.63; meas. [MH^+] 542.3. (system 1)

***Tert*-butyl ((2*S*)-1-(((2*S*)-1-((2-((2-hydroxy-3-(naphthalen-1-yloxy)propyl)amino)ethyl)amino)-1-oxo-3-phenylpropan-2-yl)amino)-1-oxo-3-phenylpropan-2-yl)carbamate (31).**

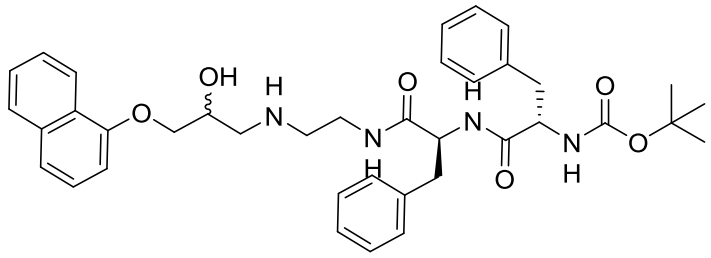

Compound **31** was synthesized *via* general procedure B to afford the title compound as a yellow oil (0.130 g, 61%).

^{1}H NMR (CD_3OD): δ 1.40 (9H, s), 3.14-2.94 (2H, m), 3.44-2.67 (4H, m), 3.88 (2H, d, *J*=5.3Hz), 4.06 (2H, m), 4.10-3.97 (2H, m), 4.21-4.14 (3H, m), 5.45 (1H, s), 6.75-6.50 (2H, m), 7. 10-7.05 (10H, m), 7.42-7.32 (3H, m), 7.62-7.52 (3H, m), 7.98-7.88 (1H, m), 8.25-8.17 (1H, m).

^{13}C NMR (CD_3OD): δ 28.32 (3), 37.26, 38.28, 54.26, 55.57 (2), 59.72, 69.12, 71.22, 78.33, 70.14, 70.19, 110.09 (2), 120.03, 122.79, 124.71, 125.61 (2), 125.95, 126.40, 126.93, 127.90 (2), 129.91 (4), 135.20 (2), 138.44 (2), 155.19, 156.36, 174.59 (2).

LC-MS: 2.60 min, m/z: theo. 654.81; meas. [MH^+] 655.6 (system 1)

(±)-*Tert*-butyl (3-((3-((2-((2-hydroxy-3-(naphthalen-1-yloxy)propyl)amino)ethyl)amino)-3-oxopropyl)amino)-3-oxopropyl)carbamate (32)

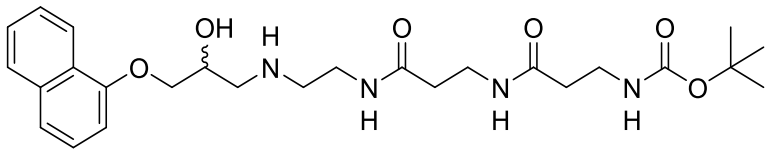

Compound **32** was synthesized *via* general procedure B to afford the title compound as a transparent oil (0.260 g, 51%).

^{1}H NMR (DMSO-d$_6$): δ 1.40 (9H, s), 2.84-2.60 (6H, m), 2.95 (4H, m), 3.70 (2H, m), 5.12 (1H, s), 4.22-4.10 (4H, m), 6.32 (2H, m), 7.55 (1H, m), 7.65 (3H, m), 8.10 (2H, s), 8.13 (1H, m), 8.35 (1H, m)

^{13}C NMR (DMSO-d$_6$): δ 28.62 (3), 34.42, 38.22, 38.11, 41.61, 41.70, 50.01, 52.42, 70.02, 75.56, 82.09, 110.71, 121.41, 124.83, 126.04, 126.42, 127.50, 127.57, 128.61, 136.41 (2), 156.21, 158.17, 177.03 (2).

LC-MS: 2.34 min, m/z: theo. 502.75; meas. [MH$^+$] 503.5 (system 1)

(2*S*)-2-amino-N-(2-((2-((2-hydroxy-3-(naphthalen-1-yloxy)propyl)amino)ethyl)amino)-2-oxoethyl)propanamide dihydrochloride (33a)

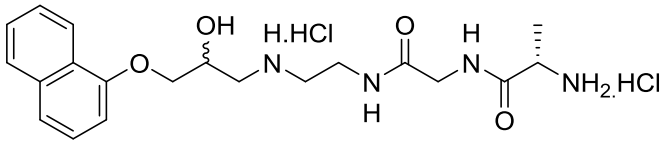

Compound **33a** was synthesized *via* general procedure C to yield the product as an oil in quantitative yield, which was dried and used without further purification.

^{1}H NMR (DMSO-d$_6$): δ 2.97-2.50 (4H, m), 3.87-3.79 (2H, m), 3.99-3.89 (2H, m), 4.18-4.00 (3H, m,), 4.28-4.16 (2H, m), 5.28 (1H, s), 5.32 (1H, s), 6.79 (2H, d, J=7.5Hz), 7.35-7.30 (2H, m), 7.44-7.36 (3H, m), 7.681 (1H, s), 7.80-7.66 (2H, m), 8.25-8.19 (2H, m)

^{13}C NMR (DMSO-d$_6$): δ 17.82, 43.42, 51.79, 54.43, 66.73, 67.07, 67.77, 107.82, 120.40, 121.68, 125.11, 125.89, 126.27, 127.40, 128.45, 129.38, 134.71, 154.18, 157.73, 164.53, 169.40.

LC-MS: 2.17 min, m/z: theo. 388.21; meas. [MH$^+$] 389.2 (system 1)

HPLC Rt: 9.73 (system 5)

(2*S*)-2-amino-N-(2-((2-((2-hydroxy-3-(naphthalen-1-yloxy)propyl)amino)ethyl)amino)-2-oxoethyl)-3-phenylpropanamide dihydrochloride (33b)

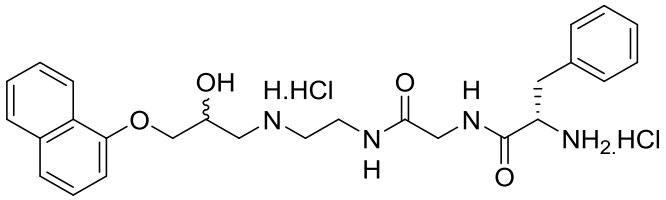

Compound **33b** was synthesized *via* general procedure C to yield the product as an oil in quantitative yield, which was dried and used without further purification.

^{1}H NMR (DMSO-d$_6$): δ 2.97-2.50 (4H, m), 3.50-3.69 (2H, m), 3.87-3.79 (2H, m), 3.99-3.89 (2H, m), 4.18-4.00 (3H, m), 4.28-4.16 (2H, m), 5.28 (1H, s),.32 (1H, s),

6.75-6.62 (3H, m), 6.80-6.78 (2H, m), 7.07-6.97 (2H, m) 7.35-7.30 (2H, m), 7.44-7.36 (3H, m), 7.681 (1H, s), 7.80-7.66 (2H, m), 8.25-8.20 (2H, m)

^{13}C NMR (DMSO-d$_6$): δ 40.42, 43.42, 51.79, 54.43, 66.73, 67.07, 104.79, 119.20, 120.44, 121.58, 121.62, 125.08, 125.27, 125.69, 126.27, 127.19, 127.29, 127.49, 127.51, 128.75, 128.77, 134.31, 134.69, 154.18, 164.53, 169.40.

LC-MS: 2.34 min, m/z: theo. 424.24; meas [MH^+] 425.5 (system 1)

HPLC Rt: 11.27 (system 5)

(2*S*)-2-amino-N-(2-((2-((2-hydroxy-3-(naphthalen-1-yloxy)propyl)amino)ethyl)amino)-2-oxoethyl)-3-(4-hydroxyphenyl)propanamide dihydrochloride (33c)

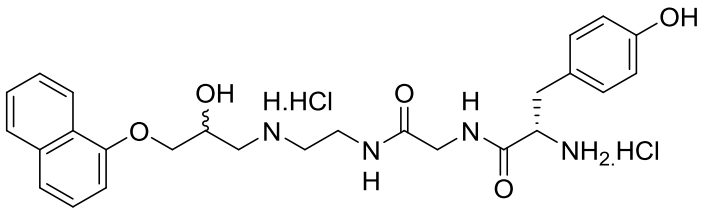

Compound **33c** was synthesized *via* general procedure C to yield the product as an oil in quantitative yield, which was dried and used without further purification.

^{1}H NMR (DMSO-d$_6$): δ 2.97-2.50 (4H, m), 3.87-3.79 (2H, m), 3.99-3.89 (2H, m), 4.18-4.00 (3H, m), 4.28-4.16 (2H, m), 5.28 (1H, s), 5.32 (1H, s), 6.75-6.62 (3H, m), 6.80-6.78 (2H, d, J=7.5Hz), 7.07-6.97 (2H, m), 7.35-7.30 (2H, m), 7.36-7.40 (1H, m), 7.44-7.36 (3H, m), 7.68 (1H, s), 7.80-7.66 (2H, m), 8.25-8.19 (1H, m)

^{13}C NMR (CDCl$_3$): δ 42.62, 43.42, 51.79, 54.43, 66.73, 71.07, 72.17, 107.82, 120.40, 121.53, 121.61, 125.08, 125.24, 127.27, 127.43, 129.40, 129.79, 131.08, 131.01, 134.55, 134.72, 153.85, 156.85, 159.42, 169.53, 172.40.

LC-MS: 2.08 min, m/z: theo. 440.23; meas [MH^+] 441.2 (system 1)

HPLC Rt: 10.59 (system 5)

(2*S*)-2-amino-3-hydroxy-N-(2-((2-((2-hydroxy-3-(naphthalen-1-yloxy)propyl)amino)ethyl)amino)-2-oxoethyl)propanamide dihydrochloride (33d)

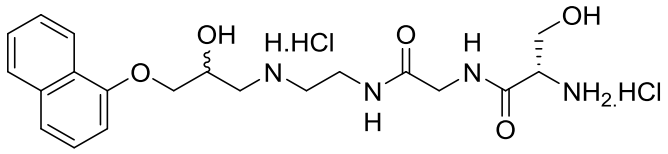

Compound **33d** was synthesized *via* general procedure C to yield the product as an oil in quantitative yield, which was dried and used without further purification.

^{1}H NMR (DMSO-d$_6$): δ 2.97-2.50 (4H, m), 3.50-3.69 (2H, m), 3.87-3.79 (2H, m), 3.99-3.89 (2H, m), 4.00-4.16 (2H, m), 4.18-4.00 (3H, m), 4.28-4.16 (2H, m), 5.28 (1H, s), 5.32 (1H, s),6.75-6.62 (3H, m), 6.80-6.78 (2H, m), 7.07-6.97 (2H, m) 7.35-7.30 (2H, m), 7.44-7.36 (3H, m), 7.681 (1H, s), 7.80-7.66 (2H, m), 8.27-8.22 (2H, m)

^{13}C NMR (DMSO-d$_6$): δ 40.42, 43.42, 51.79, 54.43, 67.07, 67.77, 107.82, 119.20, 121.68, 125.11, 126.27, 127.40, 127.80, 129.38, δ134.75, 154.18, 164.53, 169.40.

LC-MS: 2.40 min, m/z: theo. 404.20; meas. [MH^+] 411.3 (system 1)

HPLC Rt: 9.92 (system 5)

(2*S*)-2-amino-N^1-(2-((2-((2-hydroxy-3-(naphthalen-1-yloxy)propyl)amino)ethyl)amino)-2-oxoethyl)pentanediamide dihydrochloride (33e)

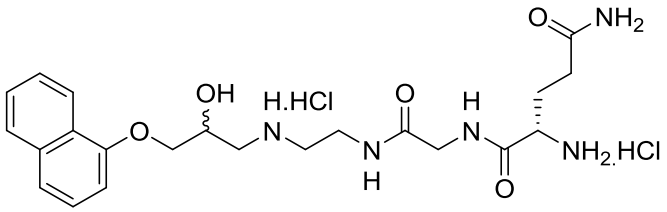

Compound **33e** was synthesized *via* general procedure C to yield the product as an oil in quantitative yield, which was dried and used without further purification.

^{1}H NMR (DMSO-d$_6$): δ 2.35-2.20 (4H, m), 2.97-2.50 (4H, m), 3.99-3.89 (2H, m), 4.28-4.16 (2H, m), 5.28 (1H, s), 5.82 (1H, s), 6.75-6.62 (1H, m), 6.80-6.78 (1H, m), 7.10-6.97 (1H, m), 7.35-7.30 (1H, m), 7.36-7.40 (2H, m), 7.44-7.36 (1H, m), 7.681 (1H, s), 7.80-7.66 (2H, m), 8.18-8.15 (2H, m), 8.25-8.19 (1H, m).

^{13}C NMR (DMSO-d$_6$): δ 40.00, 43.42, 51.79, 54.43, 66.73, 67.07, 67.77, 70.13, 107.82, 119.20, 121.68, 125.11, 126.50, 127.40, 129.38, 134.20, 135.07, 154.18, 164.53, 169.40, 173.05.

LC-MS: 1.95 min, m/z: theo. 445.23; meas. [MH$^+$] 442.2 (system 1)

HPLC Rt: 10.50 (system 5)

(2*S*)-2-amino-N-((2*S*)-1-((2-((2-hydroxy-3-(naphthalen-1-yloxy)propyl)amino)ethyl)amino)-1-oxo-3-phenylpropan-2-yl)-3-phenylpropanamide dihydrochloride (34)

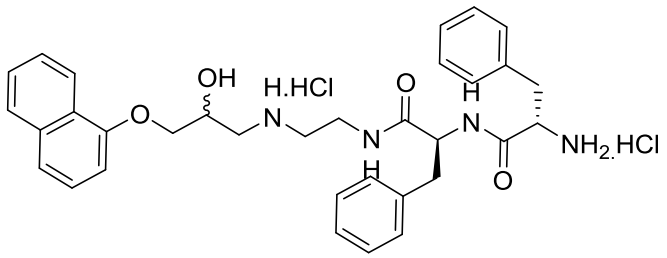

Compound **34** was synthesized *via* general procedure C to yield the product as an oil in quantitative yield, which was dried and used without further purification.

^{1}H NMR (CD_3OD): δ 1.40 (2H, s), 3.14-2.94 (2H, m), 3.44-2.67 (4H, m), 3.88 (2H, d, *J*=5.3Hz), 4.06 (2H, m), 4.10-3.97 (2H, m), 4.21-4.14 (3H, m), 5.45 (1H, s), 6.75-6.50 (2H, m), 7. 10-7.05 (10H, m), 7.42-7.32 (3H, m), 7.62-7.52 (3H, m), 7.98-7.88 (1H, m), 8.25-8.17 (1H, m).

^{13}C NMR (CD_3OD): δ 37.26, 38.28, 54.26, 55.57 (2), 59.72, 69.12, 71.22, 70.14, 70.19, 110.09 (2), 120.03, 122.79, 124.71, 125.61 (2), 125.95, 126.40, 126.93, 127.90 (2), 129.91 (4), 135.20 (2), 138.44 (2), 155.19, 156.36, 174.59.

LC-MS: 2.02 min, m/z: theo. 554.28; meas. [MH^+] 555.5 (system 1)

HPLC Rt: 2.49 min, 655.3 (system 1)

(±)-3-amino-*N*-(3-((2-((2-hydroxy-3-(naphthalen-1-yloxy)propyl)amino)ethyl)amino)-3-oxopropyl)propanamide dihydrochloride (35)

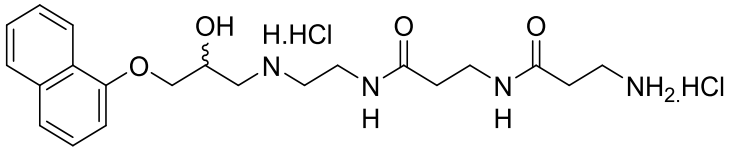

Compound **39** was synthesized *via* general procedure C to yield the title compound as an oil in quantitative yield,

^{1}H NMR (DMSO-d_6): δ 1.79 (2H, s), 2.84-2.60 (6H, m), 2.95 (4H, m), 3.70 (2H, m), 5.12 (1H, s), 4.22-4.10 (4H, m), 6.32 (2H, m), 7.55 (1H, m), 7.65 (3H, m), 8.10 (2H, s), 8.13 (1H, m), 8.35 (1H, m)

^{13}C NMR (DMSO-d$_6$): δ 34.42, 38.22, 38.11, 41.61, 41.70, 50.01, 52.42, 70.02, 75.56, 110.71, 121.41, 124.83, 126.04, 126.42, 127.50, 127.57, 128.61, 136.41 (2), 156.21, 177.03 (2).

m/z: HRMS (TOF ES$^+$) $C_{21}H_{30}N_4O_4$, $[MH]^+$ calcd. 402.2267; found 402.2671

HPLC Rt: 10.00 (system 5), 0.68 min (system 1)

(2*S*)-2-acetamido-*N*-(2-((2-((2-hydroxy-3-(naphthalen-1-yloxy)propyl)amino)ethyl)amino)-2-oxoethyl)propanamide (36a).

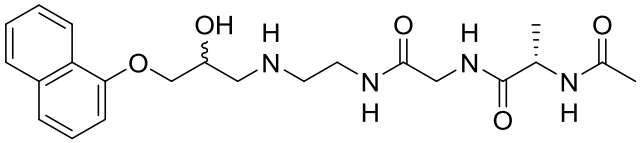

This compound was synthesized *via* general procedure D to afford the titled compound as a transparent oil (4.85 mg, 42%).

^{1}H NMR (CD$_3$OD): δ 1.36 (3H, d, *J*=7.2Hz), 1.99 (3H, s), 2.99-2.80 (4H, m), 3.45-3.38 (2H, m), 3.90-3.77 (2H, m), 4.28-4.15 (4H, m), 4.87-4.60 (1H, m), 5.00 (1H, s), 6.79 (2H, d, *J*=7.4Hz), 7.00-6.84 (1H, m), 7.55-732 (4H, m), 7.88-7.73 (1H, m), 8.35-8.29 (1H, m), 8.58 (1H, s).

^{13}C NMR (CD$_3$DO): δ 15.62, 21.07, 43.42, 44.11, 50.04, 51.60, 51.62, 68.59, 68.64, 70.52, 70.54, 104.55, 120.02, 121.64, 124.68, 125.58, 127.05, 134.65, 154.45, 170.51, 172.80, 174.40.

m/z: HRMS (TOF ES$^+$) $C_{22}H_{30}N_4O_5$, $[MH]^+$ calcd. 431.2294; found 431.2289.

HPLC Rt: 11.89 (system 5), 2.99 (system 1)

(2*S*)-2-acetamido-*N*-(2-((2-((2-hydroxy-3-(naphthalen-1-yloxy)propyl)amino)ethyl)amino)-2-oxoethyl)-3-phenylpropanamide (36b).

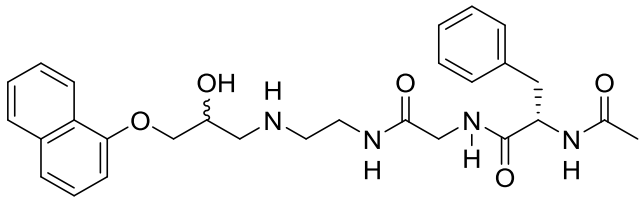

This compound was synthesized *via* general procedure D to afford the titled compound as a transparent oil (3.57 mg, 50%).

^{1}H NMR (CD_3DO): δ 1.93 (3H, s), 3.02-2.76 (5H, m), 3.17-3.10 (1H, m), 3.42-3.38 (2H, m), 3.60-3.54 (2H, m), 3.90-3.87 (1H, m), 4.28-4.15 (3H, m), 4.45-4.40 (1H, m), 5.00 (1H, s), 6.92 (2H, d, *J*=7.2Hz), 6.96-6.91 (1H, m), 7.32-7.20 (5H, m) , 7.41-7.36 (1H, m), 7.51-742 (3H, m), 7.83-7.78(1H, m), 8.34-8.30 (1H, m), 8.58 (1H, s).

^{13}C NMR (CD_3OD): δ 21.10, 36.73, 38.50, 42.25, 51.66, 55.91, 68.61, 68.66, 70.57, 104.55, 120.44, 120.03, 121.63, 124.69, 125.69, 126.27, 125.59, 125.97, 126.43, 127.05, 128.11, 128.81, 134.65, 136.91, 154.45, 170.38, 172, 38, 173.08.

m/z: HRMS (TOF ES^+) $C_{28}H_{34}N_4O_5$, $[MH]^+$ calcd. 507.2607; found 507.2602.

HPLC Rt: 15.75 (system 5), 13.55 (system 2)

(2*S*)-2-acetamido-*N*-(2-((2-((2-hydroxy-3-(naphthalen-1-yloxy)propyl)amino)ethyl)amino)-2-oxoethyl)-3-(4-hydroxyphenyl)propanamide (36c).

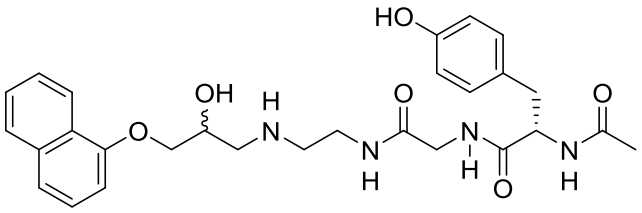

This compound was synthesized *via* general procedure D to afford the titled compound as a transparent oil (3.99 mg, 34.7%).

^{1}H NMR (CD_3OD): δ 2.97-2.50 (4H, m), 3.87-3.79 (2H, m), 3.99-3.89 (2H, m), 4.18-4.00 (3H, m), 4.28-4.16 (2H, m), 5.28 (1H, s), 5.32 (1H, s), 6.75-6.62 (3H, m), 6.80-6.78 (2H, d, *J*=7.5Hz), 7.07-6.97 (2H, m), 7.35-7.30 (2H, m), 7.36-7.40 (1H, m), 7.44-7.36 (3H, m), 7.68 (1H, s), 7.80-7.66 (2H, m), 8.25-8.19 (1H, m).

^{13}C NMR (CD_3OD): δ 21.05, 36.13,38.50, 42.30, 51.66, 56.26, 54.43, 68.66, 70.63, 104.53, 114.96, 120.03, 121.63, 124.68, 125.58, 125.97, 127.04, 127.19, 129.81, 134.64, 154.45, 156.29, 160.09, 161.43, 170.42, 172.37, 173.26.

m/z: HRMS (TOF ES^+) $C_{28}H_{34}N_4O_5$, $[MH]^+$ calcd. 523.2554; found 523.2551.

HPLC Rt: 12.23 (system 5), 2.76 min (system 1)

(2*S*)-2-acetamido-3-hydroxy-*N*-(2-((2-((2-hydroxy-3-(naphthalen-1-yloxy)propyl)amino)ethyl)amino)-2-oxoethyl)propanamide (36d).

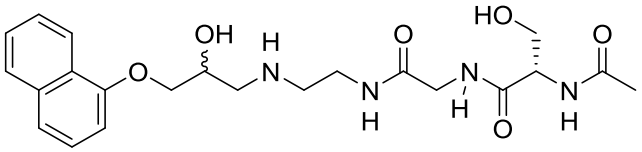

The compound was synthesized *via* general procedure D to afford the titled compound as a transparent oil (3.43 mg, 49.2%).

^{1}H NMR (CD_3OD): δ 2.97-2.50 (4H, m), 3.50-3.69 (2H, m), 3.87-3.79 (2H, m), 3.99-3.89 (2H, m), 4.00-4.16 (2H, m), 4.18-4.00 (3H, m), 4.28-4.16 (2H, m), 5.28 (1H, s), 5.32 (1H, s),6.75-6.62 (3H, m), 6.80-6.78 (2H, m), 7.07-6.97 (2H, m) 7.35-7.30 (2H, m), 7.44-7.36 (3H, m), 7.681 (1H, s), 7.80-7.66 (2H, m), 8.27-8.22 (2H, m).

^{13}C NMR (CD_3OD): δ 21.05, 29.23, 38.58, 42.44, 51.69, 56.17, 56.53, 60.20, 61.38, 68.54, 68.62, 70.07, 70.16, 107.61, 121.24, 125.40, 125.50, 137.98, 156.38, 170.44, 172.07, 172.58. **m/z:** HRMS (TOF ES^+) $C_{22}H_{30}N_4O_6$, $[MH]^+$ calcd. 450.2551; found 451.2552

HPLC Rt: 11.34 (system 5), 2.99 min (system 2)

(2S)-2-acetamido-N1-(2-((2-((2-hydroxy-3-(naphthalen-1-yloxy)propyl)amino)ethyl)amino)-2-oxoethyl)pentanediamide (36e).

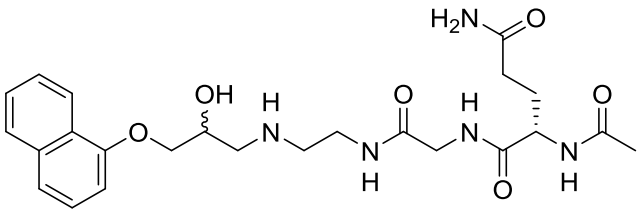

This compound was synthesized *via* general procedure D (1.51 mg, 95%).

^{1}H NMR (CD_3OD): δ 2.35-2.20 (4H, m), 2.97-2.50 (4H, m), 3.99-3.89 (2H, m), 4.28-4.16 (2H, m), 5.28 (1H, s), 5.82 (1H, s), 6.75-6.62 (1H, m), 6.80-6.78 (1H, m), 7.10-6.97 (1H, m), 7.35-7.30 (1H, m), 7.36-7.40 (2H, m), 7.44-7.36 (1H, m), 7.681 (1H, s), 7.80-7.66 (2H, m), 8.18-8.15 (2H, m), 8.25-8.19 (1H, m).

^{13}C NMR (CD_3OD): δ 21.09, 26.85, 30.99, 38.53, 39.16, 42.35, 51.56, 53.80, 68.60, 70.67, 104.49, 120.00, 121.71, 124.68, 125.61, 125.96, 127.06, 134.67, 154.44, 160.12, 170.44, 172.54, 173.21, 176.25.

m/z: HRMS (TOF ES^+) $C_{24}H_{33}N_5O_6$ $[MH]^+$ calcd. 448.2504; found 448.2506.

HPLC Rt: 11.34 (system 5), 2.09 (system 1)

(2*S*)-2-acetamido-N-((2*S*)-1-((2-((2-hydroxy-3-(naphthalen-1-yloxy)propyl)amino)ethyl)amino)-1-oxo-3-phenylpropan-2-yl)-3-phenylpropanamide (37).

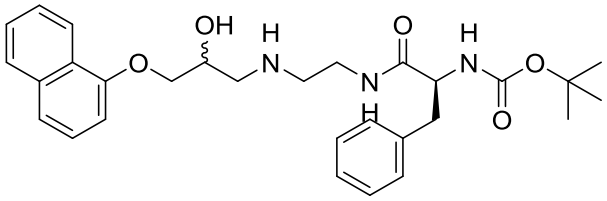

tert-butyl ((2*S*)-1-((2-((2-hydroxy-3-(naphthalen-1-yloxy)propyl)amino)ethyl)amino)-1-oxo-3-phenylpropan-2-yl)carbamate

This compound was synthesized *via* general procedure D (1.50 mg, 95%).

^{1}H NMR (CD_3OD): δ 2.04 (3H, s), 2.87-2.75 (5H, m), 3.01-2.92 (5H, m), 4.28-4.17 (4H, m), 4.95 (1H, s), 4.85 (1H, s), 6.95-6.92 (1H, m), 7.13-7.06 (4H, m), 7.32-7.16 (10H, m), 7.42-7.36 (1H, m), 7.53-7.41 (3H, m), 7.82-7.79 (1H, m), 8.31-8.29 (2H, m).

^{13}C NMR (CD_3OD): δ 21.35, 37.26 (2), 39.08, 50.87, 53.51 (2), 60.12, 69.12, 71.22, 78.33, 70.14, 70.19, 110.09 (2), 120.03, 122.79, 124.71, 125.61 (2), 125.95,

126.40, 126.93, 128.91 (3), 129.91 (4), 135.20 (2), 138.44 (2), 156.36, 172.50, 174.59 (2).

m/z: HRMS (TOF ES$^+$) $C_{49}H_{55}BF_2N_7O_7S$, $[MH]^+$ calcd. 597.3083; found 597.3071.

HPLC Rt: 17.78 (system 5), 2.34 min (system 1)

6-(2-(4-((E)-2-(5,5-difluoro-7-(thiophen-2-yl)-5H-4l4,5l4-dipyrrolo[1,2-c:2',1'-f][1,3,2]diazaborinin-3-yl)vinyl)phenoxy)acetamido)-N-((2*S*)-1-((2-((2-((2-hydroxy-3-(naphthalen-1-yloxy)propyl)amino)ethyl)amino)-2-oxoethyl)amino)-1-oxopropan-2-yl)hexanamide (38a).

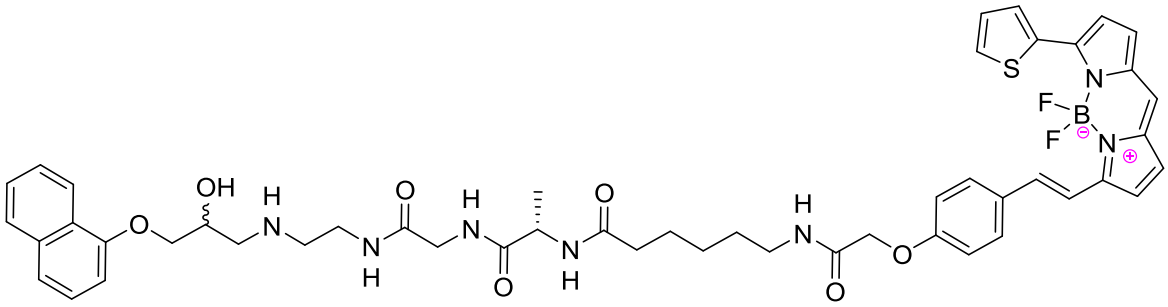

The compound was synthesized *via* general procedure E (71%).

HPLC Rt: 19.25 min (system 3), 2.57 min (system 2)

mz: HRMS (TOF ES$^+$) $C_{49}H_{54}BF_2N_7O_7S$, $[MH]^+$ calcd. 934.3939; found 934.3953

6-(2-(4-((E)-2-(5,5-difluoro-7-(thiophen-2-yl)-5H-4l4,5l4-dipyrrolo[1,2-c:2',1'-f][1,3,2]diazaborinin-3-yl)vinyl)phenoxy)acetamido)-N-((2*S*)-1-((2-((2-((2-hydroxy-3-(naphthalen-1-yloxy)propyl)amino)ethyl)amino)-2-oxoethyl)amino)-1-oxo-3-phenylpropan-2-yl)hexanamide (38b).

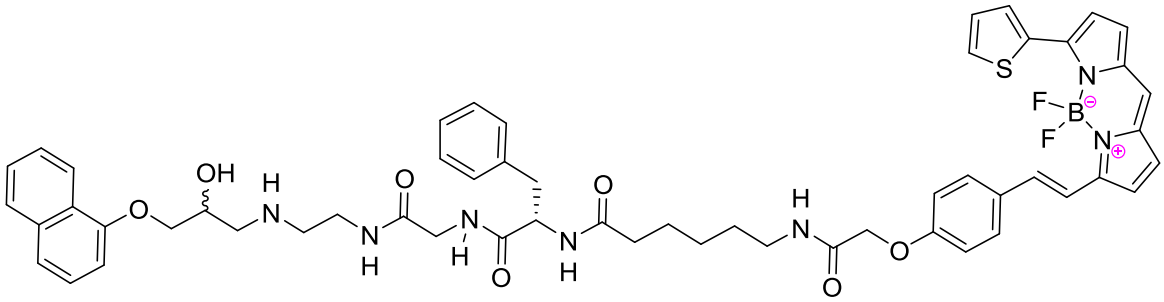

The compound was synthesized *via* general procedure E (29%).

HPLC Rt: 19.75 min (system 3), 5.68 min (system 2)

m/z: HRMS (TOF ES^+) $C_{55}H_{58}BF_2N_7O_7S$, $[MH]^+$ calcd. 1010.4252; found 1010.4222.

6-(2-(4-((E)-2-(5,5-difluoro-7-(thiophen-2-yl)-5H-4l4,5l4-dipyrrolo[1,2-c:2',1'-f][1,3,2]diazaborinin-3-yl)vinyl)phenoxy)acetamido)-N-((2*S*)-1-((2-((2-((2-hydroxy-3-(naphthalen-1-yloxy)propyl)amino)ethyl)amino)-2-oxoethyl)amino)-3-(4-hydroxyphenyl)-1-oxopropan-2-yl)hexanamide (38c).

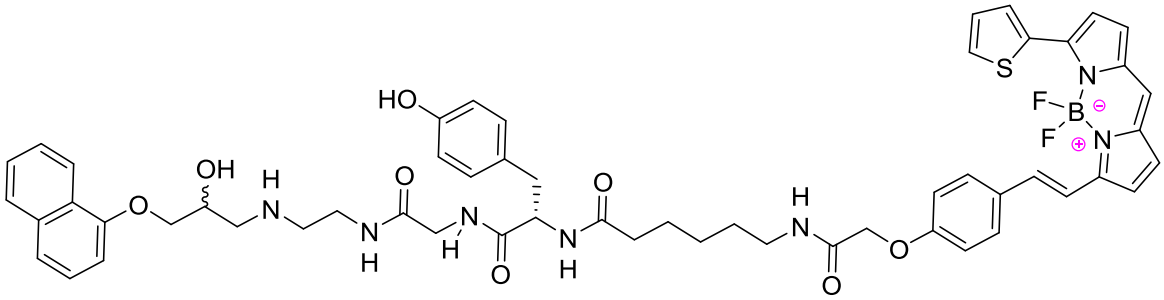

The compound was synthesized *via* general procedure E (66%).

HPLC Rt: 19.55 min. (system 3), 5.45 min (system 2)

m/z: HRMS (TOF ES^+) $C_{55}H_{58}BF_2N_7O_8S$, $[MH]^+$ calcd. 1026.9843; found 1026.4103.

6-(2-(4-((E)-2-(5,5-difluoro-7-(thiophen-2-yl)-5H-4l4,5l4-dipyrrolo[1,2-c:2',1'-f][1,3,2]diazaborinin-3-yl)vinyl)phenoxy)acetamido)-N-((2*S*)-3-hydroxy-1-((2-((2-((2-hydroxy-3-(naphthalen-1-yloxy)propyl)amino)ethyl)amino)-2-oxoethyl)amino)-1-oxopropan-2-yl)hexanamide (38d).

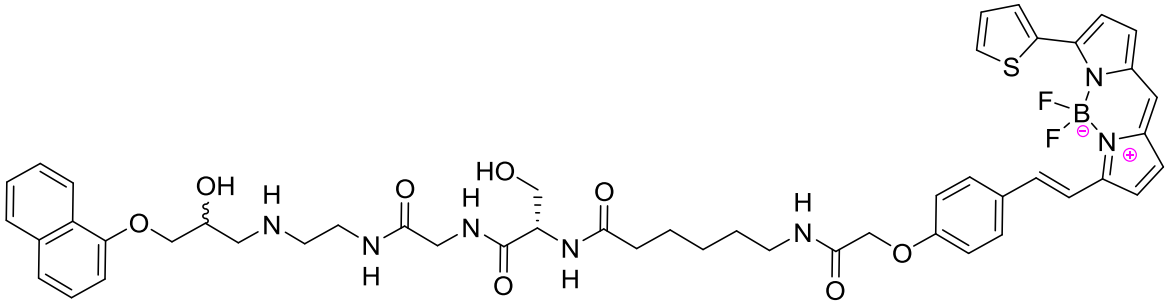

The compound was synthesized *via* general procedure E (59%).

HPLC Rt: 19.15 min (system 3), 5.40 (system 2)

m/z: HRMS (TOF ES$^+$) $C_{49}H_{54}BF_2N_7O_8S$, $[MH]^+$ calcd. 950.3861; found 950.3888

(2*S*)-2-(6-(2-(4-((E)-2-(5,5-difluoro-7-(thiophen-2-yl)-5H-4l4,5l4-dipyrrolo[1,2-c:2',1'-f][1,3,2]diazaborinin-3-yl)vinyl)phenoxy)acetamido)hexanamido)-N1-(2-((2-((2-hydroxy-3-(naphthalen-1-yloxy)propyl)amino)ethyl)amino)-2-oxoethyl)pentanediamide (38e).

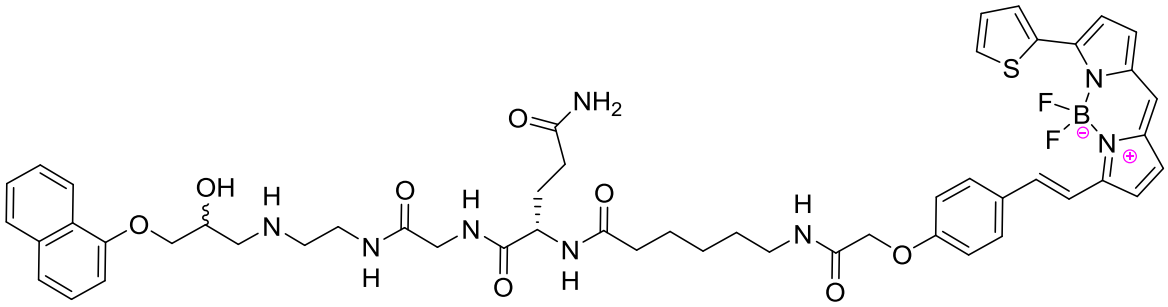

The compound was synthesized *via* general procedure E (70%).

HPLC Rt: 19.25 min (system 3), 5.21 (system 2)

m/z: HRMS (TOF ES$^+$) $C_{51}H_{58}BF_2N_8O_8S$, $[MH]^+$ calcd. 991.4154; found 991.4178**.**

6-(2-(4-((E)-2-(5,5-difluoro-7-(thiophen-2-yl)-5H-4l4,5l4-dipyrrolo[1,2-c:2',1'-f][1,3,2]diazaborinin-3-yl)vinyl)phenoxy)acetamido)-N-((2*S*)-1-(((2S)-1-((2-((2-hydroxy-3-(naphthalen-1-yloxy)propyl)amino)ethyl)amino)-1-oxo-3-phenylpropan-2-yl)amino)-1-oxo-3-phenylpropan-2-yl)hexanamide (39).

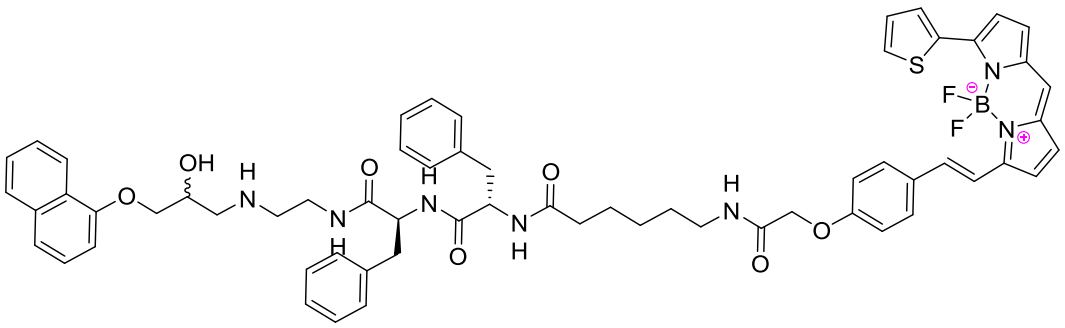

The compound was synthesized *via* general procedure E (32%).

HPLC Rt: 22 min (system 4), 4.10 (system 2)

m/z: HRMS (TOF ES^+) $C_{62}H_{64}BF_2N_7O_7S$, $[MH]^+$ calcd. 1100.4306; found 1100.4335**.**

(E)-6-(2-(4-(2-(5,5-difluoro-7-(thiophen-2-yl)-5H-4l4,5l4-dipyrrolo[1,2-c:2',1'-f][1,3,2]diazaborinin-3-yl)vinyl)phenoxy)acetamido)-N-(3-((3-((2-((2-hydroxy-3-(naphthalen-1-yloxy)propyl)amino)ethyl)amino)-3-oxopropyl)amino)-3-oxopropyl)hexanamide (40)

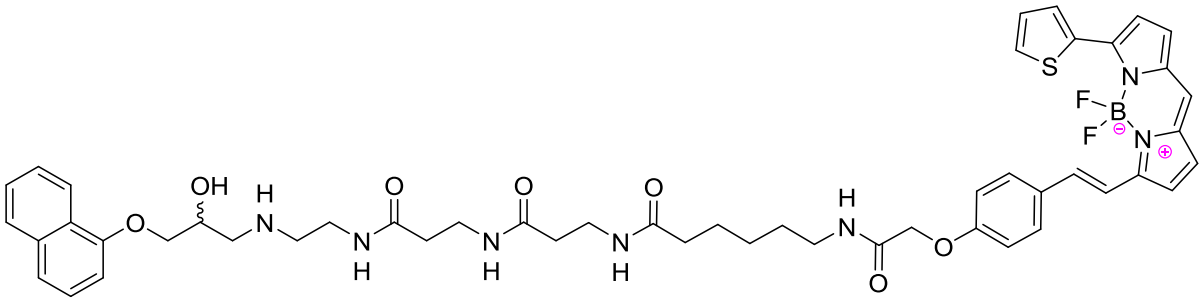

The compound was synthesized *via* general procedure E (88%).

HPLC Rt: 19 min (system 4), 4.99 min (system 1)

m/z: HRMS (TOF ES$^+$) $C_{50}H_{56}BF_2N_7O_7S$, $[MH]^+$ calcd. 944.4096; found 944.4110**.**

3-(5,5-difluoro-7,9-dimethyl-5H-4l4,5l4-dipyrrolo[1,2-c:2',1'-f][1,3,2]diazaborinin-3-yl)-N-((2*S*)-1-((2-((2-((2-hydroxy-3-(naphthalen-1-yloxy)propyl)amino)ethyl)amino)-2-oxoethyl)amino)-1-oxopropan-2-yl)propanamide (41a).

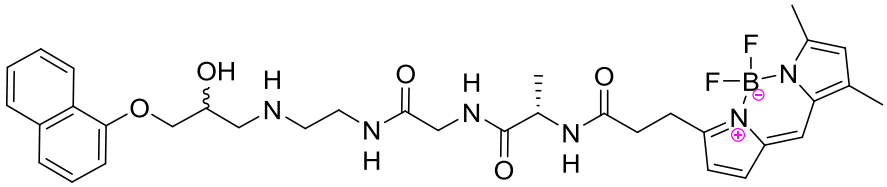

The compound was synthesized *via* general procedure E (43%).

HPLC Rt: 17 min (system 5), 4.10 min (system 1)

m/z: HRMS (TOF ES$^+$) $C_{34}H_{41}BF_2N_6O_5$, $[MH]^+$ calcd. 663.3272; found 663.3289**.**

(2*S*)-2-(3-(5,5-difluoro-7,9-dimethyl-5H-4l4,5l4-dipyrrolo[1,2-c:2',1'-f][1,3,2]diazaborinin-3-yl)propanamido)-N-(2-((2-((2-hydroxy-3-(naphthalen-1-yloxy)propyl)amino)ethyl)amino)-2-oxoethyl)-3-phenylpropanamide (41b).

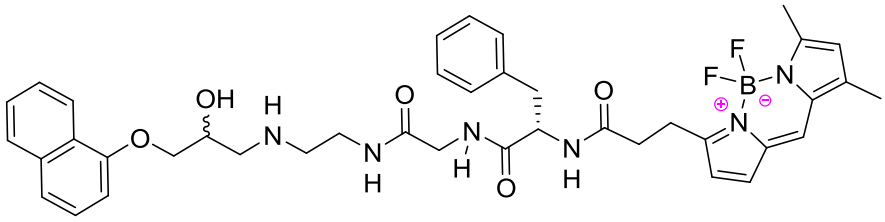

The compound was synthesized *via* general procedure E (43%).

HPLC Rt: 21 min (system 5), 4.63 min (system 1)

m/z: HRMS (TOF ES$^+$) $C_{40}H_{41b}F_2N_6O_5$, $[MH]^+$ calcd. 739.3596; found 739.3585**.**

(2*S*)-2-(3-(5,5-difluoro-7,9-dimethyl-5H-4l4,5l4-dipyrrolo[1,2-c:2',1'-f][1,3,2]diazaborinin-3-yl)propanamido)-3-hydroxy-N-(2-((2-((2-hydroxy-3-(naphthalen-1-yloxy)propyl)amino)ethyl)amino)-2-oxoethyl)propanamide (41d).

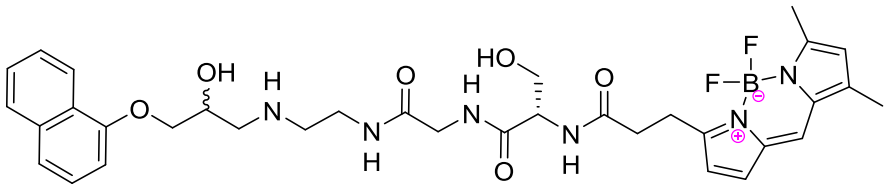

The compound was synthesized *via* general procedure E (49%).

HPLC Rt: 17.50 min (system 4), 5.31 (system 1)

m/z: HRMS (TOF ES$^+$) $C_{34}H_{41}BF_2N_6O_6$, $[MH]^+$ calcd. 684.3163; found 684.3141**.**

(2*S*)-2-(3-(5,5-difluoro-7,9-dimethyl-5H-4l4,5l4-dipyrrolo[1,2-c:2',1'-f][1,3,2]diazaborinin-3-yl)propanamido)-N-((2S)-1-((2-((2-hydroxy-3-(naphthalen-1-yloxy)propyl)amino)ethyl)amino)-1-oxo-3-phenylpropan-2-yl)-3-phenylpropanamide (42).

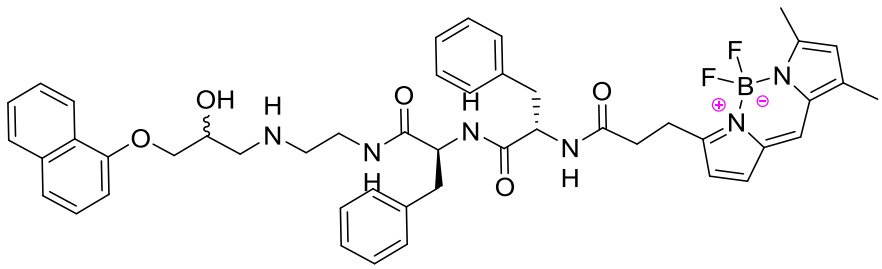

The compound was synthesized *via* general procedure E (42%).

HPLC Rt: 22 min (system 4), 5.22 min (system 1)

m/z: HRMS (TOF ES$^+$) $C_{43}H_{50}BF_2N_6O_5$ [MH]$^+$ calcd. 829.4055; found 829.4064**.**

(E)-3-(5,5-difluoro-7,9-dimethyl-5H-4l4,5l4-dipyrrolo[1,2-c:2',1'-f][1,3,2]diazaborinin-3-yl)-N-(3-((3-((2-((2-hydroxy-3-(naphthalen-1-yloxy)propyl)amino)ethyl)amino)-3-oxopropyl)amino)-3-oxopropyl)acrylamide (43)

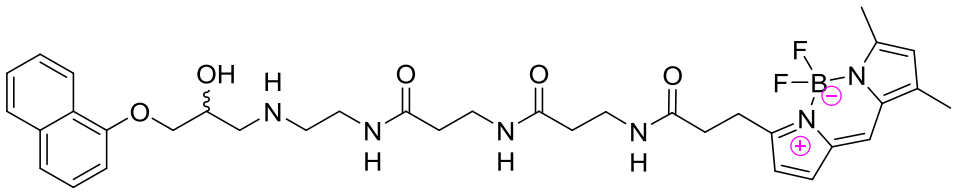

The compound was synthesized *via* general procedure E (6%).

HPLC Rt: 16.22 min (system 4), 2.36 (system 1)

m/z: HRMS (TOF ES$^+$) $C_{35}H_{43}BF_2N_6O_5$ [MH]$^+$ calcd. 677.3429; found 677.3456**.**

6-(2-(5,5-difluoro-7,9-dimethyl-5H-4l4,5l4-dipyrrolo[1,2-c:2',1'-f][1,3,2]diazaborinin-3-yl)acetamido)-N-(3-((3-((2-((2-hydroxy-3-(naphthalen-1-yloxy)propyl)amino)ethyl)amino)-3-oxopropyl)amino)-3-oxopropyl)hexanamide (44)

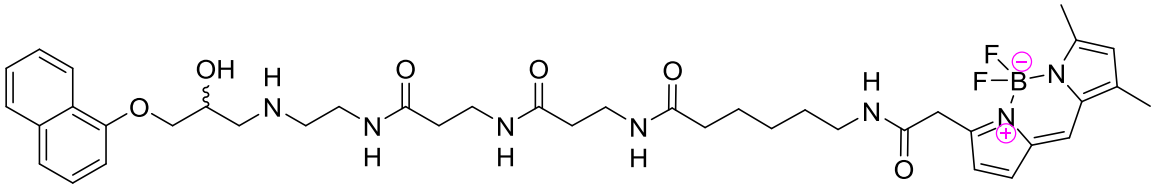

The compound was synthesized *via* general procedure E (15%).

HPLC Rt: 17.32 min (system 4), 2.37 (system 1)

m/z: HRMS (TOF ES+) $C_{41}H_{52}BF_2N_7O_6$ [MH]+ calcd. 790.4308; found 790.4306.

4.1.3 Oxindole

4-(benzyloxy)indolin-2-one (45)

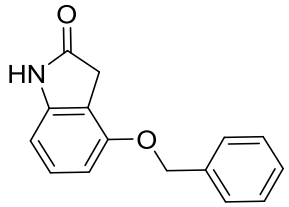

To a solution of 4-benzyloxyindole in *tert*-butanol was added drop wise NBS (1 eq.) solution in *tert*-butanol at room temperature. The reaction mixture was left to stir overnight at room temperature. The reaction mixture was dried *in vacuo* and the off-white precipitates were washed with *tert*-butanol and dried *in vacuo* to yield 75% of an off-white solid, which was used without further purification[192, 202].

^{1}H NMR ($CDCl_3$): δ 3.50 (s, 2H, CH_2), 5.11 (s, 2H, CH_2), 6.56-6.54 (d, J=8.4427Hz, 1H, ArH), 6.63-6.61 (d, J=8.4427Hz, 1H, ArH), 7.17-7.13 (t, J= 4.8Hz, 1H, ArH), 7.43-7.38 (m, 5H, ArH), 8.91 (s, 1H, NH amide).

^{13}C NMR ($CDCl_3$): δ 29.56, 60.44, 69.98, 107.66, 112.57, δ127.24, 128.58, 128.04, 129.35, 136.57, 142.70, 171.28, 178.35.

LC-MS: 2.60 min, m/z: theo 239.27; meas. [MH^+] 240.1 (system 1)

Mp: 200 - 210 °C

4-hydroxyindolin-2-one (46)

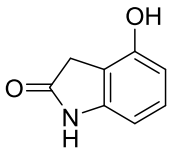

Compound **46** was synthesized *via* general procedure A to afford the title compound as a brown solid in quantitative yield.

^{1}H NMR (CD_3)$_2$OS: δ 3.28 (s, 2H, CH_2), 6.31-6.29 (d, J=7.4427Hz, 1H, ArH), δ6.42-6.39 (d, J=7.4427Hz, 1H, ArH), 6.99-6.94 (t, J= 8.30Hz, 1H, ArH), 9.49 (s, 1H, OH), 10.25 (s, 1H, NH amide)

^{13}C NMR ($CDCl_3$): δ 34.00, 101.32, 109.68, 110.83, 128.91, 145.35, 153.55, 76.80.

IR (KBr disk): 3283.72 cm^{-1} (br, O-H, str), 3220. 24 cm^{-1} (br, N-H, str), 1679.24 cm^{-1} (s, aryl ketone C=O, str), 1635.93 cm^{-1} (s, C=C, str.), 770.09 cm^{-1} (s, aryl C-H, bend and ring puckering)

Mp: 277-281°C

LC-MS: 1.10 min, m/z: theo 149.15; meas. [MH^+] 150.0 (system 1)

(S)-4-(Oxiran-2-ylmethoxy)indolin-2-one (47)

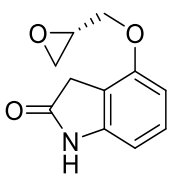

To a solution of **47** in acetone was added K_2CO_3 and (*S*)-(+)-Glycidyl 3-nitrobenzenesulfonate (nosylate)**.** The reaction was refluxed for 18-20 hours. The suspension was filtered and filtrate was then worked up. The reaction mixture was partitioned with NH_4Cl and extracted (3x) with EtOAc. The organic layer was extracted with saturated NaCl. The combined organic layer was dried using anhydrous Na_2SO_4. The excess solvent was evaporated *in vacuo* and crude was purified by flash chromatography with a gradient of 10% of diethyl ether/DCM/MeOH to afford greenish oil with 88% yield.

^{1}H NMR (CD_3OD): δ 2.76-2.74 (m, 1H, CH_2), 2.89-2.86 (m, 1H, CH_2), 3.42 (s, 2H, CH), 3.92-3.88 (m, 1H, CH), 4.17-4.04 (m, 1H, CH), 4.38-4.35 (m, 1H, CH), 6.56-6.54 (d, J=7.88Hz, 1H, ArH), 6.65-6.63 (d, J=7.72Hz, 1H, ArH), 7.17-7.14 (m, 1H, ArH), 10.14 (s, 1H, NH amide)

^{13}C NMR (CD_3OD): δ 33.29, 43.53, 49.88, 68.96, 102.71, 106.02, 112.37, 128.93, 144.29, 154.44, 178.67.

LC-MS: 2.89 min, m/z: theo 205.21; meas. [MH^+] 206.1 (system 1)

***Tert*-butyl (*S*)-(2-(benzyl(2-hydroxy-3-((2-oxoindolin-4-yl)oxy)propyl)amino)ethyl)carbamate (48)**

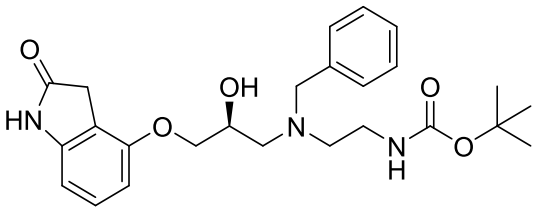

A solution of **48** (0.508g, 1 eq.) and benzyl *tert*-butyl ethane-1,2-diyldicarbamate (1.24g, 2 eq.) were dissolved in HFIP (20 mL) and stirred at room temperature for 44 h[166]. The solvent was evaporated under reduced pressure and the crude material was purified by flash column chromatography on silica employing a gradient from 0 to 15% 1N NH_3 in MeOH and DCM as eluent to afford the title compound as anto yield a brown oil (50%)

^{1}H NMR (CD_3OD): δ 1.43 (s, 9H, CH_3), 3.50 (s, 2H, CH_2), 5.11 (s, 2H, CH_2), 6.56-6.54 (d, J=8.4427Hz, 1H, ArH), 6.63-6.61 (d, J=8.4427Hz, 1H, ArH), 7.17-7.13 (t, J= 4.8Hz, 1H, ArH), 7.43-7.38 (m, 5H, ArH), 8.91 (s, 1H, NH amide)

^{13}C NMR (CD_3OD): δ 27.660 (3), 28.22, 39.43, 56.28, δ59.28, 67.94, 69.94, 78.62, 102.99, 105.82, 112.32, 126.94, 127.93, 128.86, 128.50, 139.18, 144.28, 153.60, 154.55, 157.04, 157.08, 178.71

LC-MS: 3.41 min, m/z: theo 455.56; meas. [MH^+] 456.1 (system 1)

(*S*)-4-(3-((2-aminoethyl)(benzyl)amino)-2-hydroxypropoxy)indolin-2-one hydrochloride (49)

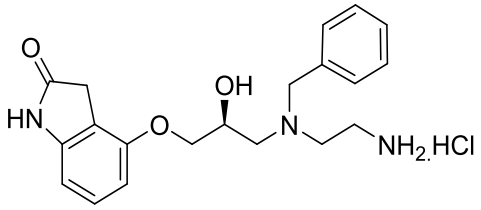

Compound **49** was synthesized *via* general procedure C to afford an orange wax (0.986 g, 90%), which was dried and used without further purification.

^{1}H NMR (CD_3OD): δ 3.50 (s, 2H, CH_2), 5.11 (s, 2H, CH_2), 6.56-6.54(d, J=8.447Hz, 1H, ArH), 6.64-6.61 (d, J=8.447Hz, 1H, ArH), 7.17-7.13 (m, 1H, ArH), 7.45-7.43 (m, 5H, ArH), 9.82 (s, 1H, NH amide)

^{13}C NMR (CD_3OD): δ 28.22, 39.43, 56.28, 59.28, 60.02, 67.94, 69.94, 78.62, 102.99, 105.82, 112.32, 126.94, δ127.93, δ128.86, 129.23, 139.18, 144.28, 154.72, 155.60, δ158.08, 177.17

LC-MS: 2.24 min, m/z: theo 355.44; meas. [MH^+] 356.1 (system 1)

***Tert*-butyl (*S*)-(2-((2-(benzyl(2-hydroxy-3-((2-oxoindolin-4-yl)oxy)propyl)amino)ethyl)amino)-2-oxoethyl)carbamate (50)**

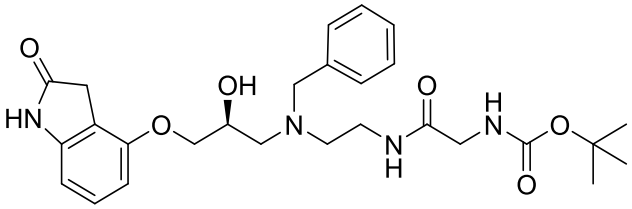

Compound (**50**) was synthesized *via* general procedure B to afford a transparent oil (0.344g, 43%).

^{1}H NMR (CD_3OD): δ 1.43 (s, 9H, CH_3), 3.54-3.46 (m, 3H, CH_2), 3.74-3.66 (m, 3H, CH_2), 3.95-3.93 (m, 2H, CH_2), 4.07-4.02 (m, 3H, CH_2), 4.38-4.31 (m, 3H, CH_2), 4.68-4.64 (m, 3H, CH_2), 4.88 (s, 1H, OH), 6.60-6.54 (m, 3H, ArH), 7.19-7.13 (m, 2H, ArH), 7.17-7.13 (m, 2H, ArH), 7.61-7.60 (m, 1H, ArH), 8.08 (s, 1H, NH amide)

^{13}C NMR (CD_3OD): δ 26.81 (3), δ33.109, 41.96, 43.34, δ58.63 (2), 60.411, 67.94, 69.298, 80.095, 102.99, 103.572, 116.79, 126.45, 127.93, 130.849 (2), 141.41, 144.07, 154.72 (2), 155.44, 157.33, 174.39, 178.62

LC-MS: 3.21 min, m/z: theo. 512.61; meas. [MH^+] 513.2 (system 1)

(*S*)-2-amino-N-(2-(benzyl(2-hydroxy-3-((2-oxoindolin-4-yl)oxy)propyl)amino)ethyl)acetamide hydrochloride (51)

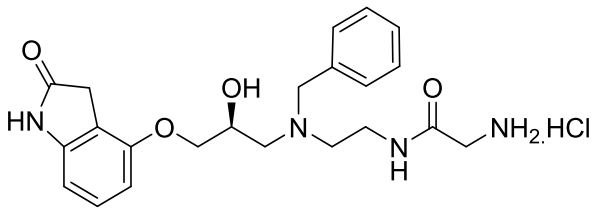

Compound **51** was synthesised *via* protocol C to afford an orange oil in quantitative yield (0.285g), which was dried *in vacuo* and used without further purification.

^{1}H NMR (CD_3OD): δ 3.25-3.16 (m, 2H, CH_2), 3.74-3.66 (m, 3H, CH_2), 3.95-3.93 (m, 2H, CH_2), 4.07-4.02 (m, 3H, CH_2), 4.38-4.31 (m, 3H, CH_2), 4.68-4.65 (m, 3H, CH_2), 4.88 (s, 1H, OH), 6.58-6.45 (m, 3H, ArH), 7.14-7.10 (m, 2H, ArH), 7.67-7.45 (m, 2H, ArH), 7.98-7.72 (m, 1H, ArH), 8.44 (s, 1H, NH amide), 8.85 (s, 2H, NH_2), 10.39 (s, 1H, AR-NH amide).

^{13}C NMR (CD_3OD): δ 37.80, 40.241, 2.35, 55.042 (2), 60.80 (2), 66.75, 69.34, 71.06, 103.41, 105.78, 112.30, 129.11, 131.28 (2), 141.41, 144.07, 154.185, 168. 25, 170.87, 178.62

LC-MS: 0.62 min, m/z: theo 412.35; meas. [MH^+] 413.00 (system 1)

***Tert*-butyl ((*S*)-1-((2-((2-(benzyl((*S*)-2-hydroxy-3-((2-oxoindolin-4-yl)oxy)propyl)amino)ethyl)amino)-2-oxoethyl)amino)-1-oxopropan-2-yl)carbamate (52a)**

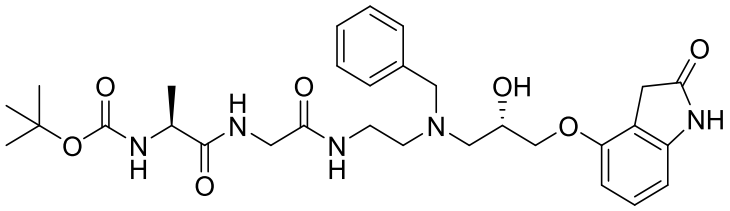

Compound **52a** was synthesized *via* general procedure C to afford an orange oil (0.105 g, 62%).

^{1}H NMR (CD_3OD): δ 1.34 (s, 9H, CH_3), 1.37 (s, 3H, CH_3), 1.80-1.74 (m, 2H, CH_2), 2.43-2.39 (s, 2H, CH_3), 2.98-2.88 (m, 2H, CH_2), 3.16-3.12 (m, 1H, CH_2), 3.36 (s, 2H, CH_2), 3.69-3.66 (m, 2H, CH_2), 3.98-3.94 (m, 2H, CH_2), 4.27 (m, 2H, CH_2), 5.42 (s, 2H, CH_2), 6.45-6.43 (m, 1H, ArH), 6.61-6.59 (m, 1H, ArH), 6.73-6.69 (d, 1H, ArH), 6.88-6.86 (m, 1H, ArH), 7.14-7.06 (m, 1H, ArH), 7.36-7.29 (m, 3H, ArH), 8.91 (s, 1H, NH amide), 8.19 (m, 2H, NH amide), 10.41 (s, 1H, AR-NH amide)

^{13}C NMR (CD_3OD): δ 22.071 (CH_3, 1-C), δ28.601 (CH, 3-C), 30.87, 34.79, 37.98, 40.24, 42.55, 50.52 (2), 65.99, 68.61, 70.59, 78.63, 103.39, 106.27, 112.72, 125.40, 128.44, 129.42, 139.62 (2), 145.32, 151.90, 154.54, 155.73, 169.85, 173.58, 176.85

LC-MS: 3.14 min, m/z: theo 583.3; meas. [MH^+] 584.1 (system 1)

***Tert*-butyl ((*S*)-1-((2-((2-(benzyl((*S*)-2-hydroxy-3-((2-oxoindolin-4-yl)oxy)propyl)amino)ethyl)amino)-2-oxoethyl)amino)-3-hydroxy-1-oxopropan-2-yl)carbamate (52b)**

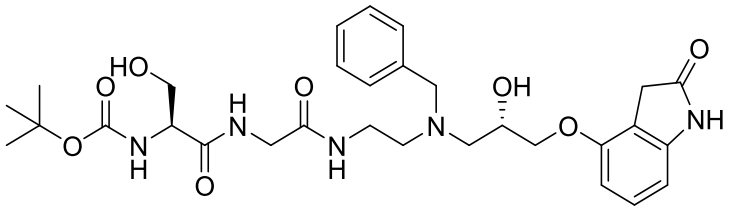

Compound **52b** was synthesized *via* general procedure B to afford a yellow oil (0.144 g, 74%).

^{1}H NMR (CD_3OD): δ 1.39 (s, 9H, CH_3), 2.17 (s, 2H, CH_3), 2.93-2.88 (m, 3H, CH_2), 3.12-3.01 (m, 1H, CH_2), 3.36 (s, 4H, CH_2), 3.65-3.52 (m, 2H, CH_2), 3.77-3.65 (m, 2H, CH_2), 4.03-3.89 (m, 3H, CH_2), 4.12-4.03 (m, 2H, OH), 4.26-4.24 (m, 1H, CH_2), 5.37 (s, 1H, OH), 6.49-6.43 (m, 2H, ArH), 6.61-6.59 (m, 2H, ArH), 6.82-6.79 (m, 1H, ArH), 6.88-6.83 (m, 2H, ArH), 7.14-7.10 (m, 1H, ArH), 7.99 (m, 1H, NH_2 amine), 8.21-8.18 (m, 2H, NH amide), 10.38 (s, 1H, AR-NH amide)

^{13}C NMR (CD_3OD): δ 28.605 (3), 30.88, 34.00, 34.82, 36.39, 42.76, 43.43, 50.51, 57.26, 62.26 (2), 66.11, 68.73, 70.43, 78.88, 103.79, 106. 81, 112.76, 125.63, 128.52, 129.35, 139.67, 142. 23, 155.63, 169.94, 171.43, 176.86, 178.31

LC-MS: 2.80 min, m/z: theo 599.69; meas. [MH^+] 600.04 (system 1)

(*S*)-2-amino-N-(2-((2-(((*S*)-2-hydroxy-3-((2-oxoindolin-4-yl)oxy)propyl)amino)ethyl)amino)-2-oxoethyl)propanamide (53a)

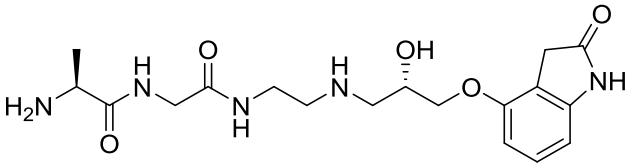

This compound was synthesised *via* protocol C to a quantitative yield an orange oil, which was dried and used without further purification

^{1}H NMR (CD_3OD): δ 1.37 (s, 3H, CH_3), 2.43-2.39 (s, 2H, CH_3), 2.98-2.88 (m, 2H, CH_2), 3.16-3.12 (m, 1H, CH_2), 3.36 (s, 2H, CH_2), 3.69-3.66 (m, 3H, CH_2), 3.98-3.94 (m, 3H, CH_2), 4.27 (m, 2H, CH_2), 5.42 (s, 2H, CH_2), 6.61-6.59 (m, 1H, ArH), 6.73-6.69 (m, 1H, ArH), 7.14-7.06 (m, 1H, ArH), 8.19 (m, 2H, NH_2 amine), 8.91 (s, 1H, NH amide), 10.42 (s, 1H, AR-NH amide)

^{13}C NMR (CD_3OD): δ 22.07, 30.86, 37.08, 40.24, 42.54, 50.50 (2), 65.99, 68.61, 103.38, 106.27, 112.72, 129.43, 145.32, 155.73, 169.84, 173.58, δ176.84

LC-MS: 0.35 min, m/z: theo 393.44; meas. [MH^+] 394.1 (system 1)

(*S*)-2-amino-3-hydroxy-N-(2-((2-(((*S*)-2-hydroxy-3-((2-oxoindolin-4-yl)oxy)propyl)amino)ethyl)amino)-2-oxoethyl)propanamide (53b)

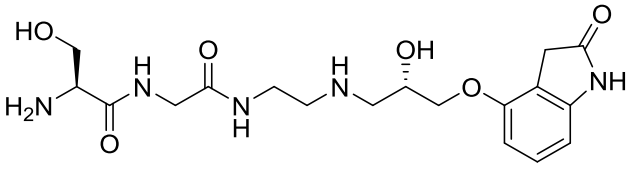

This compound was synthesised *via* protocol C to a quantitative yield an orange oil, which was dried and used without further purification

^{1}H NMR (CD_3OD): δ 2.43-2.39 (s, 2H, CH_3), 2.98-2.88 (m, 2H, CH_2), 3.16-3.12 (m, 1H, CH_2), 3.36 (s, 2H, CH_2), 3.69-3.66 (m, 4H, CH_2), 3.98-3.94 (m, 5H, CH_2), 4.00-4.17 (m, 2H, CH_2), 4.30 (s, 1H, OH), 5.37 (s, 1H, OH), 6.61-6.59 (m, 1H, ArH), 6.73-6.69 (m, 1H, ArH), 7.14-7.06 (m, 1H, ArH), 8.19 (m, 2H, NH_2 amine), 8.91 (s, 1H, NH amide), 10.41 (s, 1H, AR-NH amide)

^{13}C NMR (CD_3OD): δ 30.86, 37.80, 40.24, 42.54, 50.50, 53.88, 62.99, 68.61, 78.71, 103.38, 106.27, 112.72, 129.43, 145.32, 155.73, 169.84, 173.58, 176.84

LC-MS: 0.62 min, m/z: theo 409.44; meas. [MH^+] 411.0 (system 1)

6-(2-(4-((E)-2-(5,5-difluoro-7-(thiophen-2-yl)-5H-4l4,5l4-dipyrrolo[1,2-c:2',1'-f][1,3,2]diazaborinin-3-yl)vinyl)phenoxy)acetamido)-N-((*S*)-1-((2-((2-(((S)-2-hydroxy-3-((2-oxoindolin-4-yl)oxy)propyl)amino)ethyl)amino)-2-oxoethyl)amino)-1-oxopropan-2-yl)hexanamide (54a)

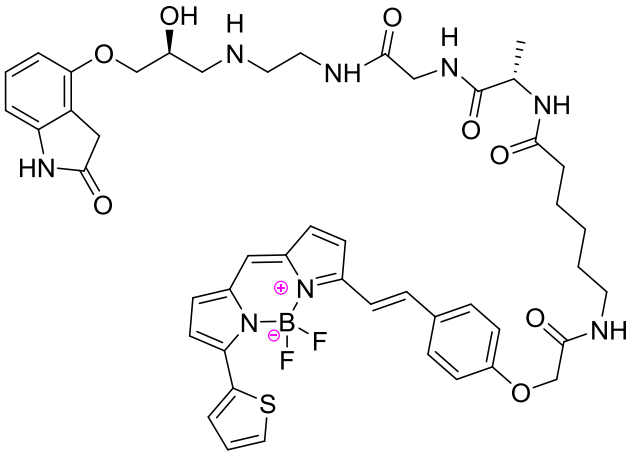

The compound was synthesized *via* general procedure E (28%).

HPLC Rt: 17.65 min (system 4), 4.62 min (system 2)

m/z: HRMS (TOF ES$^+$) $C_{43}H_{53}BF_2N_8O_8S$ [MH]$^+$ calcd. 939.3911; found 939.3923**.**

6-(2-(4-((E)-2-(5,5-difluoro-7-(thiophen-2-yl)-5H-4l4,5l4-dipyrrolo[1,2-c:2',1'-f][1,3,2]diazaborinin-3-yl)vinyl)phenoxy)acetamido)-N-((*S*)-3-hydroxy-1-((2-((2-(((S)-2-hydroxy-3-((2-oxoindolin-4-yl)oxy)propyl)amino)ethyl)amino)-2-oxoethyl)amino)-1-oxopropan-2-yl)hexanamide (54b)

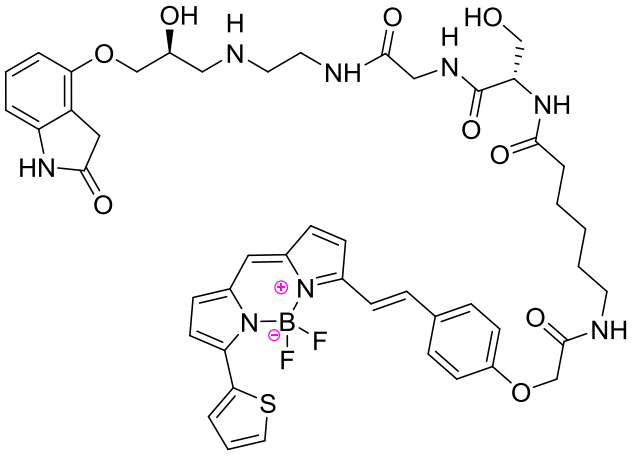

The compound was synthesized *via* general procedure E (37%).

HPLC Rt: 12.87 min (system 4), 4.44 min (system 1)

m/z: HRMS (TOF ES$^+$) $C_{43}H_{53}BF_2N_8O_9S$ [MH]$^+$ calcd. 955.3972; found 955.3956

3-(5,5-difluoro-7,9-dimethyl-10,10a-dihydro-5H-4l4,5l4-dipyrrolo[1,2-c:2',1'-f][1,3,2]diazaborinin-2-yl)-N-((*S*)-1-((2-((2-(((*S*)-2-hydroxy-3-((2-oxoindolin-4-yl)oxy)propyl)amino)ethyl)amino)-2-oxoethyl)amino)-1-oxopropan-2-yl)propanamide (55a)

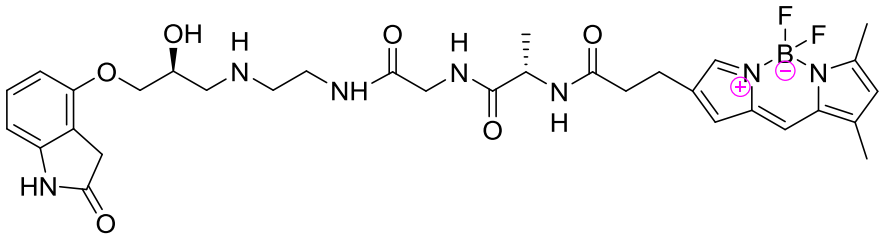

The compound was synthesized *via* general procedure E (23%).

HPLC Rt: 7.90 min (system 4), 3.36 min (system 1)

m/z: HRMS (TOF ES$^+$) $C_{32}H_{36b}F_2N_7O_6$ $[MH]^+$Na calcd. 690.3008; found 690.3002

(2*S*)-2-(3-(5,5-difluoro-7,9-dimethyl-10,10a-dihydro-5H-4l4,5l4-dipyrrolo[1,2-c:2',1'-f][1,3,2]diazaborinin-2-yl)propanamido)-3-hydroxy-N-(2-((2-(((*S*)-2-hydroxy-3-((2-oxoindolin-4-yl)oxy)propyl)amino)ethyl)amino)-2-oxoethyl)propanamide (55b)

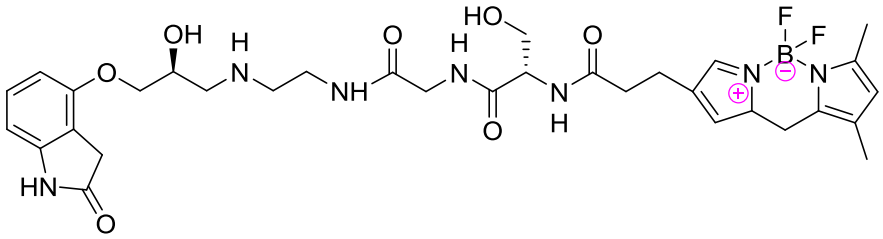

The compound was synthesized *via* general procedure E (30%).

HPLC Rt: 8.30 min (system 4), 3.26 min (system 1)

m/z: HRMS (TOF ES^+) $C_{32}H_{38b}F_2N_7O_7$ $[MH]^+$ calcd. 684.3122; found 684.3116

4.2 Pharmacology Method

Materials. Cell culture reagents were from Sigma Chemicals (Poole, Dorset, UK) except fetal calf serum, which was from PAA laboratories (Teddington, Middlesex, UK). [^{3}H]-CGP 12177 were obtained from Perkin Elmer (Workingham, UK). All other reagents were supplied by Sigma Chemicals. All plates were obtained from Corning Costar (Corning Incorporated, Corning, NY, USA), unless otherwise stated.

4.2.1 Cell Culture

CHO-CRE-SPAP and HEK 293 Nluc β_1 and β_2-ARs, and SNAP-β_1 and β_2-ARs cells were used throughout this study. CHO-CRE-SPAP β_1 and β_2-ARs cells were obtained from Dr Gherbi. HEK 293 β_1-AR Nluc cells were obtained from Dr Stoddart who performed the transfection, dilution cloning and isolation of a stable clone whereas HEK 293 β_2-AR Nluc cells were obtained from Promega UK. SNAP-β_1 and β_2-ARs cells were obtained from Dr Goulding who performed the transfection, dilution cloning and isolation of a stable clone. The CHO cell lines were cultured in Dulbecco's modified Eagle's medium/nutrient mix F12 (DMEM/F12) supplemented with 2mM L-glutamine and 10% heat-inactivated fetal calf serum (FCS) (PAA Laboratories, Teddington, Middlesex, UK). The HEK 293 cells were maintained in DMEM supplemented with 2mM L-glutamine and 10% FCS. All cell lines were incubated at 37 °C, 5% CO_2 and the culture procedures were performed in a class II laminar flow hood using sterile techniques.

4.2.1.1 Passaging of Cells

All cell lines were passaged once they had grown to 80% confluence in a 75 cm^2 tissue culture flask (T75) flask. Medium was removed by vacuum and the cells were

washed with warm Dulbecco's phosphate buffered saline (PBS) (5mL). PBS was aspirated and cells were then incubated with warm trypsin/EDTA (T/E) (1 mL) until cells were detached from the bottom of the flask. Once detached, fresh medium (10 mL) was added to the flask and the resulting suspension was spun at 1000 rpm for five minutes. The pellet was re-suspended in medium (1 mL) using a pipette, which involved rapid agitation to ensure the production of a uniform suspension. The suspended cells were then transferred to a universal flask containing 10mL medium and the resulting suspension was dispensed as appropriate into 75 mL flasks.

4.2.1.2 Seeding into plates

All cells from confluent T75 flasks were removed from the flask and centrifuged as described above. The CHO cells were grown to confluence in clear 96 well plates. For HEK 293, plates were coated with poly-D-lysine prior to the seeding; cells required for imaging were seeded into eight well chambers. HEK293 Nlucs were grown to confluence in white-walled, clear bottom 96 well plates after poly-D-lysine treatment in order to allow the cells to adhere to the plate. Cells required for radio-ligand binding and NanoBRET assays were seeded 24 hours prior to experiment, where a T75 flask was used to set up a maximum of four 96-well plates. Cells required for the SPAP assays were seeded 44 hours prior to experiment, one T75 flask was used to set up a maximum of six 96 well plates.

4.2.1.3 Cell freezing and thawing

Freezing

Cells from confluent T150 flasks were treated with trypsin and centrifuged as described previously. The cell pellet was carefully resuspended in the freezing

medium (5 mL, 10% DMSO in FCS). 1 mL of cell suspension was transferred to a cryo*via*l (Nalgene, Rochester, NY, USA) and cooled in an isopropanol-filled freezing chamber (Mr Frosty) to reduce the temperature at a rate of approximately 1 °C/min for 24 hours. The following day, cryo*via*ls were transferred to the -80 freezer. And then to liquid nitrogen for long term storage.

Thawing

The cyro*via*l from the -80 freezer was warmed to 37 °C and its contents were suspended into growth medium (10 mL) and the resulting suspension was spun at 1000rpm for five minutes. The pellet was re-suspended in medium (1 mL) and transferred to a 75 mL flask containing 20 mL of medium. After 8-12 hours, growth medium was removed and replaced with fresh growth media, removing the cell debris that did not survive the freezing/thawing process.

4.2.2 Assays

4.2.2.1 CRE-SPAP Gene Transcription.

CRE-SPAP cells β_1 and β_2-ARs were grown to confluence in clear 96-well plates. Cells were serum starved for 18 h prior to experiment before experimentation in DMEM/F12 containing 2 mM L-glutamine (serum-free media). On the day of experiment, fresh serum-free medium (DMEM/F12 supplemented with 2 mM L-glutamine) was added to the cells, and three concentrations (10, 100, 1000 nM) of fluorescent ligands were added to the appropriate wells, and cells were incubated for 30 min at 37 °C/ 5% CO_2. After 30 min, increasing concentrations of the agonist cimaterol were added to the cells, which were then incubated for a further 5 h.

Following the 5 h incubation, all medium was removed from the cells, 40 μL of fresh serum-free medium was added to each well, and cells were incubated for a further 1 h at 37 °C/ 5% CO_2. The plates were then incubated at 65 °C for 30 min to destroy any endogenous alkaline phosphatases. Plates were cooled to room temperature, and 100 μL of 5 mM 4-nitrophenyl phosphate in diethanolamine-containing buffer [10% (v/v) diethanolamine, 280 mM NaCl, 500 μM $MgCl_2$, pH 9.85] was added to each well; the plates were then incubated at 37 °C for 20 min. The absorbance at 405 nm was measured using a Dynex MRX plate reader (Chelmsford, MA).[203]

4.2.2.2 NanoBRET

β_1 and β_2-ARs NLucs HEK 293 cells were grown to confluence in clear 96-well plates. On the day of the experiment, fresh HEPES buffer [HEPES Balanced Salt Solution (HBSS), 25 mM HEPES, 10 mM glucose, 142 mM NaCl, 5 mM KCl, 1 mM $MgSO_4$, 2 mM sodium pyruvate, 1.3 mM $CaCl_2$ at pH 7.4] was added to the cells. For saturation experiments, Nlucs cells were incubated with increasing concentrations of the ten fluorescent ligands in the presence or absence of 1 μM propranolol for 2 h at 37 °C. For competition experiments using the same fluorescent ligands as previous, the β_1 and β_2-ARs NLucs HEK 293 cells were incubated with 10 nM fluorescent ligand and the required concentration of competing ligand (CGP20712A, Propranolol, cimaterol or ICI 118551) diluted in HEPES buffered saline solution for 2 h at 37 °C. The luminescence and fluorescence was measured using the PHERAstar FS plate reader (BMG Labtech) at room temperature. The filtered light emissions were read at 420 nm (80-nm bandpass) and 535 nm (60-nm

bandpass) for BY-FL labelled ligands (**41a, b & d**, **42**, **43, 44** and **59 a-b**) and at 420 nm (80-nm bandpass) and >610 nm (longpass) for the BY630-labelled compounds (**38a-e, 43, 44** and **58a-b)**. The raw BRET ratio was calculated by dividing the >610-nm emission or 535-nm emission by the 420-nm emission. The term "raw BRET ratio" refers to the unprocessed data as no background ratio has been subtracted[71].

4.2.2.3 Radioligand binding

β_1 and β_2-ARs NLucs and CRE-SPAP β_1 and β_2-ARs were seeded into 96-well white-sided plates 24 hours prior to the assay according to the seeding protocol above. For saturation binding, on the day of experimentation, all media was aspirated and twelve different concentrations of the ligand [^{3}H]-CGP 12177 (ligand was obtained from Perkin Elmer and has a specific activity of 37.7Ci/mmol) were added (100µl/well) in quadruplicate. Total and non-specific binding was defined by adding serum free media in quadruplicate (total binding) and 1 µl propranolol (non-specific binding). For competition binding experiments, cells were incubated with 100µL of various concentrations of fluorescent ligands and [^{3}H]-CGP 12177, which was made at concentrations varying between 3-9 nM in serum free media and was added to all wells (100µl/well). The cells were incubated for 2 hours at 37 °C, 5% CO_2. After 2 hour incubation, the cells were washed twice with cold PBS (200 µl/well) in order to wash any unbound ligand from the cells. White backing was added to each plate and 100 µl of microscintillant was added to each well. Finally the plates were sealed and counted on a Topcount Microplate Illuminator.

4.2.2.4 Confocal Microscopy

Cells were grown in Labtek eight-well plates (Nunc Nalgene, Rochester, NY) for at least 18 h and grown to 70-80% confluence before imaging. For β_2 (HEK 293) cells, plates were coated with poly-D-lysine prior to cell seeding. The HEK 293 cells were washed with HEPES-buffered saline solution (HBSS at pH 7.4; 25 mM HEPES, 10 mM glucose, 142 mM NaCl, 5 mM KCl, 1 mM $MgSO_4$, 2 mM sodium pyruvate, 1.3 mM $CaCl_2$). Following the washing step, cells were pre-incubated for 30 minutes with the presence or absence of unlabeled ligand propranolol hydrochloride or ICI 118551 hydrochloride and 15-30 minutes incubation with the fluorescent ligands of choice. Live cell imaging was performed at room temperature using a Zeiss LSM 710 laser scanning confocal microscope and a Zeiss Plan-Neofluar 40 x 1.3 NA oil-immersion objective. A 633 nm HeNe laser was used for the excitation of the BODIPY630/650 and 448 nm laser for BODIPY-FL for all represented fluorescent probes. The pinhole diameter (1 Airy Unit; 1.1 μm optical slice), laser power, and gain remained constant between experiments[70].

4.2.3 Data Analysis

All data are represented as mean ± S.EM. of triplicate determinations unless otherwise stated. The n in the text refers to the number of separate experiments (a separate experiment requires cells plated from a separate flask and separate drug dilution used throughout the experiment). The data is presented and analyzed using Prism software (GraphPad Prism 6) and Excel. The student unpaired t-test was used as a statistical tool in order to determine if two sets of data are significantly different from each other.

Reporter gene assay SPAP: Antagonism by acetylated and fluorescent ligands of the CRE-reporter gene response (SPAP, secreted placental alkaline phosphatase) to cimaterol in CHO cells expressing the human β_1 & β_2-adrenoceptor. For each concentration of the antagonists, the ratio (DR, dose ratio) of cimaterol concentrations required to produce the same sized response in the presence and absence of the antagonist is determined. The antagonist affinity constant (K_B) can then be determined either directly from the Gaddum equation or from a Schild plot of log (DR-1) against the log of the antagonist concentration ([B]).

Gaddum: $\mathbf{DR = 1 + [B] K_B}$ **Equation 1**

Schild: $\mathbf{Log\ (DR-1) = log\ [B] + log\ K_B}$ **Equation 2**

NanoBRET: We simultaneously fitted the total and nonspecific saturation binding curves using the following equation

$$\mathbf{BRET\ ratio} = \frac{\mathbf{B_{max}[B]}}{\mathbf{[B]+(K_D)}} + \mathbf{(M[B] + C)} \qquad \textbf{Equation 3}$$

Where B_{max} is the maximal response, [B] is the concentration of fluorescent ligand in nM, K_D is the equilibrium dissociation constant in nM, M is the slope of the nonspecific binding component, and C is the intercept with the y axis. We fitted the competition binding curves to calculate the K_i of the unlabeled ligands using the Cheng-Prusoff equation

$$\mathbf{K_i} = \frac{\mathbf{IC_{50}}}{\mathbf{1+(L/K_D)}} \qquad \textbf{Equation 4}$$

Where [L] is the concentration of fluorescent ligand in nM and K_D is the dissociation constant of fluorescent ligand in nM. The calculated K_D values used were as

calculated from the saturation binding experiments. The IC_{50} is calculated from the following equation

$$\textbf{BRET ratio} = \frac{\textbf{100 x [A]}}{\textbf{[A]+(IC}_{\textbf{50}}\textbf{)}} \qquad \textbf{Equation 5}$$

Where [A] is the concentration of competing drug and the IC_{50} is the molar concentration of ligand required to inhibit 50% of the specific binding of concentration [L] of the fluorescent ligand. We also used this equation to fit concentration-inhibition data where the affinity of the labeled ligand is unknown.

Radioligand: In order to determine the actual concentration of radioligand, 100 µl was added in triplicate to scintillation *via*ls. Scintillation fluid (5 mL) was added to each *via*l and the *via*l was counted on the Perkin Elmer Tri-Carb liquid scintillation counter. The dpm was then converted to concentration of [^{3}H]-CGP 12177 from the following:

1 Ci = 2.22 x 1012. Specific activity of [^{3}H]-CGP 12177 = 37.7 Ci/mmol

Therefore 1dpm = 1/(37.7 x 2.22 x1012) mmol.

K_D values were then determined from the IC_{50} values and concentration of radioligand according to the expression:

$$\mathbf{K_D} = \frac{\mathbf{IC_{50}}}{\mathbf{1+(A/K_{D(CGP)})}} \qquad \textbf{Equation 6}$$

Where [A] is the concentration of [^{3}H]-CGP 12177 used in the displacement, and K_d is the dissociation constant of [^{3}H]-CGP 12177.

5 REFERENCES

1. Mistry, S.; Daras, E.; Fromont, C.; Jadhav, G.; Fischer, P. M.; Kellam, B.; Hill, S. J.; Baker, J. G. Novel cyclic phenoxy compounds and improved treatments for cardiac and cardiovascular disease. In Google Patents: 2013.

2. Baker, J. G.; Adams, L. A.; Salchow, K.; Mistry, S. N.; Middleton, R. J.; Hill, S. J.; Kellam, B. Synthesis and Characterization of High-Affinity 4,4-Difluoro-4-bora-3a,4a-diaza-s-indacene-Labeled Fluorescent Ligands for Human beta 2-Adrenoceptors. *Journal of Medicinal Chemistry* **2011,** 54, 6874-6887.

3. Brodde, O.-E. Beta-adrenoceptors in cardiac disease. *Pharmacology & Therapeutics* **1993,** 60, 405-430.

4. Carr, R. A. E.; Congreve, M.; Murray, C. W.; Rees, D. C. Fragment-based lead discovery: leads by design. *Drug Discovery Today* **2005,** 10, 987-992.

5. Sell, H.; Deshaies, Y.; Richard, D. The brown adipocyte: update on its metabolic role. *The International Journal of Biochemistry & Cell Biology* **2004,** 36, 2098-2104.

6. Stoddart, L. A.; Vernall, A. J.; Denman, J. L.; Briddon, S. J.; Kellam, B.; Hill, S. J. Fragment Screening at Adenosine-A3 Receptors in Living Cells Using a Fluorescence-Based Binding Assay. *Chemistry & Biology* **2012,** 19, 1105-1115.

7. DeVree, B. T.; Mahoney, J. P.; Vélez-Ruiz, G. A.; Rasmussen, S. G. F.; Kuszak, A. J.; Edwald, E.; Fung, J.-J.; Manglik, A.; Masureel, M.; Du, Y.; Matt, R. A.; Pardon, E.; Steyaert, J.; Kobilka, B. K.; Sunahara, R. K. Allosteric coupling from G protein to the agonist-binding pocket in GPCRs. *Nature* **2016,** 535, 182-186.

8. Page, C. *Fast track Pharmacology*. 2 nd ed.; Pharmacology Press: London, 2012; Vol. 75, p 573-573.

9. Filmore, D. It's a GPCR world. *Modern Drug Discovery* **2004,** 7.

10. Tuteja, N. Signaling through G protein coupled receptors. *Plant Signaling & Behavior* **2009,** 4, 942-947.

11. Kobilka, B. K.; Frielle, T.; Dohlman, H. G.; Bolanowski, M. A.; Dixon, R. A.; Keller, P.; Caron, M. G.; Lefkowitz, R. J. Delineation of the intronless nature of the genes for the human and hamster β2-adrenergic receptor and their putative promoter regions. *Journal of Biological Chemistry* **1987,** 262, 7321-7327.

12. Rajagopal, K.; Lefkowitz, R. J.; Rockman, H. A. When 7 transmembrane receptors are not G protein–coupled receptors. *Journal of Clinical Investigation* **2005,** 115, 2971-2974.

13. Heuss, C.; Scanziani, M.; Gahwiler, B. H.; Gerber, U. G-protein-independent signaling mediated by metabotropic glutamate receptors. *Nat Neurosci* **1999,** 2, 1070-1077.

14. Lagerstrom, M. C.; Schioth, H. B. Structural diversity of G protein-coupled receptors and significance for drug discovery. *Nat Rev Drug Discov* **2008,** 7, 339-357.

15. Schiöth, H. B.; Fredriksson, R. The GRAFS classification system of G-protein coupled receptors in comparative perspective. *General and Comparative Endocrinology* **2005,** 142, 94-101.

16. Randall, M. D.; Kendall, D.; Alexander, S. *FASTtrack: Pharmacology*. 2nd ed.; Pharmaceutical Press: 2012.

17. Fredriksson, R.; Lagerström, M. C.; Lundin, L.-G.; Schiöth, H. B. The G-Protein-Coupled Receptors in the Human Genome Form Five Main Families.

Phylogenetic Analysis, Paralogon Groups, and Fingerprints. *Molecular Pharmacology* **2003,** 63, 1256-1272.

18. Hollinger, M. A. *Introduction to Pharmacology, Second Edition*. CRC Press: 2003; p 432 pp.

19. Kobilka, B. K. G protein coupled receptor structure and activation. *Biochimica et Biophysica Acta (BBA) - Biomembranes* **2007,** 1768, 794-807.

20. Jazayeri, A.; Doré, A. S.; Lamb, D.; Krishnamurthy, H.; Southall, S. M.; Baig, A. H.; Bortolato, A.; Koglin, M.; Robertson, N. J.; Errey, J. C.; Andrews, S. P.; Teobald, I.; Brown, A. J. H.; Cooke, R. M.; Weir, M.; Marshall, F. H. Extra-helical binding site of a glucagon receptor antagonist. *Nature* **2016,** 533, 274-277.

21. Chun, L.; Zhang, W.-h.; Liu, J.-f. Structure and ligand recognition of class C GPCRs. *Acta Pharmacol Sin* **2012,** 33, 312-323.

22. Dore, A. S.; Okrasa, K.; Patel, J. C.; Serrano-Vega, M.; Bennett, K.; Cooke, R. M.; Errey, J. C.; Jazayeri, A.; Khan, S.; Tehan, B.; Weir, M.; Wiggin, G. R.; Marshall, F. H. Structure of class C GPCR metabotropic glutamate receptor 5 transmembrane domain. *Nature* **2014,** 511, 557-562.

23. Salon, J. A.; Lodowski, D. T.; Palczewski, K. The Significance of G Protein-Coupled Receptor Crystallography for Drug Discovery. *Pharmacol Rev* **2011,** 63, 901-37.

24. Dijksterhuis, J. P.; Petersen, J.; Schulte, G. International Union of Basic and Clinical Pharmacology Review: WNT/Frizzled signalling: receptor–ligand selectivity with focus on FZD-G protein signalling and its physiological relevance: IUPHAR Review 3. *British Journal of Pharmacology* **2014,** 171, 1195-1209.

25. Wang, C.; Wu, H.; Katritch, V.; Han, G. W.; Huang, X.-P.; Liu, W.; Siu, F. Y.; Roth, B. L.; Cherezov, V.; Stevens, R. C. Structure of the human smoothened receptor bound to an antitumour agent. *Nature* **2013,** 497, 338-343.

26. Hamm, H. E. The many faces of G protein signaling. *J Biol Chem* **1998,** 273, 669-72.

27. Milligan, G. Constitutive activity and inverse agonists of G protein-coupled receptors: a current perspective. *Mol Pharmacol* **2003,** 64, 1271-6.

28. Li, J.; Ning, Y.; Hedley, W.; Saunders, B.; Chen, Y.; Tindill, N.; Hannay, T.; Subramaniam, S. The Molecule Pages database. *Nature* **2002,** 420, 716-717.

29. Oldham, W. M.; Hamm, H. E. Heterotrimeric G protein activation by G-protein-coupled receptors. *Nat Rev Mol Cell Biol* **2008,** 9, 60-71.

30. Milligan, G.; Kostenis, E. Heterotrimeric G-proteins: a short history. *British Journal of Pharmacology* **2006,** 147, S46-S55.

31. Stewart, A.; Fisher, R. A. Chapter One - Introduction: G Protein-coupled Receptors and RGS Proteins. In *Progress in Molecular Biology and Translational Science*, Rory, A. F., Ed. Academic Press: 2015; Vol. Volume 133, pp 1-11.

32. Dale Purves, G. J. A., David Fitzpatrick, William C. Hall, Anthony-Samuel LaMantia and Leonard E. White. Neuroscience Fith Edition. In *Neuroscience*, Sinauer Associates. Inc.: 2012; Vol. 5.

33. Dohlman, H. G.; Thorner, J.; Caron, M. G.; Lefkowitz, R. J. Model systems for the study of seven-transmembrane-segment receptors. *Annu Rev Biochem* **1991,** 60, 653-88.

34. Woodard, G. E.; Jardín, I.; Berna-Erro, A.; Salido, G. M.; Rosado, J. A. Chapter Three - Regulators of G-Protein-Signaling Proteins: Negative Modulators

of G-Protein-Coupled Receptor Signaling. In *International Review of Cell and Molecular Biology*, Kwang, W. J., Ed. Academic Press: 2015; Vol. Volume 317, pp 97-183.

35. Rasmussen, S. G. F.; DeVree, B. T.; Zou, Y.; Kruse, A. C.; Chung, K. Y.; Kobilka, T. S.; Thian, F. S.; Chae, P. S.; Pardon, E.; Calinski, D.; Mathiesen, J. M.; Shah, S. T. A.; Lyons, J. A.; Caffrey, M.; Gellman, S. H.; Steyaert, J.; Skiniotis, G.; Weis, W. I.; Sunahara, R. K.; Kobilka, B. K. Crystal structure of the [bgr]2 adrenergic receptor-Gs protein complex. *Nature* **2011,** 477, 549-555.

36. Blundell, T. L.; Patel, S. High-throughput X-ray crystallography for drug discovery. *Current Opinion in Pharmacology* **2004,** 4, 490-496.

37. Carvalho, A. L.; Trincão, J.; Romão, M. J. X-Ray Crystallography in Drug Discovery. In *Ligand-Macromolecular Interactions in Drug Discovery: Methods and Protocols*, Roque, A. A. C., Ed. Humana Press: Totowa, NJ, 2010; pp 31-56.

38. Frielle, T.; Collins, S.; Daniel, K. W.; Caron, M. G.; Lefkowitz, R. J.; Kobilka, B. K. Cloning of the cDNA for the human β1-adrenergic receptor. *Proceedings of the National Academy of Sciences of the United States of America* **1987,** 84, 7920-7924.

39. Bhattacharya, S.; Hall, S. E.; Li, H.; Vaidehi, N. Ligand-Stabilized Conformational States of Human β2 Adrenergic Receptor: Insight into G-Protein-Coupled Receptor Activation. *Biophysical Journal* **2008,** 94, 2027-2042.

40. Venkatakrishnan, A. J.; Deupi, X.; Lebon, G.; Tate, C. G.; Schertler, G. F.; Babu, M. M. Molecular signatures of G-protein-coupled receptors. *Nature* **2013,** 494, 185-194.

41. Stenkamp, R. E., Teller, D. C. and Palczewski, K. Crystal Structure of Rhodopsin: A G-Protein-Coupled Receptor. *ChemBioChem* **2002,** 3, 963–967.

42. Palczewski, K.; Kumasaka, T.; Hori, T.; Behnke, C. A.; Motoshima, H.; Fox, B. A.; Trong, I. L.; Teller, D. C.; Okada, T.; Stenkamp, R. E.; Yamamoto, M.; Miyano, M. Crystal Structure of Rhodopsin: A G Protein-Coupled Receptor. *Science* **2000,** 289, 739-745.

43. Ghosh, E.; Kumari, P.; Jaiman, D.; Shukla, A. K. Methodological advances: the unsung heroes of the GPCR structural revolution. *Nat Rev Mol Cell Biol* **2015,** 16, 69-81.

44. Rasmussen, S. G. F.; Choi, H.-J.; Rosenbaum, D. M.; Kobilka, T. S.; Thian, F. S.; Edwards, P. C.; Burghammer, M.; Ratnala, V. R. P.; Sanishvili, R.; Fischetti, R. F.; Schertler, G. F. X.; Weis, W. I.; Kobilka, B. K. Crystal structure of the human [bgr]2 adrenergic G-protein-coupled receptor. *Nature* **2007,** 450, 383-387.

45. Warne, T.; Moukhametzianov, R.; Baker, J. G.; Nehme, R.; Edwards, P. C.; Leslie, A. G. W.; Schertler, G. F. X.; Tate, C. G. The structural basis for agonist and partial agonist action on a [bgr]1-adrenergic receptor. *Nature* **2011,** 469, 241-244.

46. Wu, H.; Wacker, D.; Mileni, M.; Katritch, V.; Han, G. W.; Vardy, E.; Liu, W.; Thompson, A. A.; Huang, X.-P.; Carroll, F. I.; Mascarella, S. W.; Westkaemper, R. B.; Mosier, P. D.; Roth, B. L.; Cherezov, V.; Stevens, R. C. Structure of the human [kgr]-opioid receptor in complex with JDTic. *Nature* **2012,** 485, 327-332.

47. Dajani, R.; Cleasby, A.; Neu, M.; Wonacott, A. J.; Jhoti, H.; Hood, A. M.; Modi, S.; Hersey, A.; Taskinen, J.; Cooke, R. M.; Manchee, G. R.; Coughtrie, M. W. H. X-ray Crystal Structure of Human Dopamine Sulfotransferase. *Journal of Biological Chemistry* **1999,** 274, 37862-37868.

48. Carlsson, J.; Coleman, R. G.; Setola, V.; Irwin, J. J.; Fan, H.; Schlessinger, A.; Sali, A.; Roth, B. L.; Shoichet, B. K. Ligand Discovery from a Dopamine D(3) Receptor Homology Model and Crystal Structure. *Nature chemical biology* **2011,** 7, 769-778.

49. Haga, K.; Kruse, A. C.; Asada, H.; Yurugi-Kobayashi, T.; Shiroishi, M.; Zhang, C.; Weis, W. I.; Okada, T.; Kobilka, B. K.; Haga, T.; Kobayashi, T. Structure of the human M2 muscarinic acetylcholine receptor bound to an antagonist. *Nature* **2012,** 482, 547-551.

50. Shimamura, T.; Shiroishi, M.; Weyand, S.; Tsujimoto, H.; Winter, G.; Katritch, V.; Abagyan, R.; Cherezov, V.; Liu, W.; Han, G. W.; Kobayashi, T.; Stevens, R. C.; Iwata, S. Structure of the human histamine H1 receptor complex with doxepin. *Nature* **2011,** 475, 65-70.

51. Katritch, V.; Cherezov, V.; Stevens, R. C. Structure-function of the G protein-coupled receptor superfamily. *Annu Rev Pharmacol Toxicol* **2013,** 53, 531-56.

52. Zhang, K.; Zhang, J.; Gao, Z.-G.; Zhang, D.; Zhu, L.; Han, G. W.; Moss, S. M.; Paoletta, S.; Kiselev, E.; Lu, W.; Fenalti, G.; Zhang, W.; Muller, C. E.; Yang, H.; Jiang, H.; Cherezov, V.; Katritch, V.; Jacobson, K. A.; Stevens, R. C.; Wu, B.; Zhao, Q. Structure of the human P2Y12 receptor in complex with an antithrombotic drug. *Nature* **2014,** 509, 115-118.

53. Orellana, L.; Yoluk, O.; Carrillo, O.; Orozco, M.; Lindahl, E. Prediction and validation of protein intermediate states from structurally rich ensembles and coarse-grained simulations. *Nature Communications* **2016,** 7, 12575.

54. Vriend, G. WHAT IF: A molecular modeling and drug design program. *Journal of Molecular Graphics* **1990,** 8, 52-56.

55. Barcellos, G. B. P., Ivani; Caceres, Rafael Andrade; Macedo Timmers, Luis Fernando Saraiva; Dias, Raquel; de Azevedo Jr, Walter Filgueira. Molecular Modeling as a Tool for Drug Discovery. In *Current Drug Targets*, Bentham Science Publishers: 2008; Vol. 9, pp 1084-1091.

56. Meyer, E. F.; Swanson, S. M.; Williams, J. A. Molecular modelling and drug design. *Pharmacology & Therapeutics* **2000,** 85, 113-121.

57. Jacobson, K. A.; Gao, Z.-G.; Liang, B. T. NEOCEPTORS: REENGINEERING GPCRs TO RECOGNIZE TAILORED LIGANDS. *Trends in pharmacological sciences* **2007,** 28, 111-116.

58. Filipek, S.; Teller, D. C.; Palczewski, K.; Stenkamp, R. The Crystallographic Model of Rhodopsin and Its Use in Studies of Other G Protein–Coupled Receptors. *Annu Rev Biophys Biomol Struct* **2003,** 32, 375-97.

59. Meng, X. Y.; Mezei, M.; Cui, M. Computational Approaches for Modeling GPCR Dimerization. *Curr Pharm Biotechnol* **2014,** 15, 996-1006.

60. Vyas, V. K.; Ukawala, R. D.; Ghate, M.; Chintha, C. Homology Modeling a Fast Tool for Drug Discovery: Current Perspectives. *Indian Journal of Pharmaceutical Sciences* **2012,** 74, 1-17.

61. Kristiansen, K. Molecular mechanisms of ligand binding, signaling, and regulation within the superfamily of G-protein-coupled receptors: molecular modeling and mutagenesis approaches to receptor structure and function. *Pharmacology & Therapeutics* **2004,** 103, 21-80.

62. Kapetanovic, I. COMPUTER-AIDED DRUG DISCOVERY AND DEVELOPMENT (CADDD): in silico-chemico-biological approach. *Chem Biol Interact* **2008,** 171, 165-76.

63. Strange, P. G. Agonist binding, agonist affinity and agonist efficacy at G protein-coupled receptors. *British Journal of Pharmacology* **2008,** 153, 1353-1363.

64. Manglik, A.; Kobilka, B. The role of protein dynamics in GPCR function: insights from the β2AR and rhodopsin. *Current Opinion in Cell Biology* **2014,** 27, 136-143.

65. Christopoulos, A.; Kenakin, T. G Protein-Coupled Receptor Allosterism and Complexing. *Pharmacological Reviews* **2002,** 54, 323-374.

66. Kenakin, T.; Williams, M. Defining and characterizing drug/compound function. *Biochemical Pharmacology* **2014,** 87, 40-63.

67. Baker, J. G. The selectivity of β-adrenoceptor antagonists at the human β1, β2 and β3 adrenoceptors. *Br J Pharmacol* **2005,** 144, 317-22.

68. Baker, J. G.; Hall, I. P.; Hill, S. J. Pharmacological characterization of CGP 12177 at the human β(2)-adrenoceptor. *British Journal of Pharmacology* **2002,** 137, 400-408.

69. Bucher, E. S.; Fox, M. E.; Kim, L.; Kirkpatrick, D. C.; Rodeberg, N. T.; Belle, A. M.; Wightman, R. M. Medullary norepinephrine neurons modulate local oxygen concentrations in the bed nucleus of the stria terminalis. *Journal of Cerebral Blood Flow & Metabolism* **2014,** 34, 1128-1137.

70. Gherbi, K.; May, L. T.; Baker, J. G.; Briddon, S. J.; Hill, S. J. Negative cooperativity across beta1-adrenoceptor homodimers provides insights into the

nature of the secondary low-affinity CGP 12177 beta1-adrenoceptor binding conformation. *FASEB J* **2015**.

71. Stoddart, L. A.; Johnstone, E. K. M.; Wheal, A. J.; Goulding, J.; Robers, M. B.; Machleidt, T.; Wood, K. V.; Hill, S. J.; Pfleger, K. D. G. Application of BRET to monitor ligand binding to GPCRs. *Nat Meth* **2015,** advance online publication.

72. Kenakin, T. New concepts in pharmacological efficacy at 7TM receptors: IUPHAR Review 2. *British Journal of Pharmacology* **2013,** 168, 554-575.

73. Stephenson, R. P. A modification of receptor theory. *British Pharmacology* **1956,** 11, 379-393.

74. Thomsen, W.; Frazer, J.; Unett, D. Functional assays for screening GPCR targets. *Current Opinion in Biotechnology* **2005,** 16, 655-665.

75. Ewa Heyduk, Y. F. a. T. H. Homogeneous Fluorescence Assay for Cyclic AMP. *Combinatorial Chememistry and High Throughput Screening* **2003,** 6, 347-354.

76. Miller, T. R.; Baranowski, J. L.; Estvander, B. R.; Witte, D. G.; Carr, T. L.; Manelli, A. M.; Krueger, K. M.; Cowart, M. D.; Brioni, J. D.; Esbenshade, T. A. A robust and high-capacity [(35)S]GTPgammaS binding assay for determining antagonist and inverse agonist pharmacological parameters of histamine H(3) receptor ligands. *Assay Drug Dev Technol* **2008,** 6, 339-49.

77. Zhang, R.; Xie, X. Tools for GPCR drug discovery. *Acta Pharmacologica Sin* **2012,** 33, 372-384.

78. Flanagan, C. A. Chapter 10 - GPCR-radioligand binding assays. In *Methods in Cell Biology*, Arun, K. S., Ed. Academic Press: 2016; Vol. Volume 132, pp 191-215.

79. Liu, A. M.; New, D. C.; Lo, R. K.; Wong, Y. H. Reporter gene assays. *Methods Mol Biol* **2009,** 486, 109-23.

80. Hill, S. J.; Baker, J. G.; Rees, S. Reporter-gene systems for the study of G-protein-coupled receptors. *Current Opinion in Pharmacology* **2001,** 1, 526-532.

81. Heitman, L. H.; van Veldhoven, J. P.; Zweemer, A. M.; Ye, K.; Brussee, J.; AP, I. J. False positives in a reporter gene assay: identification and synthesis of substituted N-pyridin-2-ylbenzamides as competitive inhibitors of firefly luciferase. *J Med Chem* **2008,** 51, 4724-9.

82. Dale, M. M.; Haylett, D. G. *Pharmacology Condensed*. Churchill Livingstone: 2003; p 120 pp.

83. Torres-Marquez, M. E.; Villalobos-Molina, R.; Garca-Sainz, J. A. Adrenoceptor subtypes in aorta and liver *European Journal of Pharmacology: Molecular Pharmacology* **1991,** 206, 199-202.

84. Civantos Calzada, B.; Aleixandre de Artiano, A. Alpha-adrenoceptor subtypes. *Pharmacological Research* **2001,** 44, 195-208.

85. Gardiner, J. C.; Peters, C. J. Postsynaptic Î±1- and Î±2-adrenoceptor involvement in the vascular responses to neuronally released and exogenous noradrenaline in the hindlimb of the dog and cat. *European Journal of Pharmacology* **1982,** 84, 189-198.

86. Feng, Z.; Hou, T.; Li, Y. Studies on the Interactions between Î²2 Adrenergic Receptor and Gs Protein by Molecular Dynamics Simulations. *Journal of Chemical Information and Modeling* **2012,** 52, 1005-1014.

87. Cazzola, M.; Calzetta, L.; Matera, M. G. β2-adrenoceptor agonists: current and future direction. *British Journal of Pharmacology* **2011,** 163, 4-17.

88. Germack, R.; Starzec, A. B.; Vassy, R.; Perret, G. Y. β-Adrenoceptor subtype expression and function in rat white adipocytes. *British Journal of Pharmacology* **1997,** 120, 201-210.

89. Perrone, M. G.; Santandrea, E.; Bleve, L.; Vitale, P.; Colabufo, N. A.; Jockers, R.; Milazzo, F. M.; Sciarroni, A. F.; Scilimati, A. Stereospecific synthesis and bio-activity of novel β3-adrenoceptor agonists and inverse agonists. *Bioorganic & Medicinal Chemistry* **2008,** 16, 2473-2488.

90. Stevens, F. C.; Bloomquist, W. E.; Borel, A. G.; Cohen, M. L.; Droste, C. A.; Heiman, M. L.; Kriauciunas, A.; Sall, D. J.; Tinsley, F. C.; Jesudason, C. D. Potent oxindole based human Î²3 adrenergic receptor agonists. *Bioorganic & Medicinal Chemistry Letters* **2007,** 17, 6270-6273.

91. Tang, J.; Li, Z.; Lu, L.; Cho, C. H. β-Adrenergic system, a backstage manipulator regulating tumour progression and drug target in cancer therapy. *Seminars in Cancer Biology* **2013,** 23, 533-542.

92. Cardwell, C. R.; Coleman, H. G.; Murray, L. J.; Entschladen, F.; Powe, D. G. Beta-blocker usage and breast cancer survival: a nested case-control study within a UK Clinical Practice Research Datalink cohort. *International Journal of Epidemiology* **2013,** 42, 1852-1861.

93. Stocks, M. J.; Alcaraz, L.; Bailey, A.; Bonnert, R.; Cadogan, E.; Christie, J.; Dixon, J.; Connolly, S.; Cook, A.; Fisher, A.; Flaherty, A.; Humphries, A.; Ingall, A.; Jordan, S.; Lawson, M.; Mullen, A.; Nicholls, D.; Paine, S.; Pairaudeau, G.; Young, A. Discovery of AZD3199, An Inhaled Ultralong Acting. *ACS Med Chem Lett* **2014,** 5, 416-21.

94. Anderson, A. C. The Process of Structure-Based Drug Design. *Chemistry & Biology* **2003,** 10, 787-797.

95. Procopiou, P. A.; Barrett, V. J.; Bevan, N. J.; Biggadike, K.; Box, P. C.; Butchers, P. R.; Coe, D. M.; Conroy, R.; Emmons, A.; Ford, A. J.; Holmes, D. S.; Horsley, H.; Kerr, F.; Li-Kwai-Cheung, A.-M.; Looker, B. E.; Mann, I. S.; McLay, I. M.; Morrison, V. S.; Mutch, P. J.; Smith, C. E.; Tomlin, P. Synthesis and Structure−Activity Relationships of Long-acting β2 Adrenergic Receptor Agonists Incorporating Metabolic Inactivation: An Antedrug Approach. *Journal of Medicinal Chemistry* **2010,** 53, 4522-4530.

96. Black, J. W.; Crowther, A. F.; Shanks, R. G.; Smith, L. H.; Dornhorst, A. C. A NEW ADRENERGIC: BETA-RECEPTOR ANTAGONIST. *The Lancet* **1964,** 283, 1080-1081.

97. Crosby, N. J.; Deane, K. H.; Clarke, C. E. Beta-blocker therapy for tremor in Parkinson's disease. *Cochrane Database Syst Rev* **2003**, Cd003361.

98. Turner, P. Therapeutic uses of beta-adrenoceptor blocking drugs in the central nervous system in man. *Postgraduate Medical Journal* **1989,** 65, 1-6.

99. Paemeleire, K.; Magis, D.; Schoenen, J. Migraine, Medical Treatment of. In *Encyclopedia of the Neurological Sciences (Second Edition)*, Academic Press: Oxford, 2014; pp 49-52.

100. Brooks, A. M.; Gillies, W. E. Ocular beta-blockers in glaucoma management. Clinical pharmacological aspects. *Drugs Aging* **1992,** 2, 208-21.

101. Hoffman, J.; Grimm, W.; Maisch, B. [Beta blockers in therapy of chronic heart failure]. *Herz* **2002,** 27, 150-65.

102. Vellopoulou, K.; Kourlaba, G.; Maniadakis, N.; Vardas, P. A literature review to evaluate the economic value of ranolazine for the symptomatic treatment of chronic angina pectoris. *International Journal of Cardiology* **2016,** 211, 105-111.

103. Scrutinio, D.; Lagioia, R.; Di Biase, M.; Rizzon, P. Transient myocardial ischemia in patients with chronic angina: relation to heart rate changes and variability in exercise threshold. *International Journal of Cardiology* **1995,** 49, 215-223.

104. Diaz, E. S.; Karlan, B. Y.; Li, A. J. Impact of beta blockers on epithelial ovarian cancer survival. *Gynecologic Oncology* **2012,** 127, 375-378.

105. Bonnet, N.; Pierroz, D. D.; Ferrari, S. L. Adrenergic control of bone remodeling and its implications for the treatment of osteoporosis. *Journal of Musculoskeletal Neuronal Interactions* **2008,** 8, 94-104.

106. Baker, J. G.; Hill, S. J.; Summers, R. J. Evolution of beta-blockers: from anti-anginal drugs to ligand-directed signalling. *Trends in Pharmacological Sciences* **2011,** 32, 227-234.

107. Lundgren, B.; Carlsson, E.; Herrmann, I. β-Adrenoceptor blockade by atenolol, metoprolol and propranolol in the anaesthetized cat. *European Journal of Pharmacology* **1979,** 55, 263-268.

108. Morgan, T. O.; Anderson, A. I. E.; MacInnis, R. J. Ace inhibitors, beta-blockers, calcium blockers, and diuretics for the control of systolic hypertension. *American Journal of Hypertension* **2001,** 14, 241-247.

109. Rosendorff, C.; Lackland, D. T.; Allison, M.; Aronow, W. S.; Black, H. R.; Blumenthal, R. S.; Cannon, C. P.; de Lemos, J. A.; Elliott, W. J.; Findeiss, L.; Gersh, B. J.; Gore, J. M.; Levy, D.; Long, J. B.; O'Connor, C. M.; O'Gara, P. T.; Ogedegbe,

O.; Oparil, S.; White, W. B. Treatment of hypertension in patients with coronary artery disease: A scientific statement from the American Heart Association, American College of Cardiology, and American Society of Hypertension. *Journal of the American Society of Hypertension* **2015,** 9, 453-498.

110. Bylund, D. B. Propranolol☆. In *Reference Module in Biomedical Sciences*, Elsevier: 2015.

111. Tabacova, S. A.; Kimmel, C. A. Atenolol: pharmacokinetic/dynamic aspects of comparative developmental toxicity. *Reproductive Toxicology* **2002,** 16, 1-7.

112. L. P. Boulet, Y. L., J. Milot and N. Lampron. Comparative effects of dilevalol and atenolol on lung function and airway response to methacholine in hypertensive subjects. *British Journal of Clinical Pharmacology* **1990,** 29, 725-731.

113. Giles, T. D. The Role of Vasodilating β-Blockers in Patients with Complicated Hypertension: Focus on Nebivolol. *The American Journal of Medicine* **2010,** 123, S16-S20.

114. Cheng, J. W. M. Nebivolol: A third-generation β-blocker for hypertension. *Clinical Therapeutics* **2009,** 31, 447-462.

115. Salpeter, S. R.; Buckley, N. S. Use of β-blockers and β-agonists in COPD: A review of clinical outcomes. *Respiratory Medicine: COPD Update* **2007,** 2, 133-139.

116. Walters, J. A. E.; Wood-Baker, R.; Walters, E. H. Long-acting -agonists in asthma: an overview of Cochrane systematic reviews. *Respiratory Medicine* **2005,** 99, 384-395.

117. Cazzola M, M. M., Lotvall J. Ultra long-acting β2-agonists in development for asthma and chronic obstructive pulmonary disease. *Expert Opinion on Investigational Drugs* **2005,** 14, 775-783.

118. Connolly, S.; Alcaraz, L.; Bailey, A.; Cadogan, E.; Christie, J.; Cook, A. R.; Fisher, A. J.; Hill, S.; Humphries, A.; Ingall, A. H.; Kane, Z.; Paine, S.; Pairaudeau, G.; Stocks, M. J.; Young, A. Design-driven LO: The discovery of new ultra long acting dibasic β2-adrenoceptor agonists. *Bioorganic & Medicinal Chemistry Letters* **2011,** 21, 4612-4616.

119. Vernall, A. J.; Stoddart, L. A.; Briddon, S. J.; Hill, S. J.; Kellam, B. Highly Potent and Selective Fluorescent Antagonists of the Human Adenosine A3 Receptor Based on the 1,2,4-Triazolo[4,3-a]quinoxalin-1-one Scaffold. *Journal of Medicinal Chemistry* **2012,** 55, 1771-1782.

120. Magalhaes, A. C.; Dunn, H.; Ferguson, S. S. G. Regulation of GPCR activity, trafficking and localization by GPCR-interacting proteins. *British Journal of Pharmacology* **2012,** 165, 1717-1736.

121. Stephen J. Briddon, B. K., and Stephen Hill. Design and use of fluorescent ligands to study ligand-receptor interactions in single living cells. In *Receptor signal transduction protocols*, Third ed.; Challiss, G. B. W. a. R. A. J., Ed. Humana Press: 2011; Vol. 746, pp 211-236.

122. Ferre, S.; Casado, V.; Devi, L. A.; Filizola, M.; Jockers, R.; Lohse, M. J.; Milligan, G.; Pin, J. P.; Guitart, X. G protein-coupled receptor oligomerization revisited: functional and pharmacological perspectives. *Pharmacol Rev* **2014,** 66, 413-34.

123. Bouvier, M.; Heveker, N.; Jockers, R.; Marullo, S.; Milligan, G. BRET analysis of GPCR oligomerization: newer does not mean better. *Nat Meth* **2007,** 4, 3-4.

124. Maudsley, S.; Martin, B.; Janssens, J.; Etienne, H.; Jushaj, A.; van Gastel, J.; Willemsen, A.; Chen, H.; Gesty-Palmer, D.; Luttrell, L. M. Informatic deconvolution of biased GPCR signaling mechanisms from in vivo pharmacological experimentation. *Methods* **2016,** 92, 51-63.

125. Stoddart, L. A.; White, C. W.; Nguyen, K.; Hill, S. J.; Pfleger, K. D. G. Fluorescence- and bioluminescence-based approaches to study GPCR ligand binding. *British Journal of Pharmacology* **2015**, n/a-n/a.

126. Valeur, B. Introduction. In *Molecular Fluorescence*, Wiley-VCH Verlag GmbH: 2001; pp 3-19.

127. Falck, B.; Hillarp, N. A.; Thieme, G.; Torp, A. Fluorescence of catecholamine and related compounds condensed with formaldehyde. *Journal of Histochemistry & Cytochemistry* **1962,** 10, 348-354.

128. McGrath, J. C.; Arribas, S.; Daly, C. J. Fluorescent ligands for the study of receptors. *Trends in Pharmacological Sciences* **1996,** 17, 393-399.

129. Corey P. Neu, G. M. G. *Handbook of Imaging in Biological Mechanics*. CRC Press: London/New York, 2005.

130. Kozma, E.; Suresh Jayasekara, P.; Squarcialupi, L.; Paoletta, S.; Moro, S.; Federico, S.; Spalluto, G.; Jacobson, K. A. Fluorescent ligands for adenosine receptors. *Bioorganic & Medicinal Chemistry Letters* **2013,** 23, 26-36.

131. Baker, J. G.; Middleton, R.; Adams, L.; May, L. T.; Briddon, S. J.; Kellam, B.; Hill, S. J. Influence of fluorophore and linker composition on the pharmacology

of fluorescent adenosine A1 receptor ligands. *British Journal of Pharmacology* **2010,** 159, 772-786.

132. Cottet, M.; Faklaris, O.; Zwier, J. M.; Trinquet, E.; Pin, J.-P.; Durroux, T. Original Fluorescent Ligand-Based Assays Open New Perspectives in G-Protein Coupled Receptor Drug Screening. *Pharmaceuticals* **2011,** 4, 202-214.

133. Cordeaux, Y.; Briddon, S. J.; Alexander, S. P.; Kellam, B.; Hill, S. J. Agonist-occupied A3 adenosine receptors exist within heterogeneous complexes in membrane microdomains of individual living cells. *Faseb j* **2008,** 22, 850-60.

134. Daly, C. J.; McGrath, J. C. Fluorescent ligands, antibodies, and proteins for the study of receptors. *Pharmacology & Therapeutics* **2003,** 100, 101-118.

135. Schembri, L. S.; Stoddart, L. A.; Briddon, S. J.; Kellam, B.; Canals, M.; Graham, B.; Scammells, P. J. Synthesis, Biological Evaluation, and Utility of Fluorescent Ligands Targeting the μ-Opioid Receptor. *Journal of Medicinal Chemistry* **2015,** 58, 9754-9767.

136. Sridharan, R.; Zuber, J.; Connelly, S. M.; Mathew, E.; Dumont, M. E. Fluorescent approaches for understanding interactions of ligands with G protein coupled receptors. *Biochimica et Biophysica Acta (BBA) - Biomembranes* **2014,** 1838, 15-33.

137. Stoddart, L. A.; Kilpatrick, L. E.; Briddon, S. J.; Hill, S. J. Probing the pharmacology of G protein-coupled receptors with fluorescent ligands. *Neuropharmacology* **2015,** 98, 48-57.

138. Kilpatrick, L. E.; Hill, S. J. The use of fluorescence correlation spectroscopy to characterize the molecular mobility of fluorescently labelled G protein-coupled receptors. *Biochem Soc Trans* **2016,** 44, 624-9.

139. Middleton, R. J.; Kellam, B. Fluorophore-tagged GPCR ligands. *Current Opinion in Chemical Biology* **2005,** 9, 517-525.

140. Stoddart, L. A.; Vernall, A. J.; Briddon, S. J.; Kellam, B.; Hill, S. J. Direct visualisation of internalization of the adenosine A3 receptor and localization with arrestin3 using a fluorescent agonist. *Neuropharmacology* **2015,** 98, 68-77.

141. Kardos, J. Radiotracer Studies of Interfaces. In *Interfaces Science and Technology*, Horanyi, G., Ed. Elsevier Academic Press: 2004; Vol. 3, pp 220-226.

142. Valenzano, K. J.; Miller, W.; Kravitz, J. N.; Samama, P.; Fitzpatrick, D.; Seeley, K. Development of a Fluorescent Ligand-Binding Assay Using the AcroWell Filter Plate. *Journal of Biomolecular Screening* **2000,** 5, 455-461.

143. Shapiro, E.; Biezuner, T.; Linnarsson, S. Single-cell sequencing-based technologies will revolutionize whole-organism science. *Nat Rev Genet* **2013,** 14, 618-630.

144. Basu, S., Campbell, H. M., Dittel, B. N., Ray, A. Purification of Specific Cell Population by Fluorescence Activated Cell Sorting

(FACS). *Journal of Visualized Experiments* **2010**.

145. Macháň, R.; Wohland, T. Recent applications of fluorescence correlation spectroscopy in live systems. *FEBS Letters* **2014,** 588, 3571-3584.

146. Caballero-George, C.; Sorkalla, T.; Jakobs, D.; Bolaños, J.; Raja, H.; Shearer, C.; Bermingham, E.; Häberlein, H. Fluorescence Correlation Spectroscopy in Drug Discovery: Study of Alexa532-Endothelin 1 Binding to the Endothelin ET(A) Receptor to Describe the Pharmacological Profile of Natural Products. *The Scientific World Journal* **2012,** 2012, 524169.

147. Kilpatrick, L. E.; Briddon, S. J.; Holliday, N. D. Fluorescence correlation spectroscopy, combined with bimolecular fluorescence complementation, reveals the effects of β-arrestin complexes and endocytic targeting on the membrane mobility of neuropeptide Y receptors. *Biochimica et Biophysica Acta (BBA) - Molecular Cell Research* **2012,** 1823, 1068-1081.

148. Trache, A.; Meininger, G. A. Total internal reflection fluorescence (TIRF) microscopy. *Curr Protoc Microbiol* **2008,** Chapter 2, Unit 2A.2.1-2A.2.22.

149. Xie, Q.; Soutto, M.; Xu, X.; Zhang, Y.; Johnson, C. H. Bioluminescence resonance energy transfer (BRET) imaging in plant seedlings and mammalian cells. *Methods Mol Biol* **2011,** 680, 3-28.

150. Hall, M. P.; Unch, J.; Binkowski, B. F.; Valley, M. P.; Butler, B. L.; Wood, M. G.; Otto, P.; Zimmerman, K.; Vidugiris, G.; Machleidt, T.; Robers, M. B.; Benink, H. A.; Eggers, C. T.; Slater, M. R.; Meisenheimer, P. L.; Klaubert, D. H.; Fan, F.; Encell, L. P.; Wood, K. V. Engineered luciferase reporter from a deep sea shrimp utilizing a novel imidazopyrazinone substrate. *ACS Chem Biol* **2012,** 7, 1848-57.

151. Machleidt, T.; Woodroofe, C. C.; Schwinn, M. K.; Méndez, J.; Robers, M. B.; Zimmerman, K.; Otto, P.; Daniels, D. L.; Kirkland, T. A.; Wood, K. V. NanoBRET—A Novel BRET Platform for the Analysis of Protein–Protein Interactions. *ACS Chemical Biology* **2015**.

152. Joubert, J.; Dyk, S. V.; Malan, S. F. Small molecule fluorescent ligands as central nervous system imaging probes. *Mini Rev Med Chem* **2013,** 13, 682-96.

153. Pygall, S. R.; Whetstone, J.; Timmins, P.; Melia, C. D. Pharmaceutical applications of confocal laser scanning microscopy: The physical characterisation of pharmaceutical systems. *Advanced Drug Delivery Reviews* **2007,** 59, 1434-1452.

154. Lochner, M.; Thompson, A. J. A review of fluorescent ligands for studying 5-HT3 receptors. *Neuropharmacology* **2015,** 98, 31-40.

155. Vernall, A. J.; Hill, S. J.; Kellam, B. The evolving small-molecule fluorescent-conjugate toolbox for Class A GPCRs. *British Journal of Pharmacology* **2014,** 171, 1073-1084.

156. Briddon, S. J.; Hill, S. J. Pharmacology under the microscope: the use of fluorescence correlation spectroscopy to determine the properties of ligand–receptor complexes. *Trends in Pharmacological Sciences* **2007,** 28, 637-645.

157. Middleton, R. J.; Briddon, S. J.; Cordeaux, Y.; Yates, A. S.; Dale, C. L.; George, M. W.; Baker, J. G.; Hill, S. J.; Kellam, B. New Fluorescent Adenosine A1-Receptor Agonists That Allow Quantification of Ligand−Receptor Interactions in Microdomains of Single Living Cells. *Journal of Medicinal Chemistry* **2007,** 50, 782-793.

158. Vernall, A. J.; Stoddart, L. A.; Briddon, S. J.; Ng, H. W.; Laughton, C. A.; Doughty, S. W.; Hill, S. J.; Kellam, B. Conversion of a non-selective adenosine receptor antagonist into A3-selective high affinity fluorescent probes using peptide-based linkers. *Organic & Biomolecular Chemistry* **2013,** 11, 5673-5682.

159. Jacobson, K. A.; Kirk, K. L.; Padgett, W. L.; Daly, J. W. A functionalized congener approach to adenosine receptor antagonists: amino acid conjugates of 1,3-dipropylxanthine. *Mol Pharmacol* **1986,** 29, 126-33.

160. Briddon, S. J.; Kellam, B.; Hill, S. J. Design and use of fluorescent ligands to study ligand-receptor interactions in single living cells. *Methods Mol Biol* **2011,** 746, 211-36.

161. Baker, J. G. A Full Pharmacological Analysis of the Three Turkey Î²-Adrenoceptors and Comparison with the Human Î²-Adrenoceptors. *PLoS ONE* 5, e15487.

162. Song, L.; Hennink, E. J.; Young, I. T.; Tanke, H. J. Photobleaching kinetics of fluorescein in quantitative fluorescence microscopy. *Biophysical journal* **1995,** 68, 2588-2600.

163. Olah, M. E.; Stiles, G. L. Adenosine receptor subtypes: characterization and therapeutic regulation. *Annu Rev Pharmacol Toxicol* **1995,** 35, 581-606.

164. Philippe, C.; Milcent, T.; Crousse, B.; Bonnet-Delpon, D. Non Lewis acid catalysed epoxide ring opening with amino acid esters. *Organic & Biomolecular Chemistry* **2009,** 7, 2026-2028.

165. Li, G.-X.; Qu, J. Friedel-Crafts alkylation of arenes with epoxides promoted by fluorinated alcohols or water. *Chemical Communications* **2010,** 46, 2653-2655.

166. Das, U.; Crousse, B.; Kesavan, V.; Bonnet-Delpon, D.; Bégué, J.-P. Facile Ring Opening of Oxiranes with Aromatic Amines in Fluoro Alcohols. *The Journal of Organic Chemistry* **2000,** 65, 6749-6751.

167. Sajiki, H.; Hattori, K.; Hirota, K. The Formation of a Novel Pd/C−Ethylenediamine Complex Catalyst: Chemoselective Hydrogenation without Deprotection of the O-Benzyl and N-Cbz Groups. *The Journal of Organic Chemistry* **1998,** 63, 7990-7992.

168. Bayer, E.; Mutter, M. Liquid Phase Synthesis of Peptides. *Nature* **1972,** 237, 512-513.

169. Grant, G. *Synthetic Peptides* 2ed.; Oxford University press: New York, 2002.

170. Knorr, R.; Trzeciak, A.; Bannwarth, W.; Gillessen, D. New coupling reagents in peptide chemistry. *Tetrahedron Letters* **1989,** 30, 1927-1930.

171. Carpino, L. A. 1-Hydroxy-7-azabenzotriazole. An efficient peptide coupling additive. *Journal of the American Chemical Society* **1993,** 115, 4397-4398.

172. Han, G.; Tamaki, M.; Hruby, V. J. Fast, efficient and selective deprotection of the tert-butoxycarbonyl (Boc) group using HCl/dioxane (4 m). *The Journal of Peptide Research* **2001,** 58, 338-341.

173. Labrid, C.; Rocher, I.; Guery, O. Structure-Activity Relationships as a Response to the Pharmacological Differences in Beta- Receptor Ligands. *American Journal of Hypertension* **1989,** 2, 245S-251S.

174. Smith, G. P. Kinetics of amine modification of proteins. *Bioconjug Chem* **2006,** 17, 501-6.

175. Jankovic, S. M.; Milovanovic, D. R.; Jankovic, S. V. Schild's equation and the best estimate of pA2 value and dissociation constant of an antagonist. *Croat Med J* **1999,** 40, 67-70.

176. Soave, M.; Stoddart, L. A.; Brown, A.; Woolard, J.; Hill, S. J. Use of a new proximity assay (NanoBRET) to investigate the ligand-binding characteristics of three fluorescent ligands to the human β1-adrenoceptor expressed in HEK-293 cells. *Pharmacology Research & Perspectives* **2016,** 4, n/a-n/a.

177. Baker, J. G.; Hall, I. P.; Hill, S. J. Influence of agonist efficacy and receptor phosphorylation on antagonist affinity measurements: differences between second messenger and reporter gene responses. *Mol Pharmacol* **2003,** 64, 679-88.

178. Hulme, E. C.; Trevethick, M. A. Ligand binding assays at equilibrium: validation and interpretation. *Br J Pharmacol* **2010,** 161, 1219-37.

179. Cheng, Y.; Prusoff, W. H. Relationship between the inhibition constant (K1) and the concentration of inhibitor which causes 50 per cent inhibition (I50) of an enzymatic reaction. *Biochem Pharmacol* **1973,** 22, 3099-108.

180. Lane, J. R.; Sexton, P. M.; Christopoulos, A. Bridging the gap: bitopic ligands of G-protein-coupled receptors. *Trends in Pharmacological Sciences* **2013,** 34, 59-66.

181. Kamal, M.; Jockers, R. Bitopic ligands: all-in-one orthosteric and allosteric. *F1000 Biology Reports* **2009,** 1, 77.

182. Katritch, V.; Reynolds, K. A.; Cherezov, V.; Hanson, M. A.; Roth, C. B.; Yeager, M.; Abagyan, R. Analysis of full and partial agonists binding to beta2-adrenergic receptor suggests a role of transmembrane helix V in agonist-specific conformational changes. *J Mol Recognit* **2009,** 22, 307-18.

183. Byrem, T. M.; Beermann, D. H.; Robinson, T. F. The beta-agonist cimaterol directly enhances chronic protein accretion in skeletal muscle. *J Anim Sci* **1998,** 76, 988-98.

184. Terai, T.; Nagano, T. Fluorescent probes for bioimaging applications. *Current Opinion in Chemical Biology* **2008,** 12, 515-521.

185. Kallal, L.; Benovic, J. L. Using green fluorescent proteins to study G-protein-coupled receptor localization and trafficking. *Trends in Pharmacological Sciences* **2000,** 21, 175-180.

186. Koenig, J. Assessment of Receptor Internalization and Recycling. In *Receptor Signal Transduction Protocols*, Willars, G.; Challiss, R. A. J., Eds. Humana Press: 2004; Vol. 259, pp 249-273.

187. Kaumann, A. J.; Molenaar, P. The low-affinity site of the β1-adrenoceptor and its relevance to cardiovascular pharmacology. *Pharmacology & Therapeutics* **2008,** 118, 303-336.

188. Konkar, A. A.; Zhu, Z.; Granneman, J. G. Aryloxypropanolamine and catecholamine ligand interactions with the beta(1)-adrenergic receptor: evidence for interaction with distinct conformations of beta(1)-adrenergic receptors. *J Pharmacol Exp Ther* **2000,** 294, 923-32.

189. Taira, C. A.; Carranza, A.; Mayer, M.; Di Verniero, C.; Opezzo, J. A.; Hocht, C. Therapeutic implications of beta-adrenergic receptor pharmacodynamic properties. *Curr Clin Pharmacol* **2008,** 3, 174-84.

190. Arch, J. R. S. Do low-affinity states of β-adrenoceptors have roles in physiology and medicine? *British Journal of Pharmacology* **2004,** 143, 517-518.

191. Ximenes, V. F.; Campa, A.; Catalani, L. H. The Oxidation of Indole Derivatives Catalyzed by Horseradish Peroxidase Is Highly Chemiluminescent. *Archives of Biochemistry and Biophysics* **2001,** 387, 173-179.

192. Hinman, R. L.; Bauman, C. P. Reactions of N-Bromosuccinimide and Indoles. A Simple Synthesis of 3-Bromooxindoles1. *The Journal of Organic Chemistry* **1964,** 29, 1206-1215.

193. Molander, K. Comprehensive Organic Synthesis, 2nd Edition. In Johnson, J., Ed. Elsevier: Netherland, Uninited Kingdom and United States of Americas, 2014; Vol. 1, p 9816.

194. Stevens, F. C.; Bloomquist, W. E.; Borel, A. G.; Cohen, M. L.; Droste, C. A.; Heiman, M. L.; Kriauciunas, A.; Sall, D. J.; Tinsley, F. C.; Jesudason, C. D. Potent oxindole based human β3 adrenergic receptor agonists. *Bioorganic & Medicinal Chemistry Letters* **2007,** 17, 6270-6273.

195. Ferrell, J. E. Q&A: Cooperativity. *Journal of Biology* **2009,** 8, 53-53.

196. Jeremy M Berg, J. L. T., and Lubert Stryer. *Biochemistry, 5th edition*. 5 ed.; W H Freeman: New York, 2002.

197. Rahul Gauro*, M. G., Pradeep Kumar Goyal, Bhupendra Vyas. Role of Combinatorial Chemistry in the Field of New Drug Design. *International Journal of Pharmaceutical Erudition* **2016,** 5, 24-36.

198. Dale, C. L.; Hill, S. J.; Kellam, B. New potent, short-linker BODIPY-630/650[trade mark sign] labelled fluorescent adenosine receptor agonists. *MedChemComm* **2012,** 3, 333-338.

199. Simpson, L. M.; Taddese, B.; Wall, I. D.; Reynolds, C. A. Bioinformatics and molecular modelling approaches to GPCR oligomerization. *Current Opinion in Pharmacology* **2010,** 10, 30-37.

200. Lorsch, J. R.; Collins, F. S.; Lippincott-Schwartz, J. Cell Biology. Fixing problems with cell lines. *Science* **2014,** 346, 1452-3.

201. Kaur, G.; Dufour, J. M. Cell lines: Valuable tools or useless artifacts. *Spermatogenesis* **2012,** 2, 1-5.

202. Kawakita, Y.; Banno, H.; Ohashi, T.; Tamura, T.; Yusa, T.; Nakayama, A.; Miki, H.; Iwata, H.; Kamiguchi, H.; Tanaka, T.; Habuka, N.; Sogabe, S.; Ohta, Y.; Ishikawa, T. Design and Synthesis of Pyrrolo[3,2-d]pyrimidine Human Epidermal Growth Factor Receptor 2 (HER2)/Epidermal Growth Factor Receptor (EGFR) Dual Inhibitors: Exploration of Novel Back-Pocket Binders. *Journal of Medicinal Chemistry* **2012,** 55, 3975-3991.

203. Baker, J. G.; Hall, I. P.; Hill, S. J. Temporal Characteristics of cAMP Response Element-Mediated Gene Transcription: Requirement for Sustained cAMP Production. *Molecular Pharmacology* **2004,** 65, 986-998.